



Polyoxometalate-based materials for sustainable and clean energy conversion and storage

Yu Zhang,^a Jiang Liu,^{*,a} Shun-Li Li,^a Zhong-Min Su,^b and Ya-Qian Lan^{*,a}

^aJiangsu Collaborative Innovation Centre of Biomedical Functional Materials, Jiangsu Key Laboratory of New Power Batteries, College of Chemistry and Materials Science, Nanjing Normal University, Nanjing 210023, PR China

^bJilin Provincial Science and Technology Innovation Center of Optical Materials and Chemistry, School of Chemistry and Environmental Engineering, Changchun University of Science and Technology Changchun, Changchun 130022, PR China

*Correspondence: liuj@njnu.edu.cn (J. L.), yqlan@njnu.edu.cn (Y.-Q. L.)

ABSTRACT: In order to relieve current energy crisis and the related environment pollutions arising with fossil fuel, the development and application of sustainable and clean energy, such as solar and hydrogen, is anticipated as a prospective issue. It is urgent and significant to develop and construct various energy storage and conversion technologies and materials for the generation and utilization of clean energy sources. Polyoxometalates (POMs), a class of metal oxide polyanion clusters, can serve as outstanding candidates in energy-related fields like electrocatalysis, rechargeable battery, photocatalysis, and proton conduction, based on their plentiful redox property, semiconductor-like feature and acidity. Here, the selected recent and significant advances in the development of POM-based materials for sustainable and clean energy conversion and storage are reviewed and summarized, and special emphases are shown to the applications of POMs as platforms for hydrogen production, water oxidation, carbon dioxide reduction, Li-ion rechargeable batteries, supercapacitors, proton-exchange membrane fuel cells, dye-sensitized solar cells and so on. The results obtained from different catalytic/energy storage systems have been compared and we try to give a better understanding on catalytic reactivity-catalysts structure correlation as well as to put a picture for the rational design of electrochemical electrodes.

KEYWORDS: Polyoxometalates, Electrocatalysis, Photocatalysis, Rechargeable batteries, Energy conversion and storage

INTRODUCTION

The global energy crisis has already become one of the most urgent issues that human beings face. As the excessive overexploitation and persistent utilization of the accessible fossil fuel, these nonrenewable energy sources, such as petroleum and coal, are going to be depleted, making the exploitation and utilization of the sustainable and clean energy resources widely concerned. Solar energy is still the most likely source of sustainable energy for the medium and longer-term future. Therefore, strategies have been proposed to improve the current situation. First, the development of novel energy systems that convert photo/electrical energy into chemical energy powered by renewable-generated energy from solar, such as hydrogen from water splitting and photocatalytic/electrochemical reduction of carbon dioxide (CO₂) to chemical fuels, is considered as one of the most perspective strategies.^{1,2} Second, the construction of improved energy storage devices, such as lithium ion batteries, lithium metal batteries, supercapacitors, proton-exchange membrane fuel cell, and so on, for efficient energy conversion from stored chemical energy in substance to available electrical energy is also at the forefront of both fundamental and applied research in energy technology.^{3,4} Thirdly, since solar energy is the original source for all energy carriers, the development of solar cells to convert light into electricity is definitely of great significance.⁵

Polyoxometalates (POMs), a special class of metal (e.g. V^V, Mo^V, Nb^V, Ta^V, Mo^{VI}, and W^{VI}) oxide polyanion clusters with linked together by shared oxygen atoms to form well-defined cluster frameworks with highly variable functional properties,

recently have been widely applied in energy-related fields due to their unique features such as plentiful and reversible redox chemistry, adjustable structure, and variety compositions.⁶ The first polyoxometalate was found in 1826 and until the year of 1934, the structure of Keggin POM was confirmed by powder X-ray diffraction.^{7,8} In 1991, a review article that noted the versatile features and revealed the potentials of these unique kind of compound significantly promoted the research surge in the structural development of POM chemistry.⁹ Furthermore, the vast development of POM chemistry including the novel structure construction, the synthesis route development, and the wide application of POM in molecular magnetism, medicine and catalysis, have also been reported and well-organized in several review articles, giving a comprehensive summary of possibilities offered by POMs.^{7,8,10}

The structure and composition of POM is adjustable. Cronin et al. have predicted and summarized the building block nuclearity of POMs using a classification based on the virtual building blocks (VBB), the isolable (IBB) and the parent-cluster-based building blocks (PCBB) (Fig. 1).⁷ In accordance with their controllable structure and variable composition, the properties of POMs such as solubility, redox ability, and acidity can be delicately adjusted by varying constituent elements. One of

Received: August 3, 2019

Revised: October 8, 2019

Accepted: October 10, 2019

Published: 2 November 2019



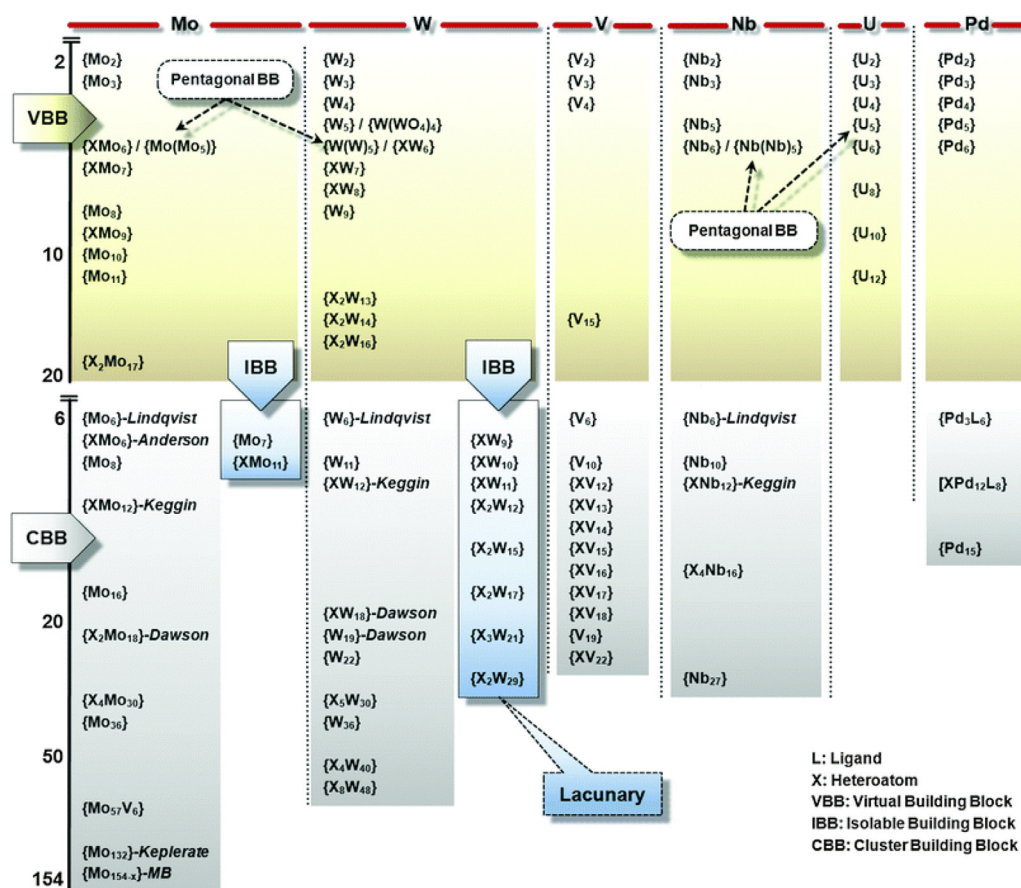


Fig. 1. Building block nuclearity. Reproduced with permission.⁷ Copyright 2012, Royal Society of Chemistry.

the most striking properties of POMs is the chargeable redox properties to reversibly gain and lose electrons,^{11,12} making them received widespread interest as ideal candidates for designing electrocatalysts or electrode materials in energy storage and conversion field. Notably, the ability to undergo reversible multi-valence reductions/oxidations of POMs leads to the formation of mixed-valence species, bringing favorable catalytic or capacitive properties with regard to several electrochemical application fields, such as electrocatalysis and rechargeable batteries.¹³ In addition, POMs possess semiconductor-like feature that is similar to metal oxides, which makes them as promising platforms for photocatalysis related applications, such as photocatalytic hydrogen production and water oxidation as well as solar cells.¹⁴ Furthermore, the acidity of POMs is favorable to proton conduction applications which is an significant identity for the proton-exchange membrane fuel cells. The essential breakthroughs of the POM-based materials for electrocatalysis and photocatalysis mentioned in this review are presented in timeline form as shown in Schemes 1 and 2.

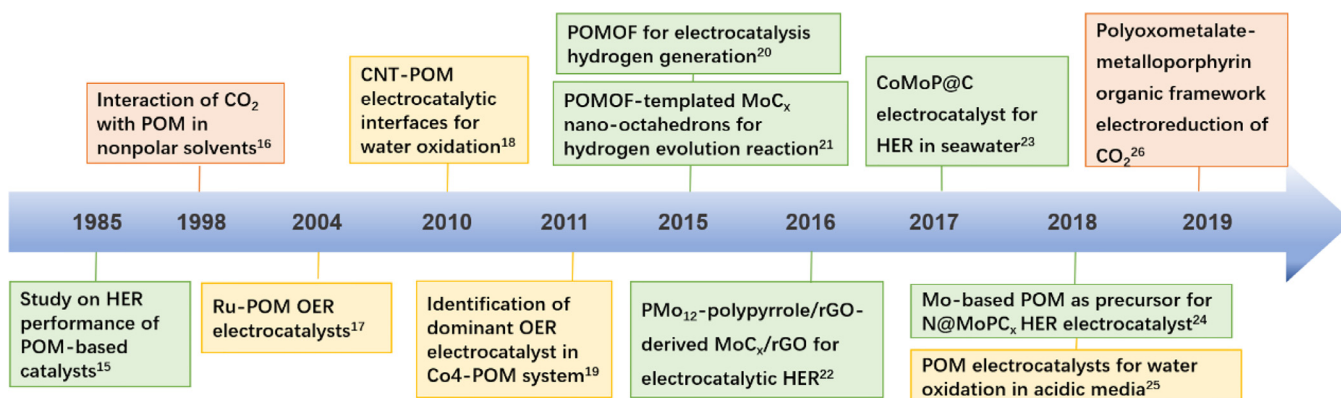
In this review, progress on the energy conversion among solar energy, electrical energy as well as chemical energy based on POM-based materials has been summarized and reviewed (Fig. 2). We focus on the important researches about the POM-based materials, including POMs, POM-based metal organic frameworks, POM-based nanocomposites, and POM-based derivatives for the application in sustainable and clean energy conversion and storage systems, especially POM-based materials as catalysts for hydrogen production, water oxidation,

and CO₂ reduction by electrocatalysis/photocatalysis, and POM-based electrode materials for rechargeable batteries, supercapacitors, proton-exchange fuel cells, dye-sensitized solar cells and so on.

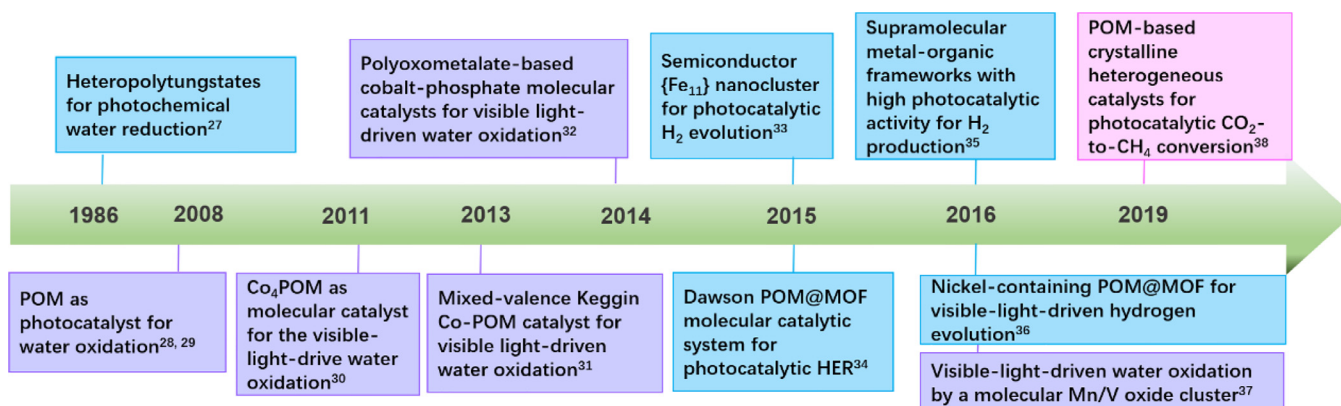
Great emphasis is paid to the emerging strategies for the activity improvement of POM-based photo/electro-catalysts and better understanding on the fundamental catalytic mechanisms as well as the rational design of the POM-based electrode materials for enhanced energy storage performance. In addition, the key factors determining the efficiencies of catalytic processes for hydrogen generation, water oxidation, and CO₂ reduction, and the performance of rechargeable batteries and supercapacitors, are also be addressed. Finally, the perspectives of POM-based materials for sustainable and clean energy conversion and storage systems are presented and discussed.

POM-BASED ELECTROCATALYSTS

Due to their fast mediate electron, proton, and oxygen atom transfer abilities,³⁹ POM-based materials have been extensively investigated in the field of the energy-related electrocatalytic reaction applications including hydrogen evolution reaction (HER), oxygen evolution reaction (OER), oxygen reduction reaction (ORR), carbon dioxide reduction reaction (CO₂RR), methanol oxidation reaction (MOR) and so on.^{40,41} Herein, recent progress of the POM-based materials as promising electrocatalysts for sustainable and clean energy conversion applications, such as HER and OER and CO₂RR, is reviewed and summarized.



Scheme 1. Timeline of important breakthroughs of POM-based electrocatalysts for sustainable and clean energy conversion processes including hydrogen production (green), water oxidation (yellow), and carbon dioxide reduction (orange).



Scheme 2. Timeline of important breakthroughs for POM-based photocatalysts for sustainable and clean energy conversion processes, such as hydrogen production (blue), water oxidation (violet), and carbon dioxide reduction (pink).

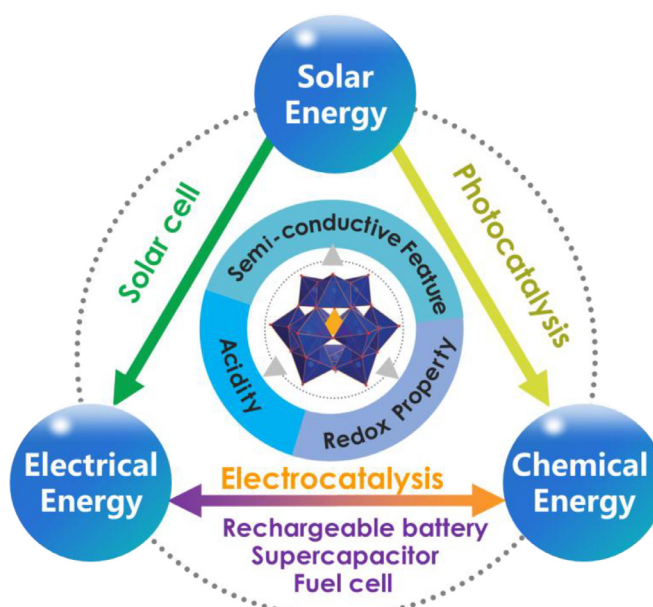


Fig. 2. POM-based materials for sustainable and clean energy conversion and storage.

POM-based electrocatalysts for hydrogen production

As one of the cleanest energy carriers on the earth, hydrogen, which has a higher energy content of 120 MJ kg^{-1} compared to 44 MJ kg^{-1} for gasoline, is essential to several key industrial processes and may play a major role in the further energy supply.⁴² Therefore, production and industrialization of hydrogen garner well-deserved attentions from the researchers in energy storage and conversion fields. The carbon-free hydrogen energy whose combustion product is just water may be used as clean fuel for vehicles to replace the declining petroleum. Unfortunately, the majority hydrogen energy currently used stems from reformation of fossil fuels, which is accompanied by the additionally increasing emission of CO_2 into atmosphere.⁴³ The most promising and eco-friendly hydrogen energy source generates from water splitting using renewable-generated power with the simultaneously production of H_2 and O_2 .

The water electrolysis can be viewed as a prospective approach to sustainably obtain clean H_2 energy. However, in addition to the issues of effective separation from the mixed generated gases, safe transportation and secure storage of H_2 , the slow kinetics during the electrolysis process and the accompanying high electric energy consumption hinder the industrial applications to some extent.⁴⁴ Noble-metal-based catalysts (e.g., Pt/C, IrO_2 and RuO_2) have been identified as the most active HER or OER catalysts,^{45,46} whereas their high cost and low abundance impede the large-scale application, making it an urgent mission to develop efficient, durable and low-cost electrocatalysts. As referred above, POMs have stable oxidation/reduction states, which can act as both acceptors and/or donors during the electron transfer reactions owing to their excellent electron/proton storage and transfer capabilities.¹⁴ POM-based materials are ideal candidates to address the challenge of constructing active non-noble-metal-based electrocatalysts as they can be chemically modified with highly redox-active metals,³⁹ covalently or non-covalently functionalized on conductive carbon materials,^{47,48} or tactfully chosen as precursors to obtain transition-metal-based nanocomposites.^{21,24,49}

POMs and their assemblies for electrocatalytic hydrogen production

The POM-based HER catalyst was firstly reported in 1985 by Nadjo and Keita, in which the HER activity was later found to come from trace amounts of Pt deposited on the working electrode resulting from anodic dissolution of the Pt counter electrode.^{15,50} Following this strategy, Wang and Lin et al. proposed a research on the simultaneous co-deposition of Pt and POM on working electrode.⁵¹ The co-deposition of POM is crucial for the excellent HER performance due to their ability to capture dissolved Pt(IV)-oxo species to lead to the uniform Pt deposition. Remarkable HER activity was achieved by using the unsaturated lacunary POM $\text{SiW}_{11}\text{O}_{39}^{8-}$ (SiW_{11}) rather than the saturated POMs ($\text{SiW}_{12}\text{O}_{40}^{4-}$ and $\text{P}_2\text{W}_{18}\text{O}_{62}^{6-}$). Additionally, the research works of Cronin's group have given the breakthroughs in POM-based water electrolysis systems for hydrogen production.^{43,45} By using the POM $\text{H}_3\text{PMo}_{12}\text{O}_{40}$ as a redox mediator, Cronin et al. introduced the concept of the electron-coupled-proton buffer (ECPB) to design a novel water splitting system, in which the O_2 and H_2 could be produced at separate times during water electrolysis.⁴³ In the proposed system, the electrons and protons generated during the oxidation of water can be taken up reversibly by PMo_{12} (an ECPB), and H_2 and O_2 can be obtained at completely different times, preventing

their mixture and thus avoiding the electrolyzer degradation. This research has broken through the transitional water electrolysis process in which the H_2 and O_2 are produced simultaneously. Furthermore, their group designed another water splitting system by introducing a recyclable redox mediator ($\text{H}_4[\text{SiW}_{12}\text{O}_{40}]$) that enables the prevention of product gases from mixing over a range of current densities and that make more effective use of the precious metal catalysts.⁴⁵ With the employment of the $\text{H}_4[\text{SiW}_{12}\text{O}_{40}]$ mediator, a platinum-catalyzed system produces pure hydrogen over 30 times faster than proton exchange membrane electrolyzers at equivalent platinum loading. However, Pt was still used as HER catalyst in these researches and the catalysis of POM was less investigated. And the limited stability of Pt-based catalysts during continuously reaction is still an obstacle, making it a challenge to construct noble-metal-free catalysts with stable structures.

A few early reported Pt-free POM-based HER catalysts, including polyanions of $[\text{Co}_6(\text{H}_2\text{O})_{30}\{\text{Co}_9\text{C}_{12}(\text{OH})_3(\text{H}_2\text{O})_9(\beta\text{-SiW}_8\text{O}_{31})_3\}]^{5-}$ and $[\text{Cu}^{\text{II}}_2\text{Pd}^{\text{II}}_{22}\text{P}^{\text{V}}_{12}\text{O}_{60}(\text{OH})_8]^{20-}$ were synthesized by Kortz et al.⁵² However, the HER performance was not discussed in detail. Additionally, most of POMs as electron and proton reservoirs could undergo reversible multi-electron processes in a homogeneous liquid medium, making them difficult to be isolated or recycled from the solution. The construction of POM-based metal-organic frameworks (POMOFs) by using POMs as building blocks for MOFs is an effective strategy to immobilize and prevent POMs from dissolving. POMOFs combine the redox nature of POMs and the porosity of MOFs. In 2014, Lan and Su et al. organized a review article on POM-based MOF materials, including their definition, synthesis, and catalysis application.⁵³ As shown in Fig. 3, POM-based MOF materials were divided into POM-based MOF single-crystal materials and POM-loaded MOF materials. Based on the position of POMs in the MOFs, the POM-based MOF single-crystal materials could be classified into three main types: (i) d/f-block metal ion-modified POM units directly connected with organic ligands, (ii) POM anions residing within the cages of MOFs as templates, and (iii) porous inorganic-organic materials with POM anions as pillars. Fig. 3b presents the POM units, which were employed to build up POM-based MOF materials in the published researches.

In 2011, Dolbecq et al. synthesized a POMOF compound of $(\text{TBA})_3[\text{PMo}^{\text{V}}_8\text{Mo}^{\text{VI}}_4\text{O}_{36}(\text{OH})_4\text{Zn}_4][\text{C}_6\text{H}_3(\text{COO})_3]_{4/3} \cdot 6\text{H}_2\text{O}$ ($\epsilon(\text{trim})_{4/3}$, TBA^+ = tetrabutylammonium ion) and primarily studied the cation effect on its electrocatalytic activities in XCl ($\text{X}=\text{Li}, \text{Na}, \text{K}, \text{Cs}$) media.⁵⁴ It was the first report on the non-noble POM-based HER electrocatalyst, and this POMOF showed a turnover frequency (TOF) as high as ca. 6.7 s^{-1} at the overpotential of 200 mV. In 2015, Su and Lan et al. reported two novel POM-based MOFs of $[\text{TBA}]_3[\epsilon\text{-PMo}^{\text{V}}_8\text{Mo}^{\text{VI}}_4\text{O}_{36}(\text{OH})_4\text{Zn}_4][\text{BTB}]_{4/3} \cdot x\text{Guest}$ (NENU-500, BTB = benzene tribenzoate) and $[\text{TBA}]_3[\epsilon\text{-PMo}^{\text{V}}_8\text{Mo}^{\text{VI}}_4\text{O}_{37}(\text{OH})_3\text{Zn}_4][\text{BPT}]$ (NENU-501, BPT = [1,1'-biphenyl]-3,4',5-tricarboxylate), in which the $\{\text{Zn}\text{-}\epsilon\text{-Keggin}\}$ fragments serving as nodes were connected with organic ligands directly giving rise to stable three-dimensional (3D) open frameworks.²⁰ The obtained compounds with the well-defined structure as displayed in Fig. 4 showed good stability in air as well as tolerance to acidic and basic media. Taking advantages of redox activity of the POM unit and porosity of the MOF, NENU-500 exhibited outstanding HER activity with a low overpotential of 237 mV at the current density of 10 mA cm^{-2} and long-term stability of maintaining its electrocatalytic activities after 2000

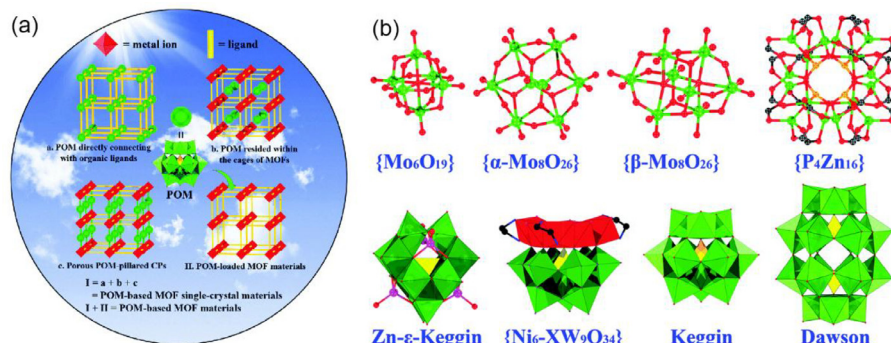


Fig. 3. (a) The schematic overview of POM-based MOF materials and (b) the POM units used to build up POM-based MOF materials. Reproduced with permission.⁵³ Copyright 2014, Royal Society of Chemistry.

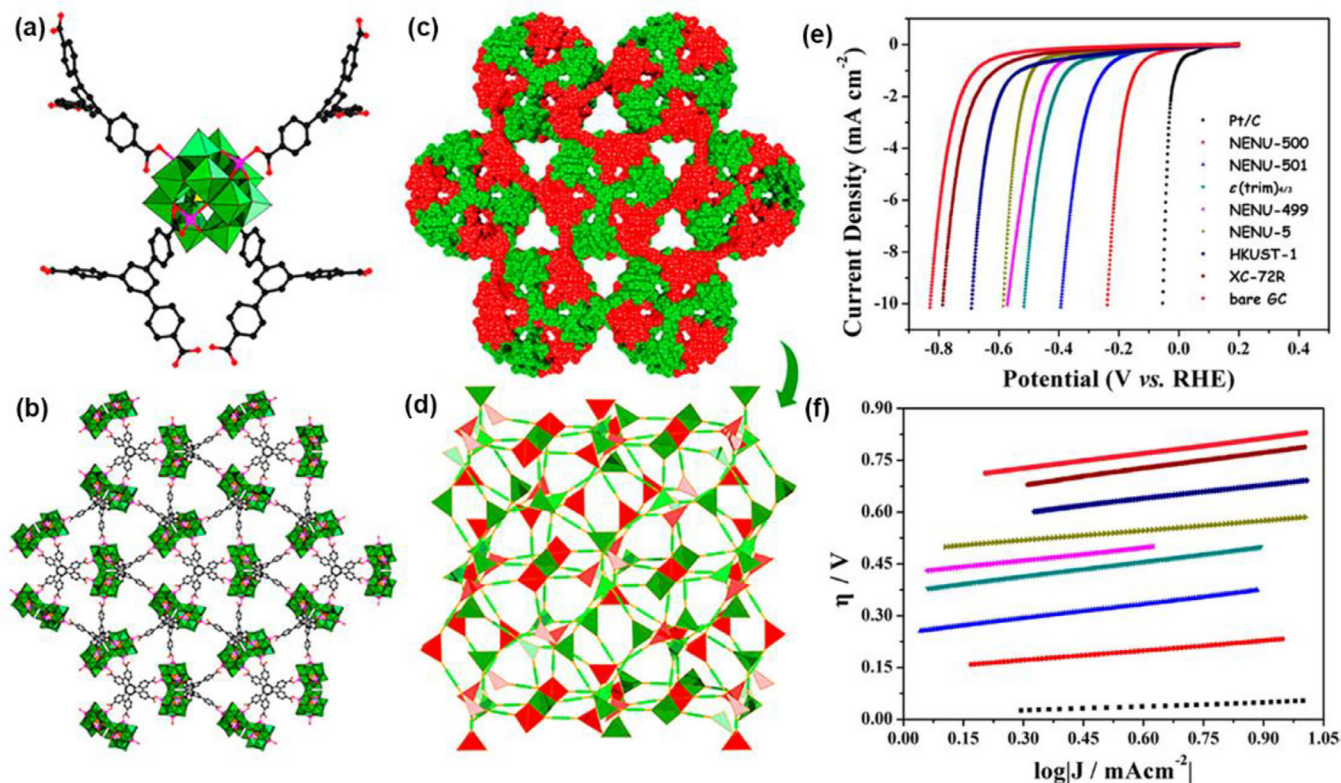


Fig. 4. Summary of the structure of NENU-500: (a) connection mode between Zn- ϵ -Keggin and BTB³⁻ fragments, (b) 3D (3,4)-connected frameworks, (c) two-fold interpenetrated structure, and (d) two-fold interpenetrated **ctu** arrays. Electrochemical characterization of the as-prepared catalysts: (e) polarization curves in 0.5 M H₂SO₄ and (f) corresponding Tafel plots. Reproduced with permission.²⁰ Copyright 2015, American Chemical Society.

cycles. Density functional theory (DFT) calculations revealed that the distinct catalytic activity of NENU-500 originated from the suitable free energy of H adsorption of the Zn- ϵ -Keggin-Cl fragment.

Due to the low specific surface area ($<10 \text{ m}^2 \text{ g}^{-1}$) and insulation of POMs, much effort has been made for POM-based electrocatalysts combined with conductive carbon materials as substrates.^{47,48,55,56} By fixing the selected POMs of phosphotungstate [H₇P₈W₄₈O₁₈₄]³³⁻ and the Co(II)-Containing silicotungstates [Co₆(H₂O)₃₀{Co₉C₁₂(OH)₃(H₂O)₉(β -SiW₈O₃₁)₃}⁵⁻ and [Co₃(β -SiW₉O₃₃(OH))(β -SiW₈O₂₉(OH))₂]₂²²⁻ on the conductive Vulcan XC-72 matrix, Nadjio et al. studied

the hydrogen-evolving behaviors of these POM proton and electron reservoirs.⁵⁷ The composite of [PW₁₂O₄₀]³⁻ Keggin ion combined with carbon nanotubes was prepared by Xing and co-workers for stable hydrogen evolution process.⁵⁸ Then, in 2016, Zhang and co-workers proposed a model system of a cyclic 48-tungsto-8-phosphate [H₇P₈W₄₈O₁₈₄]³³⁻ (P₈W₄₈)/rGO nanocomposite prepared by electroreduction to investigate the interaction between the POM and the carbon substrate.⁴⁷ The solid state ³¹P NMR spectrum of P₈W₄₈/rGO revealed a strong interaction between the individual P₈W₄₈ and the transparent rGO sheets. By taking a quarter structure of [H₂P₂W₁₂O₄₈]¹²⁻ (P₂W₁₂) as model, the DFT calculated adsorption energy for P₂W₁₂ on graphene (-1.55 eV) and

the charge transfer between P_2W_{12} and graphene ($0.66 |e|$) theoretically supported the existence of a strong interaction between POM and graphene. Notably, the P_8W_{48}/rGO hybrid displayed excellent HER activity in an acidic electrolyte with a high turnover frequency (TOF) of 11 s^{-1} at the overpotential of 295 mV, which was comparable to that of the commercial Pt/C catalyst. Later in 2018, Fernandes et al. reported the preparation of nanocomposites based on POMs (P_2W_{18} , P_5W_{30} , and P_8W_{48})/rGO via a one-step electroreduction synthesis process.⁴⁸ Among the three, the $P_5W_{30}@rGF_{ox}$ exhibited the best HER activity and the long-term electrochemical stability with the overpotential changed 9 mV at 10 mA cm^{-2} after 1000 linear sweep voltammetry cycles.

POM-derived electrocatalysts for electrocatalytic hydrogen production

Despite the progress made in the POM-based hybrid catalysts, the applications of POMs in electrocatalysis fields are still limited because of their significant solubility in reaction media, which leads to poor stability as a result of the disintegration of active sites. Recently, innovative approaches for the preparation of novel hybrid nanocomposites stemming from POM-based compounds for HER with catalytic performance that are comparable with Pt-based materials have been reported. Calcination under inert atmosphere is the most widely used treatment of the POM-based precursors to obtain expected HER electrocatalysts.

Molybdenum carbides are considered as one type of privileged noble-metal-free electrocatalysts for HER over a wide range of pH values due to their d-band electron structure that is similar to Pt.⁵⁹ Owing to the excellent redox activity of the Mo species, the Mo-containing POMs and their related derivatives have been involved as precursors to obtain molybdenum carbide-based HER electrocatalysts. In 2015, Lou et al. developed a MOFs-assisted strategy that relied on *in-situ* and confined carburization reaction between the organic ligands of MOFs and the guest POMs resided in the pores for synthesizing the porous molybdenum carbide octahedral nanocrystallite.²¹ The as-synthesized porous MoC_x nano-octahedron displayed outstanding performance with low overpotential and Tafel slope for HER in both acidic and basic electrolyte.

The latest research works indicate that the fine tuning of the electronic structure of HER electrocatalysts is the key point to improve their catalytic performance.^{60,61} The precise design of POM precursors can allow the accurate controlled synthesis of POM-derived catalysts. To develop an efficient Mo-based HER catalyst, a novel organoimido-derivatized heteropolyoxometalate, $Mo_4\text{-CNP}$, was designed as precursor for the formation of nitrogen-doped porous molybdenum carbide and phosphide ($N@MoPC_x$) hybrids by Wei et al. in 2018.²⁴ As shown in Fig. 5, the $Mo_4\text{-CNP}$ precursor crystals possessed the unique molecular and layer-by-layer packing crystal structures, which avoided the agglomeration during the thermal annealing process. This was because the Mo skeleton was surrounded by the arylimido and phenylphosphonic ligands, leading to the achievement of the *in-situ* nitrogen doping and the homogeneous carburization and phosphorization reactions on the atomic scale. Besides, the organically functionalized polyoxometalate-assisted strategy provides a novel idea for the construction of MoC_x -based HER electrocatalysts. According to this method, Wei and co-worker designed an organoimido-derivatized POM with inherent Mo-N bonds for the preparation of a MoC_2 -based catalytic HER system.⁴⁹ Their research demonstrated that the implantation of N atoms could tune the electronic structure of the Mo_2C

catalysts atomically. By changing the amount of organoimido ligands in the POM precursor, the N-doping sites in Mo_2C could be well controlled. DFT calculations also proved that the N dopants in the carbon matrix could weaken H adsorption strength and promote H_{ad} desorption, resulting in the enhanced HER performance.

By annealing the mixture of Mo-containing POMs and carbon sources, especially the heteroatom-doped ones, the composites of Mo-based materials coated by heteroatom-doped carbon layers could be fabricated. The graphitized carbon layers generated during the heat treatment can not only enhance the electrical conductivity and surface area of the catalysts but also protect the metal species from corrosion in harsh electrolytes.⁴⁶ In addition, the doped heteroatom species, such as nitrogen (N), phosphorus (P), and sulfur (S), can increase the electronic density and tune the surface properties of the carbon layers.⁶² Lan's group synthesized a porous Mo-based composite ($MoO_2@PC\text{-RGO}$) derived from a POMOFs/GO composite at a relatively low carbonization temperature (Scheme 3).⁶³ Confined in the carbon shell, the agglomeration of MoO_2 could be hindered. Due to the synergistic effects among the conductive RGO support, nanosized MoO_2 particles, P-doped carbon skeleton and the closely interconnected network, $MoO_2@PC\text{-RGO}$ exhibited a positive onset potential close to that of 20% Pt/C, low Tafel slope of 41 mV dec^{-1} , high exchange current density of 0.48 mA cm^{-2} and remarkable long-term cycle stability.

In 2016, Lan's group reported a two-dimensional (2D) coupled hybrid of molybdenum carbide and reduced graphene oxide ($Mo_2C@NPC/NPRGO$) derived from a ternary polyoxometalate-polypyrrole/reduced graphene oxide nanocomposite ($PMo_{12}\text{-PPy/RGO}$) precursor (Fig. 6).²² Due to the protection from the carbon layer, the $Mo_2C@NPC/NPRGO$ nanocomposite has showed outstanding HER performance with an overpotential of 34 mV at 10 mA cm^{-2} , a Tafel slope of 33.6 mV dec^{-1} and long-term stability in an acidic electrolyte, which is comparable to that of the commercial Pt/C catalyst. DFT calculations demonstrate that the synergistic effect between Mo_2C and C-pyridinic N contributes to the excellent HER activity of the $Mo_2C@NPC/NPRGO$ nanocomposite. Besides, Lan's group synthesized a POMOF derived HER catalyst based on the Fe_3C/Mo_2C -containing N, P-codoped graphitic carbon ($Fe_3C/Mo_2C@NPGC$) by carbonizing the mixture of $PMo_{12}@MIL\text{-}100$ (Fe) and melamine.⁶⁴ The as-prepared $Fe_3C/Mo_2C@NPGC$ demonstrated excellent electrocatalytic activity and stability towards HER with a low onset overpotential of 18 mV, small Tafel slope of 45.2 mV dec^{-1} as well as long-term durability for 10 h.

In the research of Li and co-workers, heteroatom-doped carbon coated transition metal-based electrocatalysts have been prepared and deeply investigated.^{23,65–67} A Pt-free HER catalysts based on cobalt molybdenum phosphide nanocrystal coated by a few-layer N-doped carbon ($CoMoP@C$) was prepared by a one-step pyrolysis method on a large scale with the mixture of $\{Co_{16}Mo_{16}P_{24}\}$ and dicyandiamide (DCA) (Fig. 7a).²³ The $CoMoP@C$ composite showed comparable HER activity to Pt/C catalysts in all pH range as displayed in Fig. 7d and e. Moreover, it is also an efficient and stable HER electrocatalyst in seawater with a high Faradaic efficiency of 92.5% over 10 h. Whereas, the electrocatalytic activity of 20 wt% Pt/C dramatically decreased after 4 h under the same conditions. According to the DFT calculations, the superior HER performance of $CoMoP@C$ is attributed to the synergy between $CoMoP$ and the N dopants with a small ΔG_{H^*} of 0.103 eV.

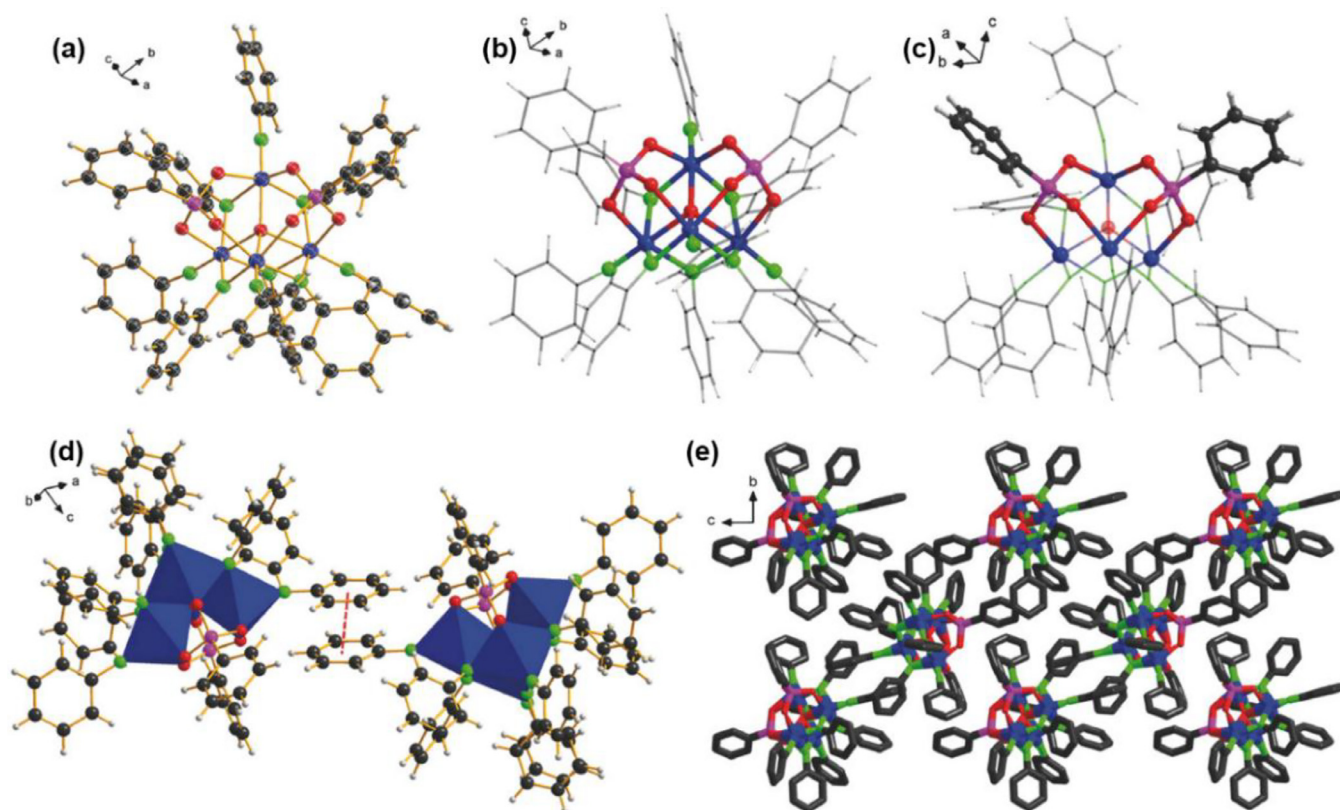
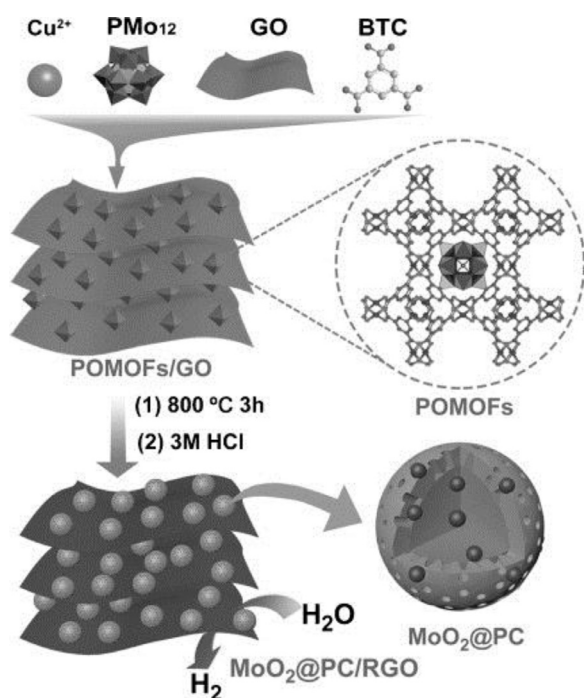


Fig. 5. Molecular and crystal structures of the Mo₄-CNP precursor. (a) ORTEP drawings of Mo₄CNP. (b, c) Mo₄ cluster and phenylphosphinic acid ligands in the Mo₄-CNP molecule. (d) Weak π-π stacking interactions between adjacent Mo₄-CNP molecules. (e) Packing structure of Mo₄-CNP. Color code: Mo, blue; C, black; N, green; P, pink; O, red; H, gray. Reproduced with permission.²⁴ Copyright 2018, Wiley-VCH. (For interpretation of the references to color in this figure legend, the reader is referred to the web version of this article.)



Scheme 3. Preparation process of the MoO₂@PC-RGO nanocomposite used as electrocatalyst for the HER. Reproduced with permission.⁶³ Copyright 2015, Wiley-VCH.

Using POM as the molecular-element-regulating platform, an electrocatalyst of molybdenum phosphide and molybdenum carbide composite nanoparticles (NPs) coated by N-doped graphitic carbon shells (MoP/Mo₂C@C) was prepared via annealing the mixture of P₄Mo₆ and dicyandiamide (DCA).⁶⁶ A P-doped Mo₂C coated by N-doped carbon (P-Mo₂C@NC) was also synthesized by calcining the mixture of H₃[PMo₁₂O₄₀] and urea-formaldehyde resin under the flowing N₂.⁶⁷ The urea-formaldehyde resin could not only serve as the carbon source but also facilitate the uniform distribution of the POM precursor to avoid the aggregation of the Mo₂C particles during calcination. Li's group selected Anderson-type POMs (NH₄)_n[TMMo₆O₂₄H₆]·5H₂O (TM=Ni²⁺, Co²⁺, n=4; TM=Fe³⁺, Cr³⁺, n=3) as precursors mixed with DCA to prepare a series of transition-metal-doped Mo₂C@C composites. The Ni-Mo₂C@C showed the lowest overpotential of 72 mV at the current density of 10 mA cm⁻² and the best long-term stability over 24 h without obvious increment of overpotential in an acidic electrolyte among all the as-prepared samples.⁵⁹ The TM dopants that exhibited a significant effect on the activity and hydrogen binding energy (ΔG_{H*}) of Mo₂C mainly accounted for the increased HER performance. The strategy of carbonization of POMs and carbon sources for posterior application as HER electrocatalysts leads to novel nanocomposites with unique architectures and improved HER activities.

Molybdenum disulfide (MoS₂) that serves as an acknowledged and highly-efficient HER electrocatalyst can be obtained derived from POM-based precursors.^{68–70} In 2016, Lan's group reported a

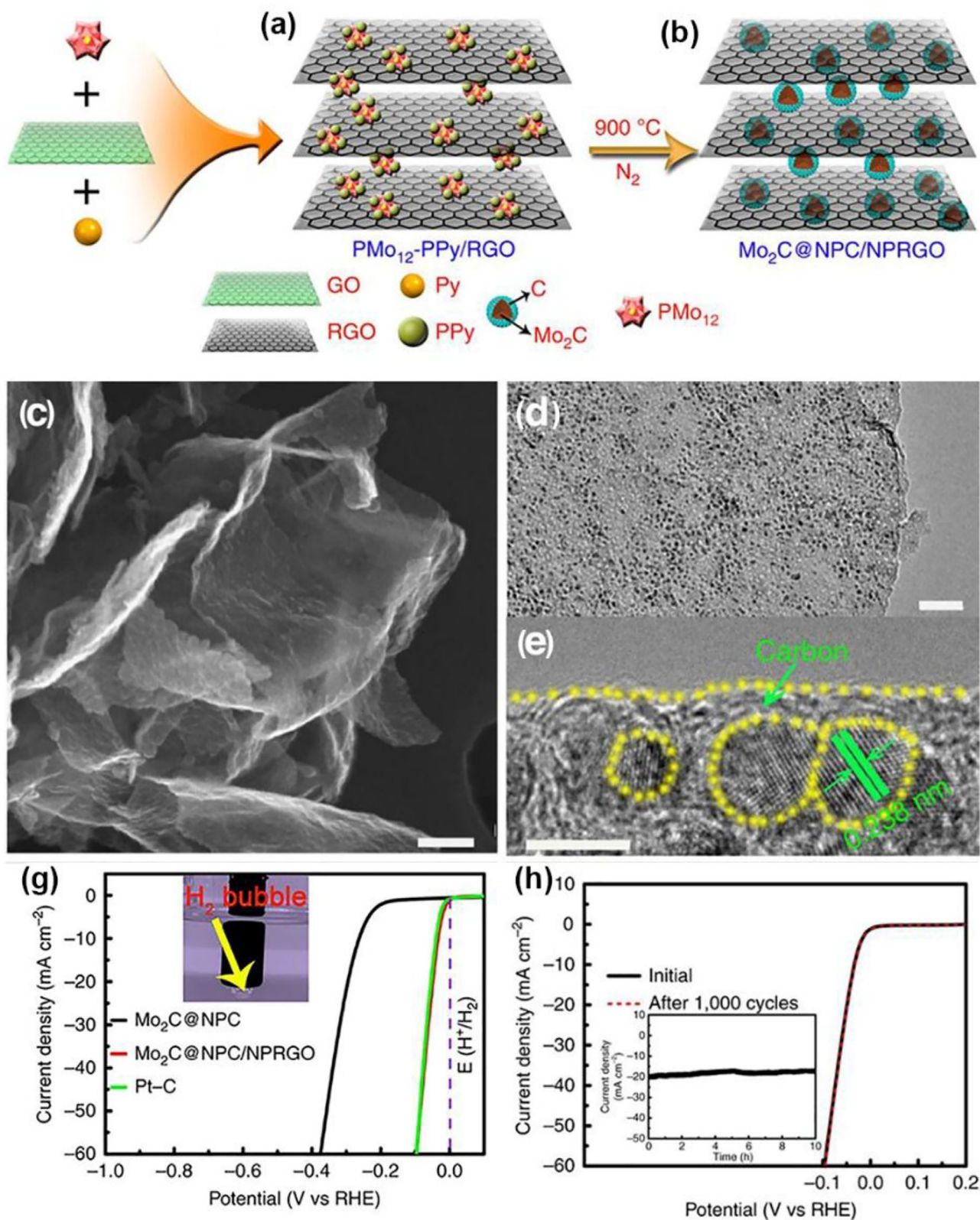


Fig. 6. Schematic illustration of (a) synthesis of the $\text{PMo}_{12}\text{-PPy}/\text{RGO}$ precursor and (b) formation of $\text{Mo}_2\text{C}@\text{NPC}/\text{NPRGO}$. Characterization of the $\text{Mo}_2\text{C}@\text{NPC}/\text{NPRGO}$ hybrid: (c) SEM, (d) TEM and (e) HRTEM images. HER performance: (f) polarization curves of different electrodes, (f) polarization curves of $\text{Mo}_2\text{C}@\text{NPC}/\text{NPRGO}$ before and after 1000 CV cycles with inset being the time-dependent current density curve under a static overpotential of 48 mV for 10 h. Reproduced with permission.²² Copyright 2015, Nature Publishing Group.

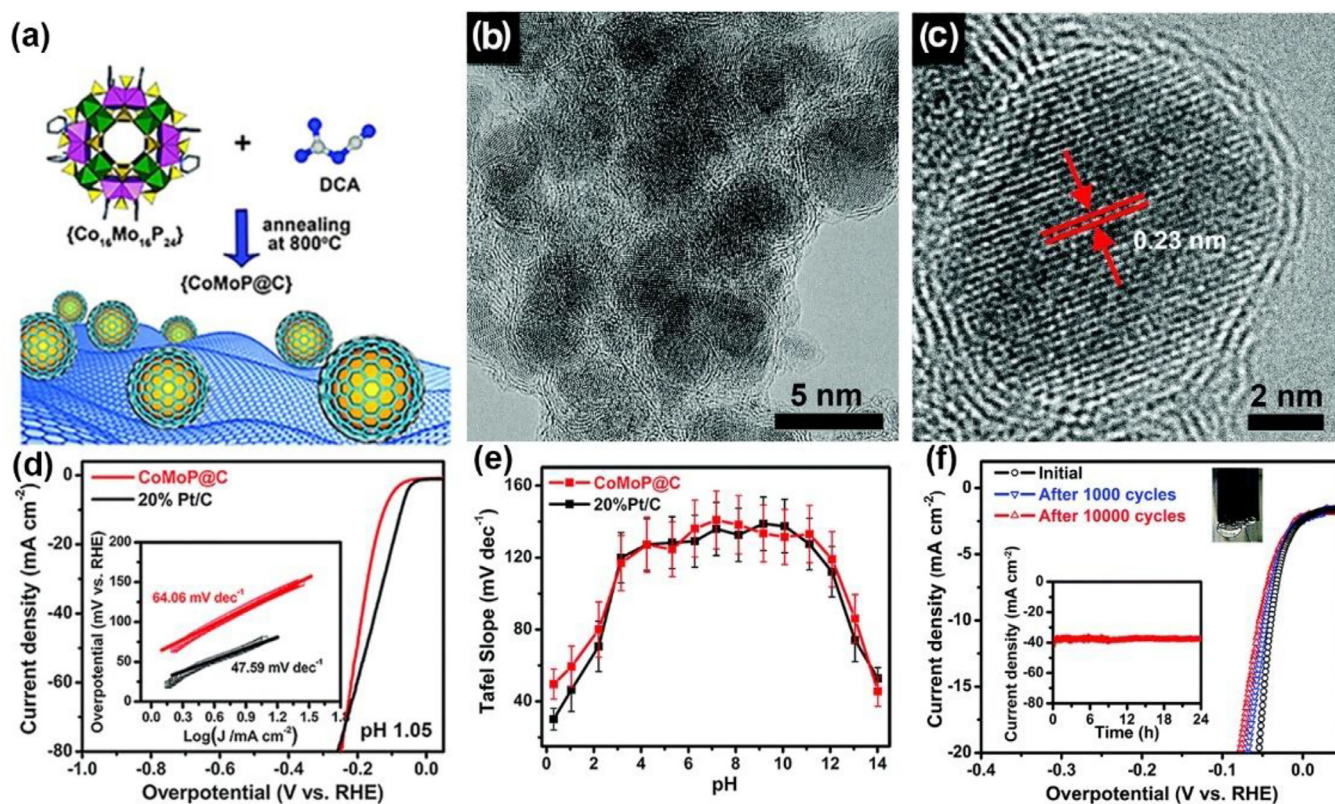


Fig. 7. (a) Illustration of the preparation of the CoMoP@C catalyst. (b) and (c) HRTEM images of CoMoP@C. (d) Polarization curves in pH 1.05 electrolytes at 5 mV s^{-1} . Inset: The corresponding Tafel plots. (e) The variation of Tafel slopes with the pH values (0–14). (f) Polarization curves of CoMoP@C initially and after 1000 and 10,000 cycles in $0.5 \text{ M H}_2\text{SO}_4$. Inset: Time-dependent current density curve of CoMoP@C under a static overpotential of 120 mV for 24 h (down) and the production of H_2 bubbles on the surface of CoMoP@C (up). Reproduced with permission.²³ Copyright 2017, Royal Society of Chemistry.

simple strategy to synthesize an ultrathin MoS_2 /nitrogen-doped reduced graphene oxide (MoS_2 /N-RGO) composite by a one-step hydrothermal method using PMo_{12} and GO as precursors.⁶⁸ By controlling the reaction temperatures, the interlayer spacing of the MoS_2 nanosheets could be enlarged from 6.2 \AA to 9.5 \AA , which prevented the stacking of the MoS_2 nanosheets and enhanced the electrocatalytic activity for HER. The optimal MoS_2 /N-RGO catalyst exhibited excellent catalytic activity with a low onset potential of 5 mV , a small Tafel slope of 41.3 mV dec^{-1} , a high exchange current density of 0.74 mA cm^{-2} and good stability over 5000 cycles under an acidic medium. More recently, Wei and Gu et al. prepared a series of transition-metal-doped MoS_2 by using reliable and tunable Anderson-type POMs $[\text{XH}_6\text{Mo}_6\text{O}_{24}]^{n-}$ ($\text{X}=\text{Fe}^{\text{III}}, \text{Co}^{\text{III}}, n=3; \text{X}=\text{Ni}^{\text{II}}, n=4$) as precursors, which achieved both the formation and the atomically engineering of metallic 1T- MoS_2 .⁶⁹ The unique structure of Anderson-type POM precursors provides fine-tuned chemical environment for 1T- MoS_2 production. Due to the metal doping sites onto the metallic 1T- MoS_2 , the high hydrogen adsorption free energy that is not beneficial for HER is decreased. As shown in Fig. 8, according to the HER catalytic performance, the optimized $\text{NiO}@1\text{T-MoS}_2$ electrocatalyst showed great enhancement in the HER with a positive onset potential of $\sim 0 \text{ V}$ and a low overpotential of 46 mV in an alkaline electrolyte, which was comparable to that of the Pt-based catalyst. The first-principles calculations revealed that the codoping transition metal atoms and oxygen into 1T- MoS_2 promoted the dissociation

of water molecule and therefore assisted hydrogen generation from the intermediate states.

Other examples based on the Mo-containing POM-derived transition metal phosphates and nitrides for posterior application as HER electrocatalysts have also been reported.^{71,72} Fu and Tian et al. developed a *in-situ* catalytic etching strategy to fabricate hololy reduced graphene oxide coupling with a small-sized $\text{Mo}_2\text{N-Mo}_2\text{C}$ heterojunction ($\text{Mo}_2\text{N-Mo}_2\text{C/HGr}$) using PW_{12} ($\text{H}_3\text{PW}_{12}\text{O}_{40}$) as a precursor.⁷² PMo_{12} not only acts as the Mo source but also provides the Mo species that can *in-situ* catalyze the decomposition of adjacent reduced GO to form HGr. The proposed $\text{Mo}_2\text{N-Mo}_2\text{C/HGr}$ showed superior activity towards HER with low onset potentials of 11 mV in $0.5 \text{ M H}_2\text{SO}_4$ and 18 mV in 1 M KOH as well as remarkable stability. The activity in alkaline media was also superior to Pt/C at current density as large as $>88 \text{ mA cm}^{-2}$. Tungsten-containing compounds are promising candidates for HER.^{73,74} In 2015, Tian and Fu et al. reported a phosphorus-modified tungsten nitride/reduced graphene oxide (P-WN/rGO) as HER electrocatalyst by using $\text{H}_3[\text{PO}_4(\text{W}_3\text{O}_9)_4]$ cluster as a W source.⁷⁴ The interaction of the doped P with rGO and WN leads to an obvious increase of work function that is close to Pt metal and favorable to trap electrons. The P-WN/rGO required overpotential of only 85 mV at current density of 10 mA cm^{-2} with Tafel slope of 54 mV dec^{-1} . More recently, Li et al. also reported nickel/tungsten carbide (Ni/WC) hybrid particles anchored on N-doped carbon sheets (Ni/WC@NC) with multi-interfacial as efficient and

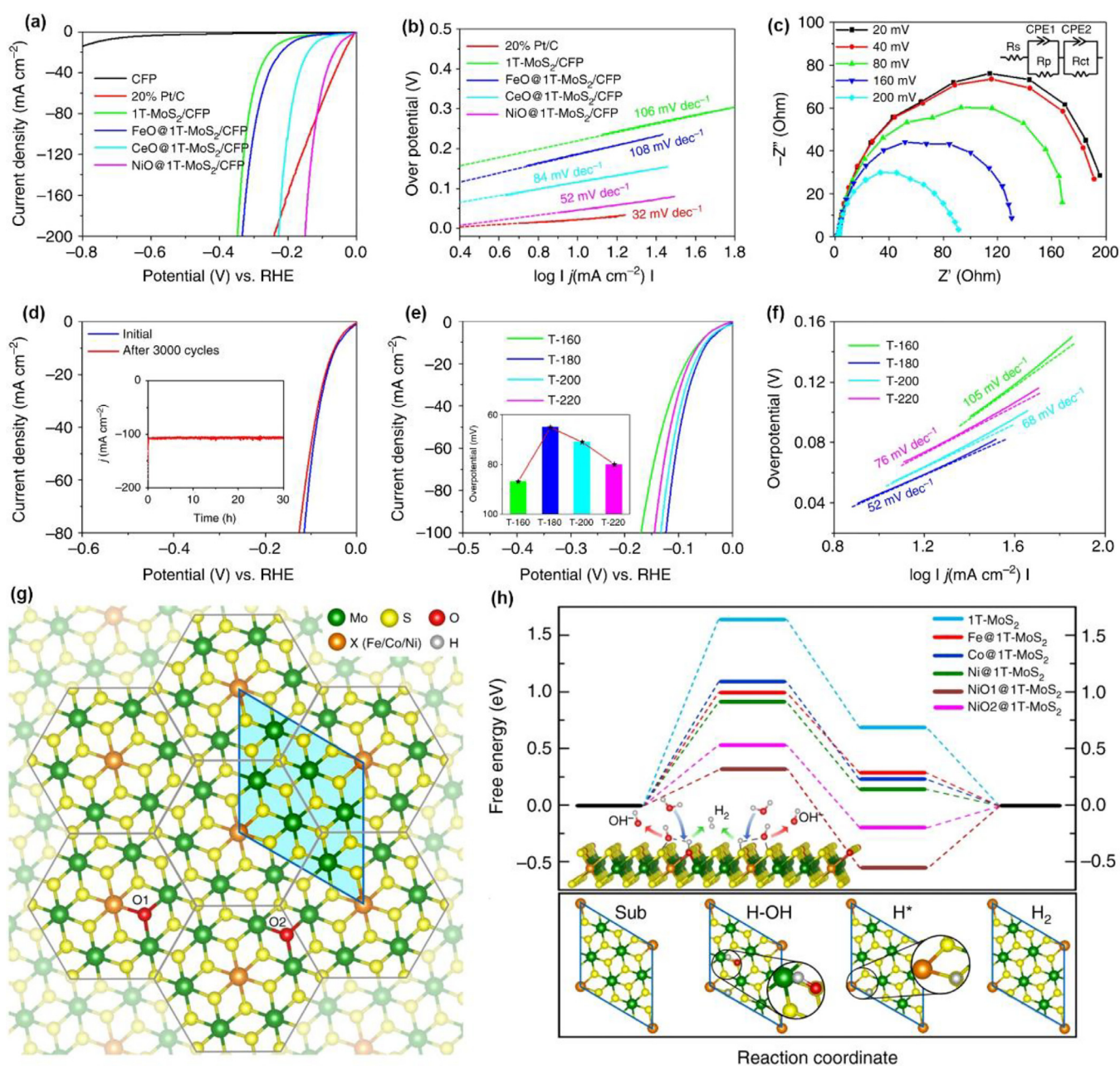


Fig. 8. HER catalytic performances for NiO@1T-MoS₂: (a) polarization curves, (b) Tafel plots, (c) electrochemical impedance spectroscopy (EIS), (d) stability tests (inset: the long-term durability at $\eta=130$ mV), (e) polarization curves (inset: overpotentials to drive 20 mA cm^{-2}), and (f) the corresponding Tafel slopes of NiO@1T-MoS₂ synthesized at various temperatures. First-principles calculations of the doping effect on HER performance: (g) the monolayer structure of XO@1T-MoS₂ formed by the XMo₆ hexagon motifs co-doped by O, (h) free energy diagrams on the surface of different catalysts in alkaline solution, with the smallest repeating unit cell used in calculations indicated in (g), and (i) the structures of predicted intermediates that bind to water and hydrogen. The green, yellow, orange and red spheres represent Mo, S, X (Fe, Co, Ni) and O atoms, respectively. Reproduced with permission.⁶⁹ Copyright 2019, Nature Publishing Group.

stable catalyst for HER over a wide pH range.⁷³ As shown in Fig. 9a, the Ni/WC@NC catalyst was obtained via a two-step pyrolysis method by employing transition-metal-substituted POM cluster of Ni₅₄W₇₂ as preassembly molecular platform. According to the DFT calculation and *in-situ* XAS spectra, the accelerated mass transfer and promoted HER kinetics were achieved by the Ni/WC@NC catalyst attributed to the multi-interfacial structure of Ni/WC hybrid NPs that could induce a synergistic improvement of electric structure via electron transfer and mass transport processes between Ni and WC, which

resulted in the excellent HER activity. The summary of HER performance of POM-derived hybrid materials is presented in Table 1.

POM-based electrocatalysts for water oxidation

As a half-reaction for water splitting, oxygen evolution reaction (OER) has caused much attentions because it encompasses the transfer of four electrons and four protons and often requires high electrochemical overpotentials to drive the reaction at appreciable rates.⁸⁰ Development of active and efficient OER

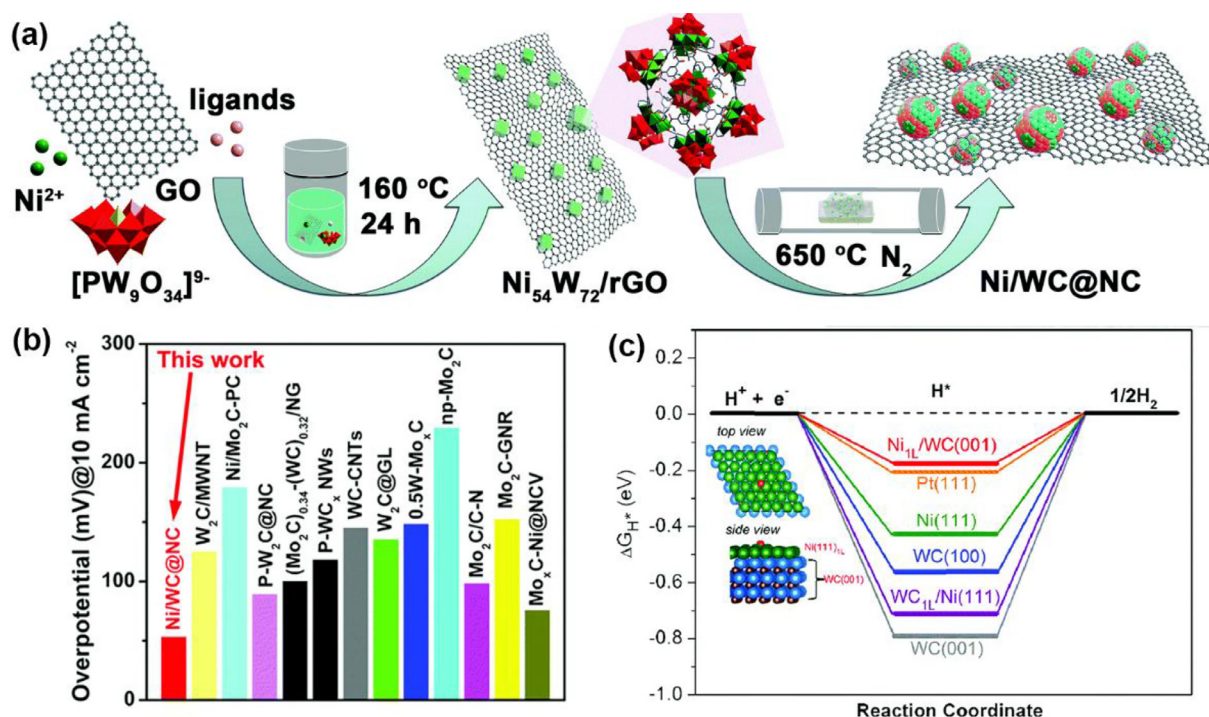


Fig. 9. (a) Illustration of the preparation of Ni/WC@NC catalyst. (b) Comparison of overpotentials of Ni/WC@NC and reported electrocatalysts at 10 mA cm^{-2} for HER. (c) Gibbs free energy diagram of HER on different surfaces. Reproduced with permission.⁷³ Copyright 2018, Royal Society of Chemistry.

electrocatalysts is the main bottleneck for practical utilization of hydrogen production by water splitting due to the sluggish kinetics caused by the complicated reaction processes involving multiple electron transfer.⁸¹ POMs with high redox activity permit the electron transfer to or from a substrate, which is extremely vital for the development of multi-electron transfer OER processes. In addition, as the ligands of POMs are all-inorganic and difficult to be oxidized during water oxidation process, POMs and their derived composites have been widely used as stable water oxidation catalysts.

POMs as molecular water oxidation catalysts

The most promising POMs used as molecular catalysts for electrocatalytic OER are modified with highly-redox active metals, such as ruthenium (Ru) and cobalt (Co). In 2004, Shannon and co-workers firstly reported a POM electrocatalyst based on di-Ru-substituted POM $[\text{Ru}^{\text{III}}_2\text{Zn}_2(\text{H}_2\text{O})_2(\text{ZnW}_9\text{O}_{34})_2]^{14-}$ for catalyzing the electrochemical generation of O_2 on Au electrode using 0.1 M sodium phosphate buffer (pH 8.0) as electrolyte.¹⁷ An approximate $E_{1/2}$ for the electrocatalytic generation of O_2 of 0.75 V vs. SHE and a Tafel slope of 120 mV dec^{-1} were calculated from electrochemical results. In accordance to the previous research, the authors demonstrated that the proximity of the two Ru atoms appeared to be a key factor in the electrocatalytic ability to generate O_2 .^{17,82}

In 2010, Hill and co-workers reported that the cobalt-based POM of $[\text{Co}_4(\text{H}_2\text{O})_2(\text{PW}_9\text{O}_{34})_2]^{10-}$ ($\text{Co}_4\text{-POM}$) showed highly catalytic activity toward water oxidation when the $\text{Ru}(\text{bpy})_3^{3+}$ was introduced as the chemical oxidant.⁸³ Nonetheless, to answered the question of “what is the true catalyst” in the $\text{Co}_4\text{-POM}$ oxygen evolution catalysts, Finke and Stracke deeply investigated the instinct active sites in $\text{Co}_4\text{-POM}$ during water oxidation process.^{19,84} Their experimental results

provided compelling evidence that the *in-situ* electrodeposited heterogeneous CoO_x using $\text{Co}_4\text{-POM}$ as the precatalyst was the dominant water oxidation catalyst on a glassy carbon electrode in 0.1 M sodium phosphate buffer at pH 8.0 in air. The Co-containing POM in solution with a pH value of 8.0 partially decomposed to release Co(II) to form a well-precedented active CoO_x under oxidizing conditions.¹⁹ Furthermore, controlled experiments under conditions (low polyoxometalate concentrations of $2.5\text{ }\mu\text{M}$ and high electrochemical potentials $\geq 1.3\text{ V vs. Ag/AgCl}$, in pH 5.8 and 8.0 sodium phosphate electrolyte at a glass carbon working electrode) specifically chosen that are favor to $[\text{Co}_4(\text{H}_2\text{O})_2(\text{PW}_9\text{O}_{34})_2]^{10-}$ POM catalyzing water oxidation but found that $\text{Co}_4\text{-POM}$ is not stable in a thermodynamic sense to the conditions examined.⁸⁴ Although the accurate distinction of $\text{Co}_4\text{-POM}$ or CoO_x as dominant catalyst was still unattained, their studies have highlighted the challenges of distinguishing homogeneous and heterogeneous water oxidation catalysis. Furthermore, the study reported by Goberna-Ferron et al. suggested that the $[\text{Co}_9(\text{H}_2\text{O})_6(\text{OH})_3(\text{HPO}_4)_2(\text{PW}_9\text{O}_{34})_3]^{16-}$ POM was more stable than $\text{Co}_4\text{-POM}$ in an acidic media. Therefore, POMs could act as the true homogeneous water oxidation electrocatalyst with a chelating ligand to trap Co^{2+} ion.⁸⁵ They proposed an OER catalyst based on an insoluble $\text{Cs}_{15}\text{K}[\text{Co}_9(\text{H}_2\text{O})_6(\text{OH})_3(\text{HPO}_4)_2(\text{PW}_9\text{O}_{34})_3]$ salt into modified amorphous carbon paste electrodes, which exhibited a Tafel slope of 148 mV dec^{-1} and robust catalytic activities over a wide pH range.⁸⁶

POM-based composites and derivative as water oxidation catalysts

In the last years, the nanostructured hybrids composed of POMs and conductive platforms have been presented as promising

Table 1. Summary of HER performance of POM-derived hybrid materials reviewed in this work.

Catalyst	Electrolyte	Overpotential @10 mA cm ⁻² (mV)	Tafel slope (mV dec ⁻¹)	Stability	Ref.
NENU-500	0.5 M H ₂ SO ₄	237	96	2000 CV	20
MoC _x	0.5 M H ₂ SO ₄	142	53	11 h	21
	1 M KOH	151	59	11 h	
Mo ₂ C@NPC/NPRGO	0.5 M H ₂ SO ₄	34	33.6	10 h	22
CoMoP@C	0.5 M H ₂ SO ₄	41	50	24 h	23
	1 M KOH	81	56	24 h	
N@MoPC _x	0.5 M H ₂ SO ₄	108	69.4	1000 CV	24
	1 M KOH	139	86.6	1000 CV	
P ₈ W ₄₈ /rGO	0.5 M H ₂ SO ₄	28	38	1000 CV	47
P ₅ W ₃₀ @rGF _{ox}	0.5 M H ₂ SO ₄	35	37	1000 CV	48
N@Mo ₂ C-3/CFP	0.5 M H ₂ SO ₄	56	51	20 h, 3000 CV	49
	1 M KOH	66	49	20 h, 3000 CV	
Ni-Mo ₂ C@C	0.5 M H ₂ SO ₄	72	65.8	24 h, 2000 CV	59
MoO ₂ @PC-RGO	0.5 M H ₂ SO ₄	64	41	5000 CV	63
Fe ₃ C/Mo ₂ C@NPGC	0.5 M H ₂ SO ₄	98	45.2	10 h	64
MoC _x @C-1	0.5 M H ₂ SO ₄	79	56	48 h	65
MoP/Mo ₂ C@C	0.5 M H ₂ SO ₄	89	45	14 h	66
	1 M KOH	75	58	14 h	
P-Mo ₂ C@NC	0.5 M H ₂ SO ₄	109	76	12 h, 3000 CV	67
	0.1 M PBS, pH = 7.0	159	N/A	12 h	
	1 M KOH	83	N/A	12 h	
MoS ₂ /N-RGO	0.5 M H ₂ SO ₄	56	41.3	5000 CV	68
NiO@1T-MoS ₂	1 M KOH	46	52	30 h, 3000 CV	69
MoS ₂ /C	0.5 M H ₂ SO ₄	207	73	25 h, 1000 CV	70
Cu-Mo-P	0.5 M H ₂ SO ₄	146	54	20 h	71
	0.5 M PBS, pH = 7.0	133	111	20 h	
	1 M KOH	91	77	20h	
Mo ₂ N-Mo ₂ C/HGr	0.5 M H ₂ SO ₄	157	55	50 h, 2000 CV	72
	1 M KOH	154	68	50 h, 2000 CV	
Ni/WC@NC	0.5 M H ₂ SO ₄	53	43.3	24 h, 5000 CV	73
P-WN/rGO	0.5 M H ₂ SO ₄	85	54	20 h, 5000 CV	74
Co-WSe ₂ /rGO	0.5 M H ₂ SO ₄	217	64	3 h	75
Co-Mo-S/CC	1 M KOH	118	84	14 h	76
O-CoMoS	1 M KOH	97	70	10 h	77
P-NiMo ₄ N ₅ @Ni	1 M KOH	118	125	24 h	78
CoP/MoP@NC/CC	1 M KOH	94	40	20 h	79

N/A These values were unavailable.

electrocatalysts for effective OER processes. The introduction of conductive platforms, such as nanocarbons,^{18,87–89} conductive polymers,⁹⁰ and nickel foam,⁹¹ allows the heterogenization of OER catalysts and provides a versatile method for the fabrication of electrocatalytic water splitting cells with increased surface area, controlled material morphologies and the additional pathways for the sequential electron transfer.

Despite the advantages of storing multiple redox equivalent in a single homogeneous catalyst,⁹² Prato and co-workers developed the heterogeneous assembly of an oxygen-evolving POM cluster with multiwalled carbon nanotubes to address the importance of hybrid interfaces and/or contacts to control and promote electron-transfer events at heterogeneous surfaces.¹⁸ Their research indicated that the combination of multi-walled carbon nanotubes and the highly robust tetraruthenate cluster of POM (M₁₀[Ru₄(H₂O)₄(μ-O)₄(μ-OH)₂(γ-SiW₁₀O₃₆)₂] (M=Cs, Li)) resulted in the enhanced oxygen evolving catalytic performance with a remarkably improved efficiency, operative voltage, current density and operational stability. Carbon nanotubes (CNTs) as heterogeneous support could prepare POM/CNT hybrids, which showed controlled material morphology, increased surface area and accelerate electron transfer ability to the electrode, thus favoring the energy dispersion

and relieving the catalytic fatigue. In 2013, Paolucci, Prato, and Bonchio et al. conducted the synthesis of graphene nanoplateform supporting Ru₄POM (Ru₄POM@d-G) (Fig. 10).⁸⁸ The proposed approach was the noninvasive and high-scale surface modification of the graphene nanoplateforms, which enabled the electron transport and accumulation across the extended π-bond network. Serving as an oxygen evolution catalyst, Ru₄POM@d-G performed better than the multiwalled carbon nanotubes supported one reported by Prato et al.^{18,88}

Almost at the same time, Hill et al. studied the electrochemistry of another Ru-containing POM of Rb₈K₂[{Ru₄O₄(OH)₂(H₂O)₄}(γ-SiW₁₀O₃₆)₂]¹⁰⁻ (Rb₈K₂-1) supported by graphene.⁸⁷ In the presence of 1.0 M Ca(NO₃)₂, the activity of the graphene supported Rb₈K₂-1 is comparable to that of IrO₂ with a TOF of 8.01 s⁻¹ at the overpotential of 0.81 V vs. SHE in neutral pH conditions. More recently, Nam and co-workers proposed a research on linker-free spontaneous binding of tetracobalt-based polyoxometalates (Co₄POMs) on nitrogen-doped carbon nanotubes (NCNTs) via electrostatic hybridization.⁸⁹ Protonated nitrogen-dopant sites at NCNTs enabled linker-free immobilization of Co₄POMs and fluent electron transfer in the resultant hybrid structure. The Co₄POM/NCNT hybrid yielded excellent electrocatalytic

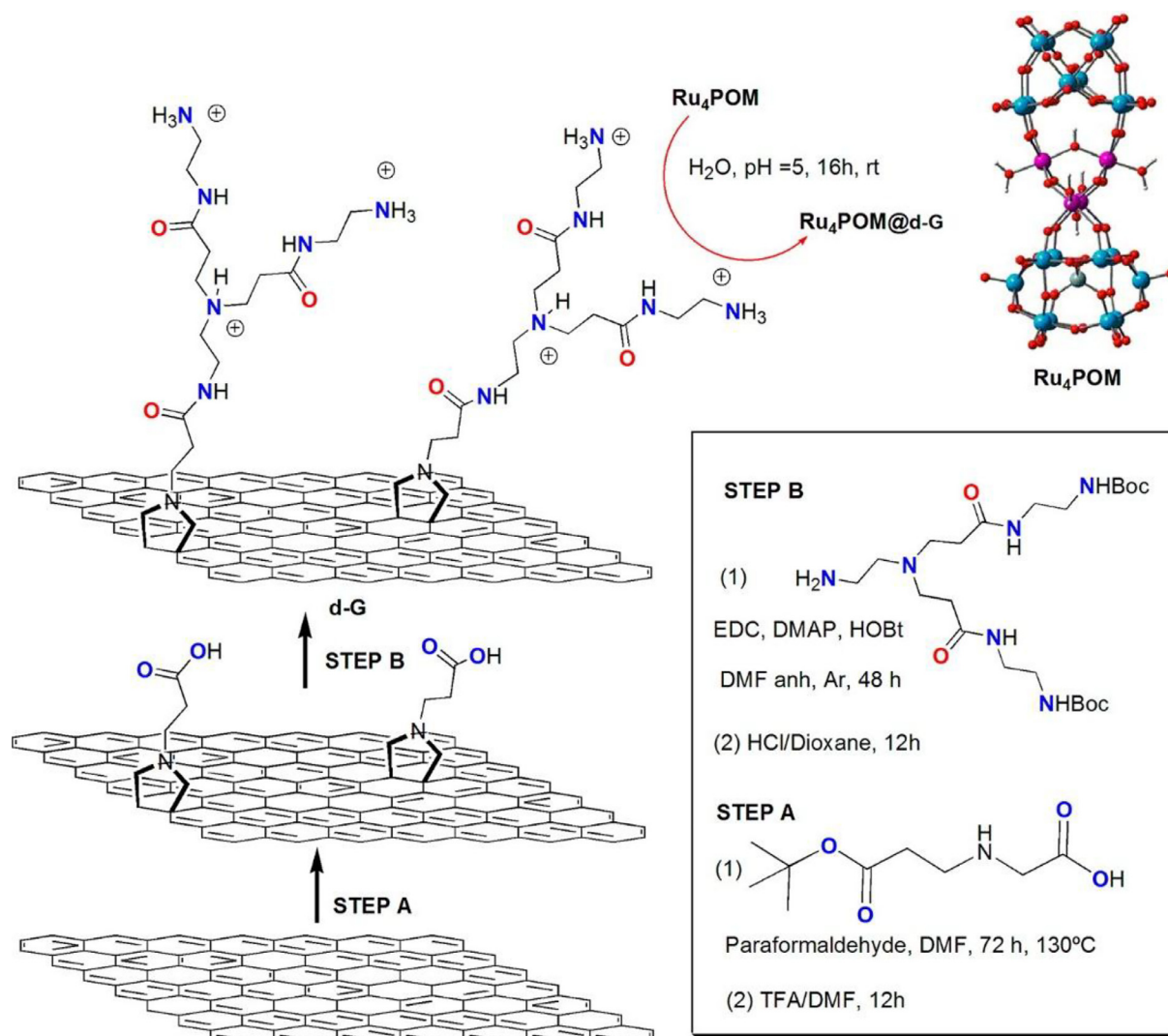


Fig. 10. Synthesis of graphene nano-platform supporting Ru₄POM. Reproduced with permission.⁸⁸ Copyright 2013, American Chemical Society.

activities for water oxidation under neutral conditions, delivering a low overpotential of 370 mV at 10 mA cm⁻², a Tafel slope of 203 mV dec⁻¹ and a high TOF of 0.211 s⁻¹.

More recently, Blasco-Ahicart et al. reported an OER electrocatalyst based on polypyrrole with embedded cobalt-based POM {Co₉(H₂O)₆(OH)₃(HPO₄)₂·(PW₉O₃₄)₃}¹⁶⁻ (Co₉).⁹⁰ Compared to reported pure Co₉ catalyst, less than 6% POM content in a polypyrrole film multiplied the OER current by one order of magnitude, reducing the required overpotentials by approximately 200 mV.^{86,90} In 2017, Song and co-workers proposed a facile one-step hydrothermal route to deposit microcrystals of a robust Dexter-Silverton POM, [Co_{6.8}Ni_{1.2}W₁₂O₄₂(OH)₄(H₂O)₈], on a commercial nickel foam electrode, as shown in Fig. 11a.⁹¹ The as-fabricated NiCo-POM/Ni electrode showed efficient and sustained electrochemical oxygen evolution at a low overpotential of 360 mV at 10 mA cm⁻², a Tafel slope 126 mV dec⁻¹ and a faradaic efficiency of ~96% in an alkaline aqueous solution (pH = 13). It was worth mentioning that the NiCo-POM/Ni composite also exhibited remarkable long-term durability during the continuous oxygen evolution electrolysis process. Such a high OER performance was in accordance with the post-catalytic characterization results that the morphology and crystal structure

of the catalyst were maintained, highlighting the stability of the composite under basic and oxidizing conditions (Fig. 11c–e).

In 2018, Galan-Mascaros and co-workers reported a water oxidation catalyst on insoluble salts of cobalt-based POMs with cesium or barium counter-cations that performed well and could compete with noble metals in strongly acidic conditions.²⁵ Particularly, the barium salt of a cobalt-phosphotungstate polyanion (Ba[Co-POM]) showed an overpotential of 189 mV vs. RHE at 1 mA cm⁻², outperformed the IrO₂ catalyst even in an acidic electrolyte (pH < 1). The significant influence of barium dications in the activity of the [Co-POM] indicates that by changing the coordinated cations the catalytic performance of POMs can be tuned. The POMs offered an intrinsic advantage in this regard, because their polyanionic nature made them easy to selectively incorporate the desired ancillary counter-cations close to their active sites, without structurally or chemically affecting their appropriate environment. In addition, it was demonstrated that the carbon-paste conducting support with a hydrocarbon binder could improve the stability of metal-oxide catalysts in acidic media by providing a hydrophobic environment (Fig. 12).

By using Co-based POM as precursors, Co-containing OER catalysts can be fabricated.^{95,96} In 2016, Lan's group synthesized a metal/metal carbide-based composite (Co-Mo-C/NRGO-1)

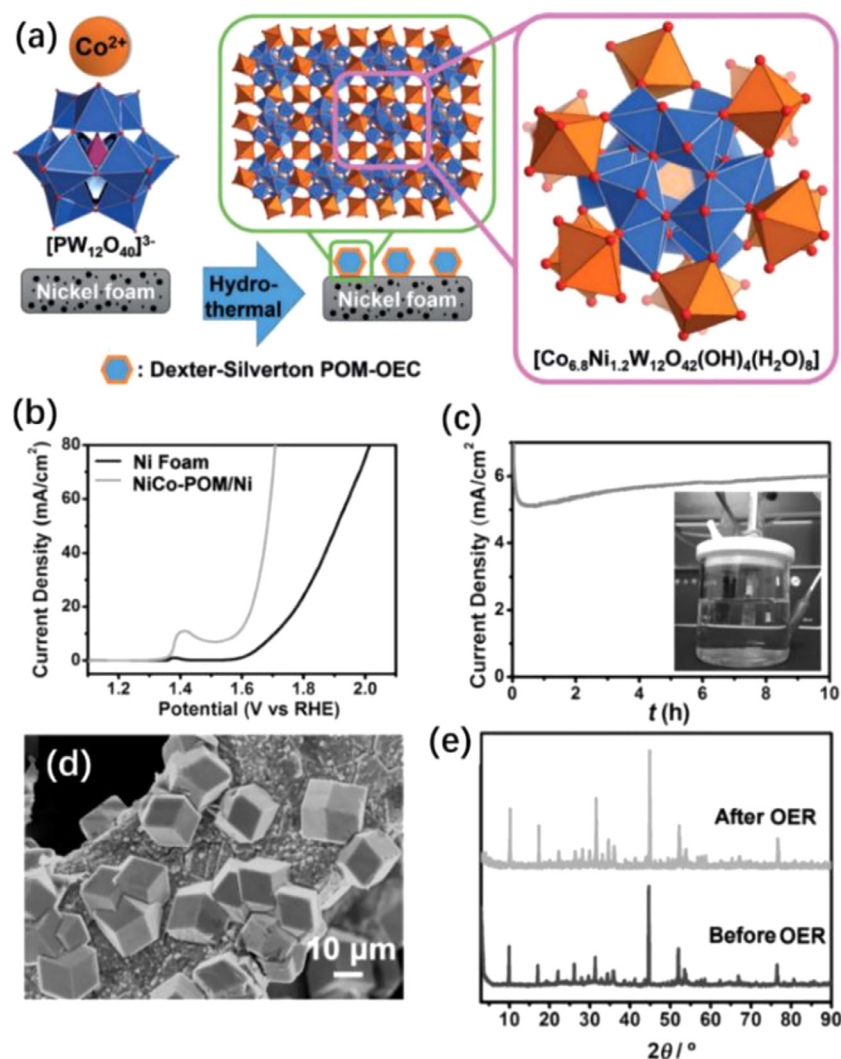


Fig. 11. (a) Deposition of Dexter-Silverton polyoxometalate microcrystals on nickel foam electrodes. (b) IR-corrected polarization curves in 0.1 M KOH at 5 mV s^{-1} . (c) Change of current density during the OER electrocatalysis at $E = 1.67 \text{ V vs. RHE}$; inset: photograph of the electrochemical setup. (d) SEM image of NiCo-POM/Ni electrode after OER stability test over 10 h; (e) PXRD spectra of NiCo-POM/Ni before and after OER stability test over 10 h. Reproduced with permission.⁹¹ Copyright 2017, Wiley-VCH.

by directly carbonizing the Co-doped PMo_{12} POM/conductive polymer/graphene precursor (Co-PCG). The obtained Co-Mo-C/NRGO-1 composite showed superior electrocatalytic activity for OER with a low Tafel slope of 42 mV dec^{-1} , a small overpotential of 330 mV at 10 mA cm^{-2} as well as the long-term stability in alkaline medium.⁹⁵ Additionally, Lan's group developed a novel bimetallic oxide composite consisting of CoV_2O_6 and V_2O_5 anchoring on nitrogen-doped reduced graphene oxide ($\text{CoV}_2\text{O}_6\text{-V}_2\text{O}_5/\text{NRGO-1}$) based on the carbonization of CoV-POM, ethylenediamine, and graphene oxide precursors (Fig. 13a).⁹⁶ Acting as a promising OER electrocatalyst, $\text{CoV}_2\text{O}_6\text{-V}_2\text{O}_5/\text{NRGO-1}$ exhibited an ultralow overpotential of 239 mV vs. RHE at the current density of 10 mA cm^{-2} and excellent stability in 1 M KOH as shown in Fig. 13. Notably, it possessed high intrinsic activity with a TOF of 1.80 s^{-1} at the overpotential of 300 mV . DFT calculations revealed the instinct reason accounting for the excellent OER performance that the hydrogen bond between V_2O_5 and intermediate HOO^* of OER decreased its adsorption energy, which was coupled with the activation of CoV_2O_6 and thus greatly reduced the overpotential. Additionally,

this research work has firstly proved that the hydrogen bond plays a key role in the water oxidation.

POM-based materials for overall water splitting

The overall water splitting by electrocatalysis with POM-based catalysts is of great practical significance to obtain hydrogen energy. The POM-based derivatives obtained by annealing the POMs under inert atmosphere can achieve high performance water splitting electrocatalysis with both excellent HER and OER catalytic activity. More recently, Anderson-type POMs derived transition metal sulfides heterojunctions have been reported as effective electrocatalysts for overall water splitting. A one-pot hydrothermal synthesis method was proposed to prepare a series of bimetallic sulfides on carbon cloth (M-Mo-S/CC , $\text{M} = \text{Co}$, Ni , Fe) by Lan and co-workers. The related growth process of M-Mo-S was studied through the nucleation-doping competition mechanism.⁷⁶ The Anderson-type POMs, represented by the formula of $[\text{XM}_6\text{O}_{24}\text{H}_x]^{n-}$ ($\text{X} = \text{Zn}$, Cu , Co , Ni , Fe , etc., $\text{M} = \text{Mo}$), not only possess precise structure, nanoscale size ($< 1 \text{ nm}$) and good water solubility but can also provide fixed proportions of

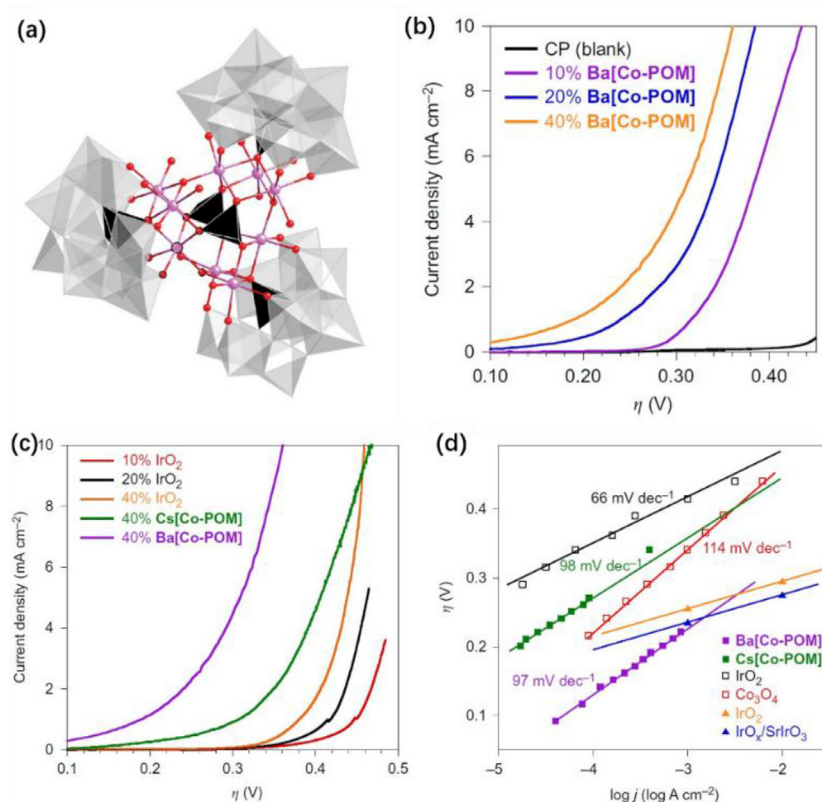


Fig. 12. (a) Molecular structure of the $[\text{Co}_9(\text{H}_2\text{O})_6(\text{OH})_3(\text{HPO}_4)_2(\text{PW}_9\text{O}_{34})_3]^{16-}$ cluster. Co, pink; O, red; WO_6 , grey octahedra; PO_4 , black tetrahedra. (b) Polarization curves measured in 1 M H_2SO_4 solution with a $\text{Ba}[\text{Co-POM}]/\text{CP}$ blend electrode. (c) Polarization curves measured in 1 M H_2SO_4 solution with an IrO_2/CP blend working electrode for different catalyst content, compared with $\text{Cs}[\text{Co-POM}]/\text{CP}$ and $\text{Ba}[\text{Co-POM}]/\text{CP}$ electrodes. (d) Tafel plots. Orange and blue triangles are taken from the literature, and represent the state of the art for IrO_2 and $\text{IrO}_x/\text{SrIrO}_3$, respectively.^{93,94} Reproduced with permission.²⁵ Copyright 2018, Nature Publishing Group. (For interpretation of the references to color in this figure legend, the reader is referred to the web version of this article.)

bimetallic sources for the controlled synthesis of M-Mo-S/CC with specific morphology and structure. The as-prepared Co-Mo-S/CC with stable heterostructure formed by the hybridization of CoS_2 and MoS_2 ensures improved activity and stability during water splitting process. Soon after, Hou et al. also reported oxygenated- CoS_2 - MoS_2 (O-CoMoS) heteronanosheets by using a Anderson-type $(\text{NH}_4)_4[\text{Co}^{\text{II}}\text{Mo}_6\text{O}_{24}\text{H}_6] \cdot 6\text{H}_2\text{O}$ as the bimetal precursor for efficient HER and OER processes in a basic electrolyte.⁷⁷ Assembled as an electrolyzer for overall water splitting, the O-CoMoS heteronanosheets as both the anode and the cathode delivered a current density of 10 mA cm^{-2} at a quite low cell voltage of 1.6 V. The disordered structure and S-vacancies confined in two-dimensional oxygenated bimetal sulfide nanosheet heterojunctions could provide large electrochemical active surface area, great number of active sites, exposed active heterointerfaces and enhanced conductivity, thus resulting in the excellent electrocatalytic performance.

Other POM-derived transition metal composites have been reported for overall water splitting as well.^{78,79,97,98} In early 2019, Lan's group reported the fabrication of P doped crystalline bimetallic nitride arrays supported on Ni foam ($\text{P-NiMo}_4\text{N}_5@\text{Ni}$) with controlled morphologies through adopting a Keggin-type POM ($\text{H}_3\text{PMo}_{12}\text{O}_{40}$, PMo_{12}) and nickel nitrate as metal sources.⁷⁸ By introducing POM with the capability of controlling the nucleation and crystal growth, the hierarchical $\text{P-NiMo}_4\text{N}_5@\text{Ni}$ catalyst with high surface-to-volume ratio of energetic actives was obtained and exhibited unprecedented

activity as a bifunctional electrocatalyst for overall water splitting approaching 50 and 100 mA cm^{-2} at low cell voltages of 1.59 and 1.66 V, respectively. Song and Streb et al. reported a scalable route via a $[\text{SiW}_{11}\text{O}_{39}]^{8-}$ POM-template for simultaneous deposition of several nanostructured mixed metal oxides on metal foam electrodes.⁹⁷ The synergy of mixed metal oxides containing cobalt oxides, copper oxides, and tungsten oxides endowed the fabricated electrode with enhanced electron transport ability, structural and chemical stability, as well as high water electrolysis activity with a low overpotential of 0.57 V at 10 mA cm^{-2} . Fu and Tian et al. prepared a bimetallic carbide of $\text{Mo}_x\text{Co}_x\text{C}$ by using $[\text{PMo}_{12}\text{O}_{40}]^{3-}$ (PMo_{12}) clusters trapped into ZIF-67 ($\text{PMo}/\text{ZIF-67}$) composite as precursor.⁹⁸ The obtained $\text{Mo}_x\text{Co}_x\text{C}$ with small particle sizes below 20 nm was confined in uniform carbon polyhedron ($\text{Mo}_x\text{Co}_x\text{C}@\text{C}$). The proper size matching of PMo_{12} (1 nm) and ZIF-67 cages (1.16 nm) ensures the contact of the Co and Mo sources during calcination, resulting in small-sized $\text{Mo}_x\text{Co}_x\text{C}$ coated by carbon layer. The optimized $\text{Mo}_x\text{Co}_x\text{C}@\text{C}$ catalyst exhibited excellent performance for overall water splitting with a low overpotential of 83 mV for hydrogen evolution and 295 mV for oxygen evolution, respectively.

POM-based electrocatalysts for CO_2 reduction

Carbon dioxide (CO_2) is one of the main combustion products of fossil fuels and its emission into the atmosphere triggers serious environmental and climate problems. According to recent reports, global CO_2 emission currently is *ca.* 37 Gt with 30.4 Gt

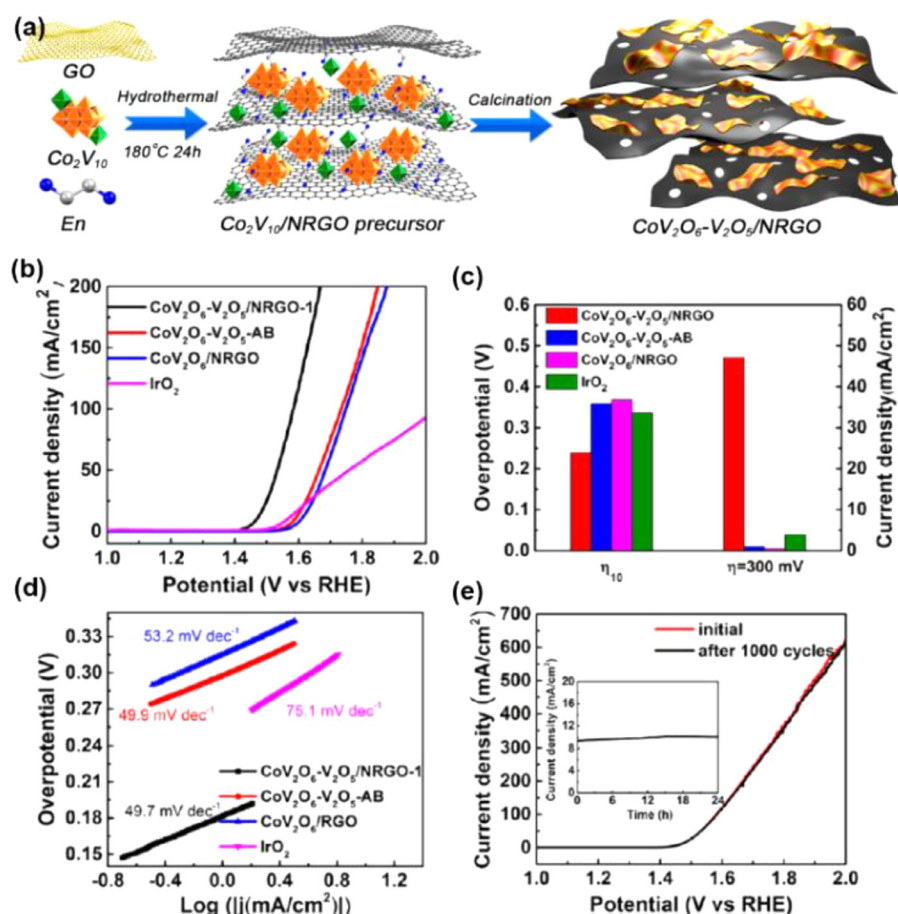


Fig. 13. (a) Synthetic process of $\text{CoV}_2\text{O}_6\text{-V}_2\text{O}_5/\text{NRGO}$ -1 composite. (b-e) OER performances: (b) polarization curves, (c) comparison of overpotentials at the current density of 10 mA cm^{-2} (η_{10}) and current densities at the overpotential of 300 mV, (d) Tafel plots, and (e) initial polarization curves and after 1000 CV cycles. Inset: time-dependent current density curve under the potential of 239 mV for 24 h. Reproduced with permission.⁹⁶ Copyright 2017, American Chemical Society.

related to the utilization of fossil fuels and predicted to increase up to 36 ~ 43 Gt by 2035.⁹⁹ The atmospheric level of CO_2 rose from 270 ppm in the preindustrial era to nearly 395 ppm in 2012, which far exceeds its natural fluctuation ($d = 180 \sim 300 \text{ ppm}$) over the past millions of years.¹⁰⁰ Consequently, the valid conversion and reasonable utilization of CO_2 is of great significance to relieve the greenhouse effect of CO_2 caused serious climate and environmental problems. Tremendous strive has been made to achieve efficient CO_2 reduction processes.^{101,102} Among them, the most representative strategy for implementing this conversion process is electrocatalytic CO_2 reduction reaction ($\text{CO}_2 \text{ RR}$), due to its characteristic advantages of easy processing, simple devices, and low energy consumption.^{103,104} Meanwhile, due to their proton- and electron-storage properties, POMs are attractive candidates to promote the multi-proton/multielectron reduction of CO_2 to useful chemicals.

In 1998, Kozik and co-workers studied the interaction of CO_2 with transition-metal-substituted heteropolyanions in nonpolar solvents.¹⁶ It was found that the α -Keggin structure could reversibly form complexes with CO_2 when substituted with Co(II) , Ni(II) , and Mn(II) . And traces of water are necessary for the reactions to take place. On basis of these previous fragmented research works, in 2015, Proust et al. proposed the first systematical investigation about electrocatalytic the four-electron reduction of CO_2 by a $(\text{TOA})_6[\alpha\text{-SiW}_{11}\text{O}_{39}\text{Co}(_)]$

(TOA = tetraoctyl ammonium) POM homogeneous catalyst.¹⁰⁵

It was demonstrated that the electrolysis of a CO_2 -saturated dichloromethane solution with the presence of the $(\text{TOA})_6[\alpha\text{-SiW}_{11}\text{O}_{39}\text{Co}(_)]$ could lead to the formation of CO. By adding acid and water into POM solution for electrolysis under CO_2 , CO was produced continuously to reach $37 \mu\text{mol}$ after 66 h of electrolysis. In addition, formaldehyde could be detected without H_2 or other CO_2 reduction products. Although, the proposed POM catalyst showed low faradic yield, this research suggested that $(\text{TOA})_6[\alpha\text{-SiW}_{11}\text{O}_{39}\text{Co}(_)]$ was capable to selectively promote the electrocatalytic reduction of CO_2 to CO or even the four-electron/four-proton reduction product of formaldehyde.

According to the reported studies on the molecular catalysts for $\text{CO}_2 \text{ RR}$, the presence of proton sources can activate the reaction.^{106–108} and the efficiency of the proton-coupled electron transfer occurs when the proton source is close to the catalytic center.^{109,110} Zhang et al. synthesized silver nanoclusters capped with bovine serum albumin (AgNC@BSA) catalysts applied for the electrocatalytic reduction of CO_2 by using an $[\alpha\text{-SiW}_{12}\text{O}_{40}]^{4-}$ anion as electron transfer mediator to facilitate the electrical communication between the electrode and the strongly protected catalyst.¹¹¹ The synergistic effect of AgNC@BSA and $[\alpha\text{-SiW}_{12}\text{O}_{40}]^{4-}$ led to the high electrocatalytic activity for CO_2 reduction in dimethylformamide containing 1% (v/v) water. As demonstrated, CO was the major product with excellent

faradaic efficiency (>75%) and the onset potential for the proposed catalytic CO₂ reduction process was about 400 mV. Then, in 2018, they proposed the research on nanostructured Ag by electrodeposition of Ag in the presence a Keggin type polyoxometalate, [PMo₁₂O₄₀]³⁻ (PMo).¹¹² The obtained Ag-PMo nanocomposite could catalyze the reduction of CO₂ to CO in DMF (0.1 M [*n*-Bu₄N]PF₆ and 0.5% (v/v) H₂O) with an onset potential of -1.70 V *vs.* Fc^{0/+} and high faradaic efficiencies of about 90% obtained over a wide range of applied potentials. The kinetics studies reveal that the enhanced catalytic activity associated with Ag-PMo was attributed to the strong interaction between the reduced PMo and CO₂, which lowered the activation energy for *CO₂. In 2019, Proust and Blanchard et al. synthesized a new organometallic derivative of POMs, (TBA)₃[α-H₂PW₁₁O₃₉-{Rh^{III}Cp*(OH₂)}], presenting an accessible coordination site on the Rh^{III} center, for electrocatalytic reduction reaction.¹¹³ The electro-assisted reduction of CO₂ in the presence of water as a proton source mainly led to the catalytic formation of hydrogen, with formic acid being a minor product.

POM ions, which represent a well-defined library of inorganic building blocks of nanoscopic scale with oxygen-rich surfaces, are ideal candidates for the design and construction of tailored framework materials.^{114–116} In 2018, Lan and co-workers developed a series of precisely designed polyoxometalate-metalloporphyrin organic frameworks for electrocatalytic CO₂ reduction.²⁶ The special structural design of involving the integration of {ε-PMo₈^VMo₄^{VI}O₄₀Zn₄} cluster and metalloporphyrin endowed the proposed M-PMOFs (M = Co, Fe, Ni, Zn) greatly advantages in terms of electron collecting and donating, which is vital to the electron migration in the multiple-electron CO₂ reduction process. As shown in Fig. 14a and b, the obtained Co-PMOF catalyst exhibited remarkable faradaic efficiency of 94% over a wide potential range from -0.8 to -1.0 V and the best faradaic efficiency could reach up to 99%, the highest in reported metal-organic frameworks to date. Particularly, Co-PMOF also showed a high TOF of 1656 h⁻¹ and excellent catalysis stability up to 36 h for continuously testing. The DFT calculations were performed to understand the highly active as well as selective reaction mechanism of Co-PMOF. The assembly of Zn-ε-Keggin POM and Co-TCP leads to the decreased ΔG of the rate-determining steps with the formation of adsorbed intermediates *COOH and *CO during CO₂ reduction. The calculation results also prove it theoretically that the favorable active site is the Co in Co-TCP rather than POM, together with the efficiently synergistic electron modulation of POM and the porphyrin metal center.

Conclusions

The energy-related electrocatalysis processes, such as HER, OER and especially CO₂RR, are still challenging due to the sluggish kinetics during multiple-electron transfer reaction routes as well as the currently used high-cost noble-metal based catalysts. POM-based materials are ideal candidates used as promising effective noble-metal-free electrocatalysts for the associated electrocatalysis owing to their compositional diversity, structural variety and well-defined redox properties. In the early researches on POMs for electrocatalytic reactions, the homogeneous POMs have been proved to be active for these energy-related electrocatalysis reactions. However, the catalytic activity and stability are far from enough as a result of the disintegrated active sites of the homogeneous POM catalysts. Therefore, heterogenizing homo-catalysts is the main strategy to improve POM-based electrocatalysts, such as anchoring POMs on to conductive matrix and incorporating POMs into MOFs. Specifically, Mo and W-based POMs, and

the related derivative are used as platform for constructing POM hybrids for efficient electrocatalytic HER processes or acting as precursors to synthesize HER catalyst by carbonization. Ru and Co-based POMs and hybrids are widely introduced as catalyst or components for the OER. Although great progress has been achieved in these fields, effort is still needed to address the challenges, such as (i) the dominant active sites of heterogeneous HER catalysts, especially the ones obtained from precursors pyrolysis, are usually unclear and rarely discussed; (ii) both the structural stability and catalytic durability of the POM-based water oxidation catalysts during reaction under high potentials need more study; (iii) in addition, the POM-based catalysts with both HER and OER electrocatalytic activity for overall water splitting are still less reported and need more attention to develop; and (iv) in terms of CO₂RR, the POMs-based materials are promising but still far from investigation to uncover the real active sites for CO₂ activation and the key factors to product selectivity.

POM-BASED PHOTOCATALYSTS

As a large family of nano-sized inorganic clusters with oxygen-rich surfaces, POMs can readily undergo multi-electron reduction and oxidation processes due to their fast, reversible and stepwise electron transfer reactions without structural alterations,¹¹⁷ thus representing excellent candidates as water reduction and water oxidation photocatalysts. Herein, researches on POM-based materials presented as promising photocatalysts for sustainable and clean energy conversion processes, such as hydrogen production, water oxidation, and CO₂ conversions have been summarized and reviewed for the further study on these fields.

POM-based photocatalysts for hydrogen production

Hydrogen evolution based on artificial photosynthesis is a major approach toward solar energy conversion and storage.^{118,119} Photocatalytic HER is an essential half reaction of water splitting, in which effective generation of charge-separated excited states (electron-hole pairs) is followed by facile transfer of the electrons to HER centers to reduce proton to hydrogen.^{120–122} Since the discovery of the photocatalytic splitting of water on TiO₂ electrodes by Fujishima and Honda in 1972,¹²³ significant progress has been made in the discovery of metal oxide semiconductor (MOS)-based photocatalysts for H₂ evolution.^{124,125} Polyoxometalates (POMs) are a large class of photocatalysts,¹²⁶ that exhibit semiconductor-like photochemical characteristics due to their similar electronic characteristics (band gap transition for MOSs and HOMO-LUMO transition for POMs) to metal oxides semiconductor.^{127,128}

POMs as photocatalysts for hydrogen production

The early studies towards photochemistry of POMs including the photo- and electrochromism of POM, their photodynamic and catalytic properties, *etc.* have been investigated by Hill et al. and Yamase.^{129,130} Then, various kinds of POMs, especially the Keggin-type heteropolytungstates, such as PW₁₂O₄₀³⁻, SiW₁₂O₄₀⁴⁻, BW₁₂O₄₀⁵⁻, FeW₁₂O₄₀⁵⁻ and H₂W₁₂O₄₀⁶⁻, have been found and known for the past several decades to be homogeneous photocatalysts for evolution of H₂ in acidic aqueous solutions under UV-light irradiation.^{27,131} Compared to the single Keggin-type polyanion unit with only one-electron-reduced species that could be formed under UV-light irradiation, the high nuclearity POM nanoclusters that formed by the combination of several polyanion units have been found undergoing

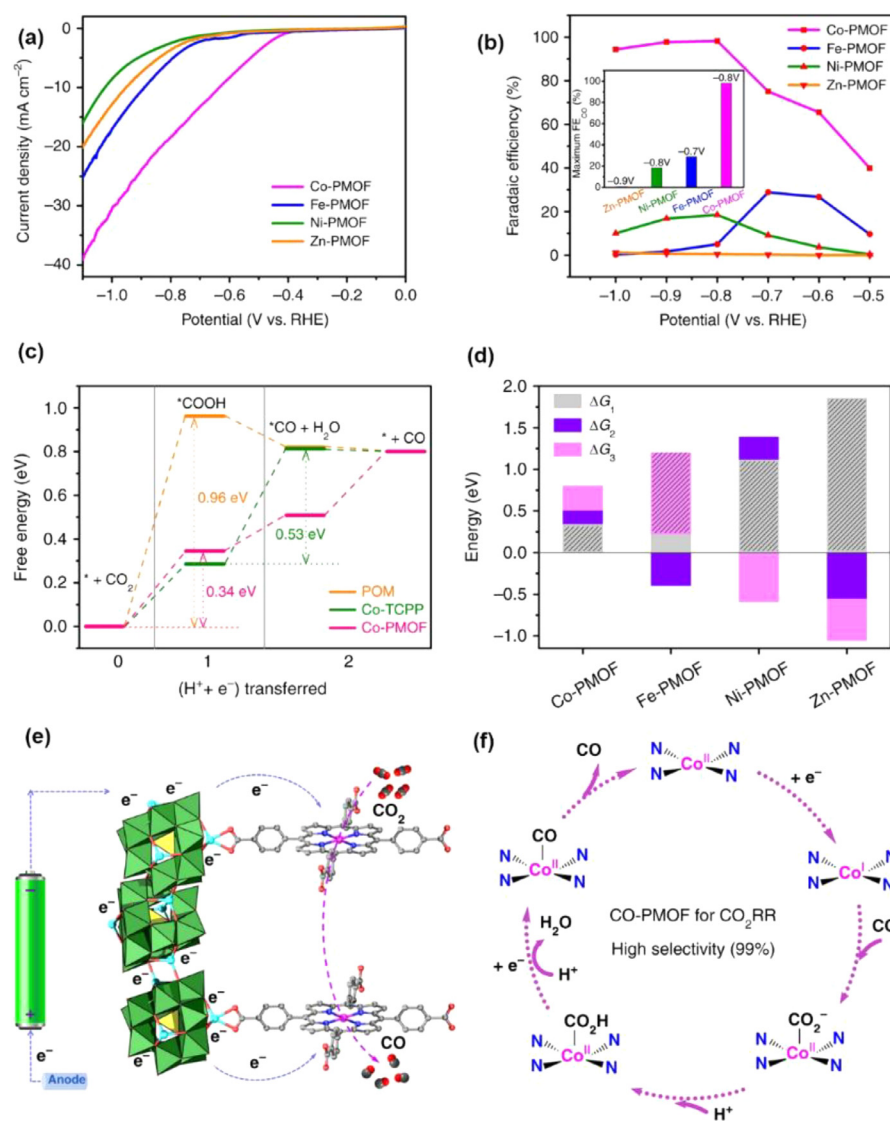


Fig. 14. (a) Polarization curves. (b) Faradaic efficiencies for CO. (c) The free energy diagrams of CO₂ reduction to CO by DFT calculation. (d) Comparison of the free energy of each elementary reaction (ΔG_1 , ΔG_2 , and ΔG_3 represent the free energy of *COOH formation, *CO formation, and CO desorption process, respectively) in CO₂ RR. (e, f) Mechanistic scheme for the CO₂ RR on Co-PMOF. Reproduced with permission.²⁶ Copyright 2018, Nature Publishing Group.

fast reversible multi-electronic processes, which can facilitate the reduction of H⁺ in water to generate H₂ with much higher efficiency.

Zhang et al. prepared a high nuclearity Co substituted POM cluster, K₁₀Na₁₂[{Co₃(B-β-SiW₉O₃₃(OH))(B-β-SiW₈O₂₉OH)₂}]₂·49H₂O (CoPOM), as photocatalyst for hydrogen evolution reaction.¹³² The CoPOM showed photocatalysis activity under UV-light irradiation in both homogenous (molecule scale) and heterogeneous (TiO₂/CoPOM composites) systems. Hill et al. reported an efficient, robust, and noble-metal-free molecular POM-based water reduction catalyst, a tetra-nickel-substituted POM, [Ni₄(H₂O)₂(PW₉O₃₄)₂]¹⁰⁻ (Na₆K₄-Ni₄P₂).¹³³ The proposed Ni₄P₂ could catalyze H₂ production over 1 week and achieved a turnover number (TON) of as high as 6500 with almost no loss in activity with (4,4'-di-tert-butyl-2,2'-dipyridyl)-bis(2-phenylpyridine(1H))-iridium(III) hexafluoro-phosphate

[Ir(ppy)₂(dtbbpy)][PF₆] as photosensitizer and triethanolamine (TEOA) as sacrificial electron donor.

Ding et al. proposed a Co-based Keggin POM K₇[Co^{III}Co^{II}(H₂O)W₁₁O₃₉] homogeneous catalyst with high efficiency for visible-light driven hydrogen evolution.¹³⁴ By using Pt acting as cocatalyst, Eosin-Y as photosensitizer, and triethanolamine sacrificial electron donor, the H₂ evolution average rate of the Co-POM reached 13,395 μmol h⁻¹ g⁻¹. Then, as displayed in Fig. 15, Ding et al. reported another eleven-Fe^{III} substituted antimoniotungstate molecular semi-conductor Na₂₇[Fe₁₁(H₂O)₁₄(OH)₂(W₃O₁₀)₂(α-SbW₉O₃₃)₆] that could exhibit outstanding photocatalytic HER catalytic property without introducing any co-catalysts at neutral conditions.³³ The proposed {Fe₁₁} nanoclusters with both five-coordinate and six-coordinate iron ions showed a hydrogen evolution rate of 820 μmol h⁻¹ g⁻¹ without adding any photosensitizers under the optimized conditions.

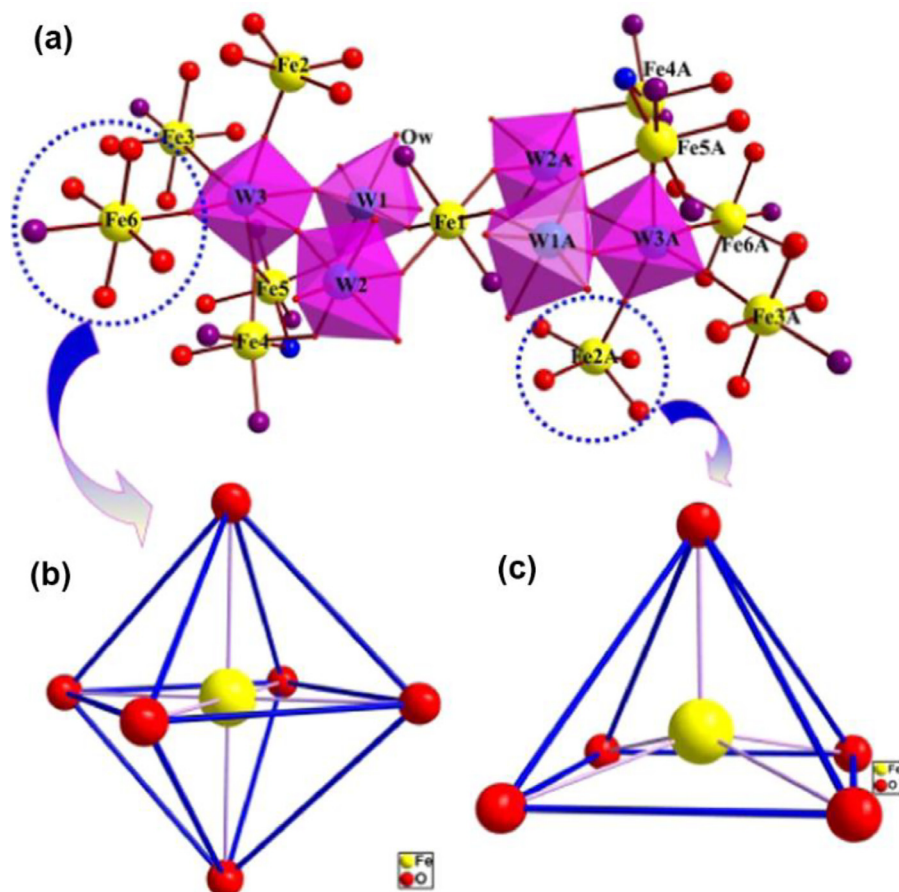


Fig. 15. (a) polyhedral/ball-and-stick model of the $[\text{Fe}_{11}(\text{H}_2\text{O})_{14}(\text{OH})_2(\text{W}_3\text{O}_{10})_2]^{27+}$ cluster, (b) the octahedral structure of the six-coordinate Fe^{3+} cations, and (c) the square pyramidal geometry of the penta-coordinate Fe^{3+} cation. Color scheme: Fe (yellow), O (red), H_2O (violet), OH (blue). Reproduced with permission.³³ Copyright 2015, Elsevier. (For interpretation of the references to color in this figure legend, the reader is referred to the web version of this article.)

Hill and co-workers prepared a new structurally unprecedented POM family, the multi-nickel carbon-free complex of $[\{\text{Ni}_4(\text{OH})_3\text{AsO}_4\}_4(\text{B}-\alpha\text{-PW}_9\text{O}_{34})_4]^{28-}$ ($\text{Ni}_{16}\text{As}_4\text{P}_4$) by one-pot synthesis.¹³⁵ The synthesized high-nuclearity Ni-POM is an efficient, water-compatible, noble-metal-free catalyst for H_2 production upon visible-light irradiation via utilizing $[\text{Ir}(\text{ppy})_2(\text{dtbbpy})][\text{PF}_6]$ as photosensitizer and triethylamine as sacrificial electron donor. It exhibited a highest turnover number (TON) of ~ 580 , corresponding to a best quantum yield of approximately 4.07%. In 2016, Niu and co-workers synthesized high-nuclearity $\{\text{Fe}_{14}\}/\{\text{Fe}_{10}\}$ POM-based nanoclusters that could also act as photocatalysts with methanol as sacrificial electron donor and platinum as cocatalyst for H_2 evolution from UV-light-driven water splitting.¹³⁶

There are two essential components in the photocatalytic HER system: photosensitizer for light harvesting and catalyst for water reduction. Except for acting as catalysts, the POMs could also be used for stabilizing the active noble metal nanoparticle catalysts.^{137,138} Hill et al. developed a hybrid catalyst POM-Pt NPs@ $\text{NH}_2\text{-MIL-53}$ for synergistic hydrogen evolution based on the self-assembly of Keggin POM ($\text{H}_3\text{PW}_{12}\text{O}_{40}$), Pt nanoparticles and metal-organic frameworks.¹³⁹ The self-assembled composite showed a TON of ca. 66 in 6 h under standard conditions with a quantum yield of 1.2×10^{-4} by using

ascorbic acid as a sacrificial electron donor under visible light irradiation. In the proposed photocatalysis system, the POM reduced H_2PtCl_6 to Pt NPs, stabilized the Pt NPs, induced a strong electrostatic association of the negatively charged Pt NPs with the protonated MOF ($\text{NH}_2\text{-MIL-53}$) sites on the particle surfaces, and facilitated the catalytic reduction reaction itself.

Introducing the photosensitizers or sacrificial electron donors into the POM catalysts structure is an effective strategy to achieve efficient electron transfer of proton reduction for H_2 production. Wang et al. designed and synthesized a series of catalysts based on Keggin-type POMs by the introduction of the sacrificial electron donors TEA (triethanolamine) into their structures.¹⁴⁰ The coordinated sacrificial electron donors to the structure of the catalysts led to higher catalytic efficiency compared to the homologous Keggin-type heteropolyacid. Douvas and co-workers showed the highly efficient hydrogen evolution with a TON of 215 induced by the zinc(II) mesotetrakis(*N*-methylpyridinium-4-yl)porphyrin (ZnTMPyP^{4+}) sensitization of a series of Dawson and Keplerate POM catalysts in a visible-light-driven system.¹⁴¹ The high efficiency for hydrogen evolution is attributed to the multi-electron reduction of POMs as well as the presence of the ZnTMPyP^{4+} sensitization. Rau and Streb et al. developed a covalent photosensitizer-POM catalyst dyad for the HER under visible-light irradiation upon the concept of the covalent linkage of coordination compounds to pyridine-

functionalized POMs.¹⁴² By combining an iridium(III) photosensitizer with a manganese-functionalized Anderson anion, the dyad showed superior HER activity compared with the non-covalent reference due to synergistic covalent interactions between functional coordination compounds and reactive molecular metal oxides.

POM-based assemblies as photocatalysts for hydrogen production

Although the pristine POM-based nanoclusters have been proven to be effective in UV-light, photosensitizers or cocatalysts based on noble metals, and/or poor activity of polyoxometalates are generally obtained, making it difficult to achieve a better catalytic performance. Recent progress has been made on various fronts lately to achieve more efficient light-driven hydrogen production, including development of POM-based hybrids,^{143–145} integration or adsorption of POMs into the structure of MOFs.^{34–36,146–150}

A hybrid polyoxometalate-aminoazobenzene dye compound, $(C_{12}H_{12}N_3)_3PW_{12}O_{40}2CH_3CN$, exhibiting effective photocatalytic H_2 evolution activity under visible-light, was synthesized by Li and co-workers.¹⁴⁵ Due to the introduction of the dye cations, the absorption edge of the prepared compound was largely red-shifted compared to the pure polyoxoanions. In 2018, Shanmugan and co-workers prepared a serious visible light responsive and water-stable inorganic-organic-inorganic POM and polyhedral oligomeric silsesquioxanes (POSS) hybrid materials.¹⁴³ Owing to improved charge carrier separation by electron-deficient metal sites and a red shift in the absorption, the synthesized hybrid materials exhibited remarkable photocatalytic H_2 production activities under visible-light irradiation and the maximum H_2 production rate of $485 \mu\text{mol h}^{-1} \text{g}^{-1}$ was obtained by the POM(MoV)-POSS catalyst. Also, in 2018, Lan et al. synthesized quaternary composite materials involving a snowflake-like CdS nanocrystal wrapped by different amounts of polyoxometalate-decorated $g\text{-C}_3\text{N}_4$ and polypyrrole (GPP@CdS) as photocatalysts for hydrogen production under visible-light irradiation.¹⁴⁴ The optimal catalyst (40%GPP@CdS composite) exhibited hydrogen production activity of $1321 \mu\text{mol}$ and excellent stability with negligible loss of activity after several cycles. The efficient synergy of CdS, $g\text{-C}_3\text{N}_4$, polypyrrole (PPy), and the POM $Ni_4(PW_9)_2$ attributed to the enhanced photocatalytic performance.

Integrating the redox POM catalyst or the photosensitizer into MOF is an effective strategy to obtain active HER photocatalysts due to the tunable structure of MOFs in which the catalytical competent moieties could be introduced via either the bridging ligands or the metal-connecting nodes. Lin et al. used the noble-metal-free Wells-Dawson POM $[P_2W_{18}O_{62}]^{6-}$ as the electron acceptor to construct the POM@MOF molecular catalytic system for photocatalytic HER. As a result of fast six-electron injection from multiple $[Ru(bpy)_3]^{2+}$ ligands to each encapsulated $[P_2W_{18}O_{62}]^{6-}$ cluster, efficient visible-light-driven hydrogen production was achieved with a TON of 79.³⁴ More recently, they reported an efficient visible-light-driven HER process with high turnover numbers as high as 1476 by encapsulating tetra-nickel-containing Ni_4P_2 POMs into the pores of phosphorescent UiO-MOFs built from $[Ir(ppy)_2(bpy)]^+$ -derived dicarboxylate ligands as shown in Fig. 16a, b and c.³⁶ The proximity of Ni_4P_2 to multiple photosensitizers in Ni_4P_2 @MOF allows for facile multi-electron transfer to enable efficient HER under visible-light irradiation with the ligand $[Ir(ppy)_2(bpy)]^+$ as photosensitizer and methanol as sacrificial electron donor. In 2018, Lin and

Zhang et al. reported on another serious of POM@MOF based composites by introducing three Wells-Dawson type polyoxoanions $P_2W_{15}V_3$ ($K_8HP_2W_{15}V_3O_{62} \cdot 9H_2O$), $P_2W_{17}Ni$ ($K_8P_2W_{17}(NiOH_2)O_{61} \cdot 17H_2O$) and $P_2W_{17}Co$ ($K_8P_2W_{17}(CoOH_2)O_{61} \cdot 16H_2O$) into a Cr-MOF of the MIL-101 for visible light-driven hydrogen production.¹⁴⁶ The MIL-101 framework absorbs the anionic POM, while the charge overcompensation in the POM@MOF composites allow them to efficiently adsorb cationic photosensitizer $Ru(bpy)_3^{2+}$ from solution, allowing the photosensitizers to surround the POM proton reduction catalysts, which results in a heterogeneous catalytic device POM@Photosensitizers@MOF with much higher photocatalytic activity than that of the corresponding homogeneous catalytic system. Additionally, this strategy was extended to sequential adsorption of anionic $Mo_2S_{12}^{2-}$ catalyst and cationic photosensitizers to lead to highly active photocatalytic proton reduction system with a H_2 evolution rate of $25,578 \mu\text{mol h}^{-1} \text{g}^{-1}$ in 8 h under visible light irradiation. As an improvement of these research works, in 2018, Li et al. developed a water-stable and novel free-noble-metal-based POM@MOF ($PW_{12}@UiO-NH_2$) HER photocatalyst through one-step solvothermal method.¹⁵⁰ The remarkable improvement of photocatalytic behavior for both H_2 evolution and RhB degradation were realized for $PW_{12}@UiO-NH_2$ composites compared with pristine $UiO-66-NH_2$.

Meanwhile, in 2016, Li and the co-workers reported on the combination of POMs with supramolecular metal-organic frameworks built from different precursors for effective visible-light driven HER. Firstly, the generation of a homogeneous supramolecular metal-organic framework (SMOF-1) by a self-assembly strategy in water from a hexa-armed $[Ru(bpy)_3]^{2+}$ -based precursor and cucurbit[8]uril (CB[8]) was reported (Fig. 17).³⁵ It has been demonstrated that the SMOF-1 could adsorb anionic Wells-Dawson-type POMs (WD-POMs) in a one-cage-one-guest manner to give WD-POM@SMOF-1 hybrid assemblies that enable fast multi-electron injection from photosensitive $[Ru(bpy)_3]^{2+}$ units to redox-active WD-POM units, leading to efficient hydrogen production in aqueous media and in organic media. Then, they proposed another self-assembly synthesis of a stable metal-covalent-supramolecular organic framework hybrid with other six-armed $[Ru(bpy)_3]^{2+}$ -based precursors and CB[8].¹⁴⁷ The discrete POMs can be adsorbed by the framework at very low concentrations to realize efficient visible light-induced reduction of proton to generate hydrogen. More recently, they reported the self-assembly of another 3D supramolecular organic framework from a rigid bipyridine-derived tetrahedral monomer and CB[8] in water, and its efficient and simultaneous intake of both $[Ru(bpy)_3]^{2+}$ -based photosensitizers and various POMs, which could take place at very low loading.¹⁴⁸ The robust intake of the framework for both photosensitizer and catalyst molecules led to improved electron transfer with 110-fold increase of the TON for HER. In addition, the high stability of the framework allowed for long-time irradiation of the resulting integrated catalytic systems and their recyclable use while maintaining high catalytic efficiency.

POM-based photocatalysts for water oxidation

Due to the plentiful redox properties and the stable inorganic ligands, POMs and their derivatives have been used as photocatalytic OER catalysts. The visible light-driven water oxidation system usually consists of three main parts, the sacrificial electron acceptor, for insurance $S_2O_8^{2-}$, the photosensitizer

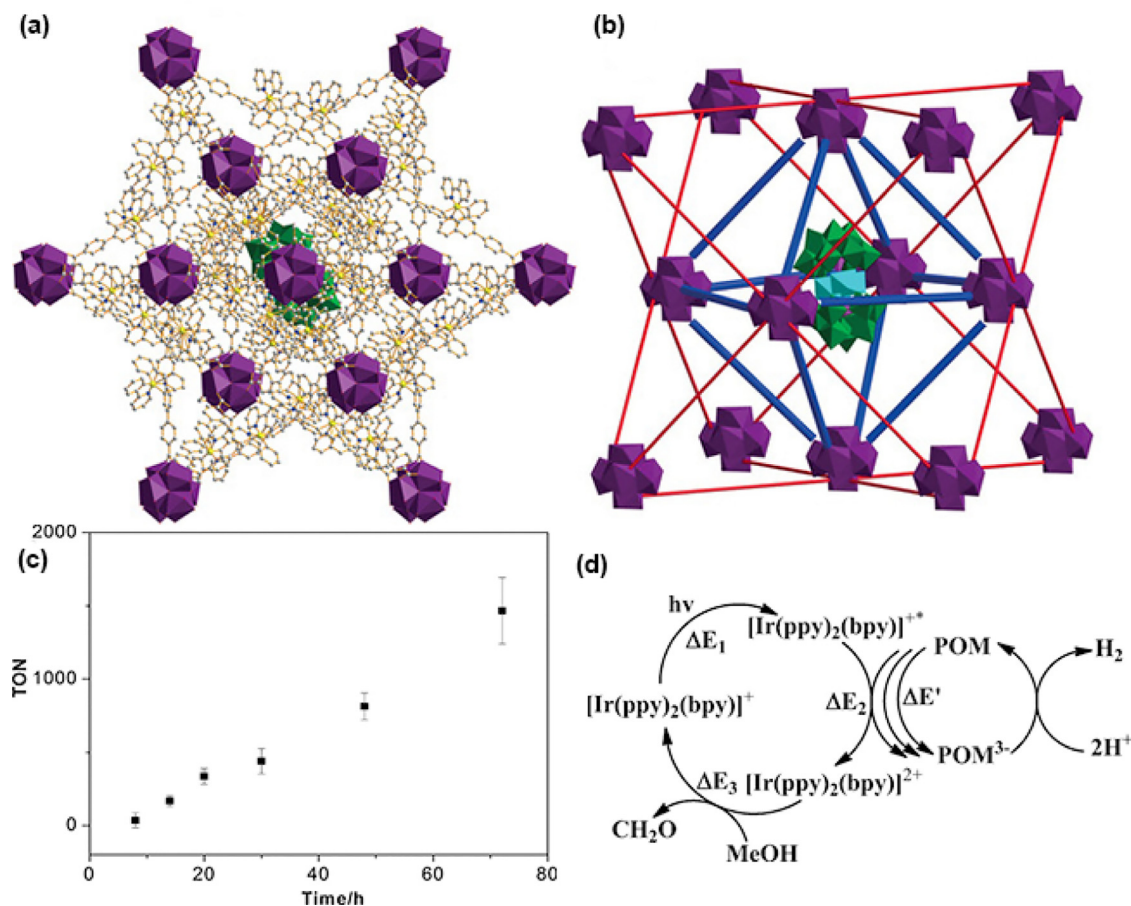


Fig. 16. (a) Structural model of Ni₄P₂@MOF as viewed along the [1,1,1] direction. (b) Structural model showing unoccupied tetrahedral cavities and the central Ni₄P₂-loaded octahedral cavity. (c) Time-dependent TONs of Ni₄P₂@MOF-1 with methanol as the sacrificial electron donor in aqueous solution (pH 1.2) under visible-light ($\lambda > 400$ nm) irradiations. (d) Proposed catalytic cycle for visible-light-driven hydrogen evolution catalyzed by Ni₄P₂@MOF-1. Reproduced with permission.³⁶ Copyright 2016, Wiley-VCH.

[Ru(bpy)₃]²⁺ (bpy = 2,2'-bipyridine) or its derivative, and water oxidation catalyst (WOC).

POM-based homogeneous molecular photocatalysts for water oxidation

The initial research was committed to develop efficient POM homogeneous molecular photocatalytic water oxidation catalysts. In 2008, the POM-based photocatalytic water oxidation catalyst of tetraruthenium(IV)-substituted POM [$\{\text{Ru}_4\text{O}_4(\text{OH})_2(\text{H}_2\text{O})_4\}\gamma\text{-SiW}_{10}\text{O}_{36}\}_2$]¹⁰⁻ was simultaneously reported by Hill et al. and Bonchio et al.^{28,29} After that, Hill and Tian et al. prepared a hydrolytically and oxidatively stable, homogeneous [Co₄(H₂O)₂(PW₉O₃₄)₂]¹⁰⁻ (Co₄POM) as efficient molecular catalyst for the visible-light-drive water oxidation, which showed superior performance compared to the firstly reported one with 30% photon-to-O₂ yield and a TON of >220 at pH 8.³⁰

There has been an inevitable challenge to distinguish heterogeneous and genuinely homogeneous catalysis, especially the Co-based POM electrocatalysts was found serving as a pre-catalyst for a heterotopic CoO_x catalyst.¹⁹ In 2013, Hill and Geletii et al. reported on differentiating homogeneous and heterogeneous water oxidation catalysis based on the confirmation of the Co-containing POM [Co₄(H₂O)₂(α -PW₉O₃₄)₂]¹⁰⁻ (Co₄POM)

molecular light-driven WOC.¹⁵¹ They quantified the amount of Co²⁺(aq) released from Co₄POM for thorough examination of active species under catalytic condition to provide strong evidence that this amount of cobalt, whatever speciation state it may exist in, cannot account for the observed water oxidation under the conditions initially reported for water oxidation using Co₄POM.⁸³ and the POM anion could function as a molecular catalyst, not a precursor for CoO_x. It was also proposed that catalytic O₂ evolution by Co₄POM, Co²⁺(aq), and CoO_x have different dependences on buffers, pH, and WOC concentration. Then, Hill and co-workers synthesized another Co-containing all-inorganic, oxidatively and thermally stable, homogeneous WOC based on redox-active (vanadate(V)-centered) POM ligands, Na₁₀[Co₄(H₂O)₂(VW₉O₃₄)₂] \cdot 35H₂O.¹⁵² The synthetic catalyst is highly active under mild conditions with a TOF > 1 \times 10³ s⁻¹ and a quantum efficiency of \sim 68% for O₂ formation at 6.0 μ M catalyst. Under light-driven conditions, it exhibited higher selectivity for water oxidation *versus* bpy ligand oxidation, and the final O₂ yield using the synthetic catalyst was twice as high as that using the previously reported Co₄POM. However, Folkman and Finke still have doubt on the high hydrolytic stability of this reported "Na₁₀[Co₄(H₂O)₂(VW₉O₃₄)₂] \cdot 35H₂O" (denoted as Co₄V₂W₁₈) WOC.¹⁵³ And they proposed a research to answer the question of "what is the stability of Co₄V₂W₁₈ in aqueous

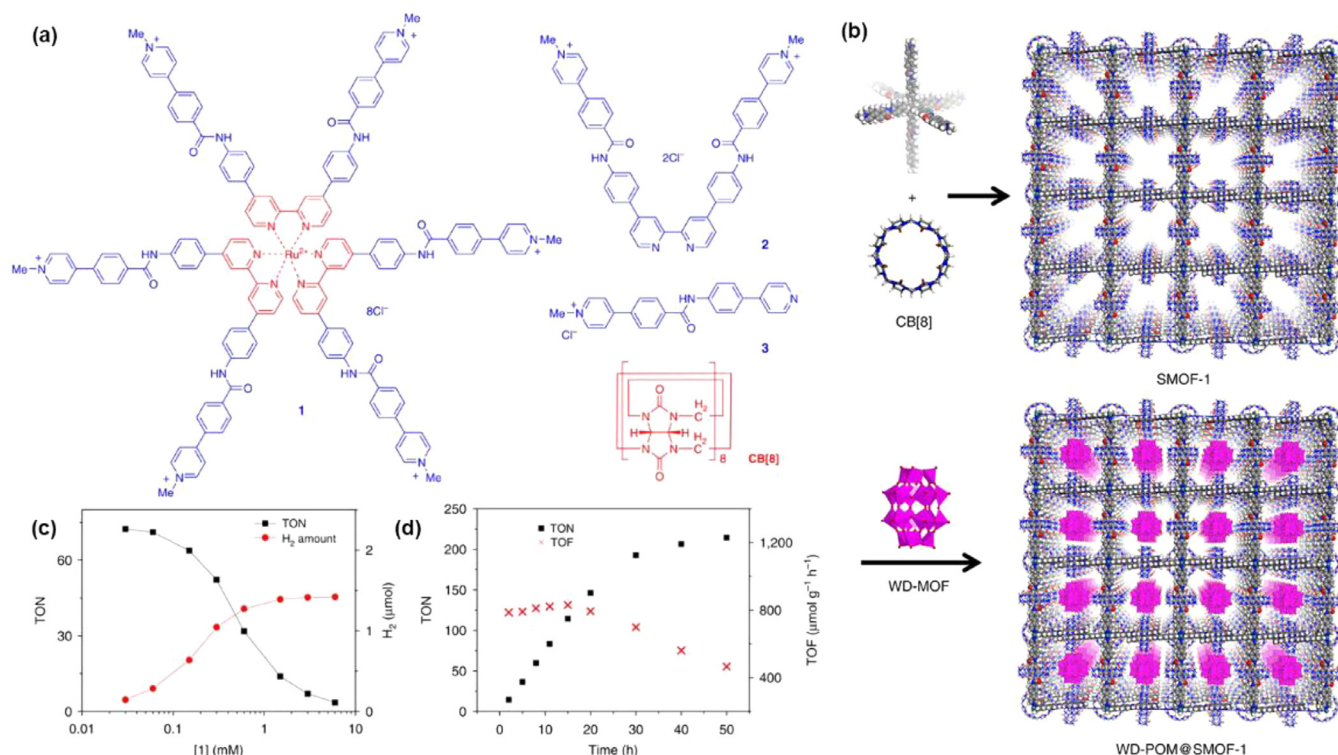


Fig. 17. Supramolecular metal-organic frameworks/POM for photocatalytic HER. (a) The structures of synthesized SMOF compounds and CB[8]. (b) Self-assembly of 3D cubic SMOF-1 and WD-POM loading. Formation of SMOF-1 and WD-POM@SMOF-1. The space-filling structural models were obtained using Materials Studio 7.0. H, white; C, light grey; N, blue; O, red; Ru, cyan; WD-POM ($[P_2W_{18}O_{62}]^{6-}$), purple polyhedron. (c) TONs of the solution of WD-POM@SMOF-1 and H₂ production amount after irradiating for 7 h. $[SMOF-1]/[WD-POM] = 15$, $[SMOF-1] = 0.03$ to 6 mM. (d) Time-dependent TON and TOF of the solution of WD-POM@SMOF-1. $[SMOF-1] = 0.3$ mM, $[WD-POM] = 0.02$ mM. Methanol was used as the sacrificial electron donor. Reproduced with permission.³⁵ Copyright 2016, Nature Publishing Group.

solution using 0.1 M NaPi pH 5.8 and 8.0 as well as sodium borate (NaB) pH 9.0'' in 2017. Their study summarized seven main findings from ³¹P NMR, electrochemical tests, and some other controlled experiments results, which provides evidence that Co(II) derived from Co₄V₂W₁₈ forms a CoO_x film on the electrode and Co₄V₂W₁₈ WOC is not as stable as previously reported. Although the disputation about the stability of POM-based molecular WOCs is still on-going, increasing numbers of researches have been devoted to uncovering the truth and making contribution to the development of the field.

In 2013, Ding and co-workers reported the stable water-soluble cobalt-containing Keggin POM $K_7[Co^{III}Co^{II}(H_2O)W_{11}O_{39}]$ (1) catalyst with mixed-valence Co(III) and Co(II) for efficient O₂ production via visible-light driven water oxidation (Fig. 18a and b).³¹ They systemically studied all possible variables of photocatalytic reaction and presented the optimal reaction condition (photoirradiation at $\lambda \geq 420$ nm, $[Ru(bpy)_3]Cl_2$ as the photosensor, Na₂S₂O₈ as the oxidant in borate buffer at pH 9.0) for (1) with an oxygen yield of 30%, TON of 51, and TOF (at the first 60 s) of 0.5 s⁻¹, respectively. Multiple experiments, including laser flash photolysis, CV tests, FT-IR spectra, dynamic light scattering and EDX characterization, ruled out the possibility that neither the free Co²⁺ ions were present in the reaction solution nor were cobalt oxide/hydroxide nanoparticles *in-situ* formed from the assumed decomposition, which collectively proved that (1) was a true molecular catalyst. The stability of catalyst was tested and confirmed (1) with excellent photocatalytic water oxidation stability and durability with catalyst recycling or aging

(Fig. 18c and d). It has also been demonstrated that the Co(III) center in (1) played a vital role in maintaining the structural integrity.

With respect to the variable combinations of metal cores with POM shells, catalytically active metal sites of water oxidation, such as Co and Ru, could be introduced, offering the advantage of sterically exposed and accessible active metal centers within a chemically stable POM shell. In 2012, Patzke and Car et al. introduced small "open" Ru-POMs with exposed catalytic centers as new building blocks to construct a trivalent triruthenium Keggin-type silicotungstate $\alpha-K_6Na[\{Ru_3O_3(H_2O)Cl_2\}SiW_9O_{34}]\cdot 17H_2O$ WOC.¹⁵⁴ The TOF is 0.7 s⁻¹ after 5 min of visible light illumination for 50 μM catalyst. Additionally, the interaction of POM with the photosensitizer (PS, $[Ru(bpy)_3]^{2+}$) during water oxidation results in a stable POM-PS complex that is recyclable and affords constant oxygen production rates. The immobilization of POM with PS promotes their stability as catalytically active molecular species. Then, Patzke et al. reported another tungstobismutate $[\{Co(H_2O)_3\}_2\{CoBi_2W_{19}O_{66}(OH)_4\}]^{10-}$ with a disordered Co/W core.¹⁵⁵ Subtle differences in the core disorder patterns of the as-proposed isostructural POM-WOC was revealed to be decisive for the catalytic activity with a maximum TON of 21 and 97% oxygen yield for 115 μM catalyst.

In most formerly mentioned POM water oxidation catalysts, the polyoxometalated unit(s) were mainly used as stabilizing shells, with the catalytically active metals not belonging to the polyoxometalated scaffold. Santoni et al. firstly demonstrated

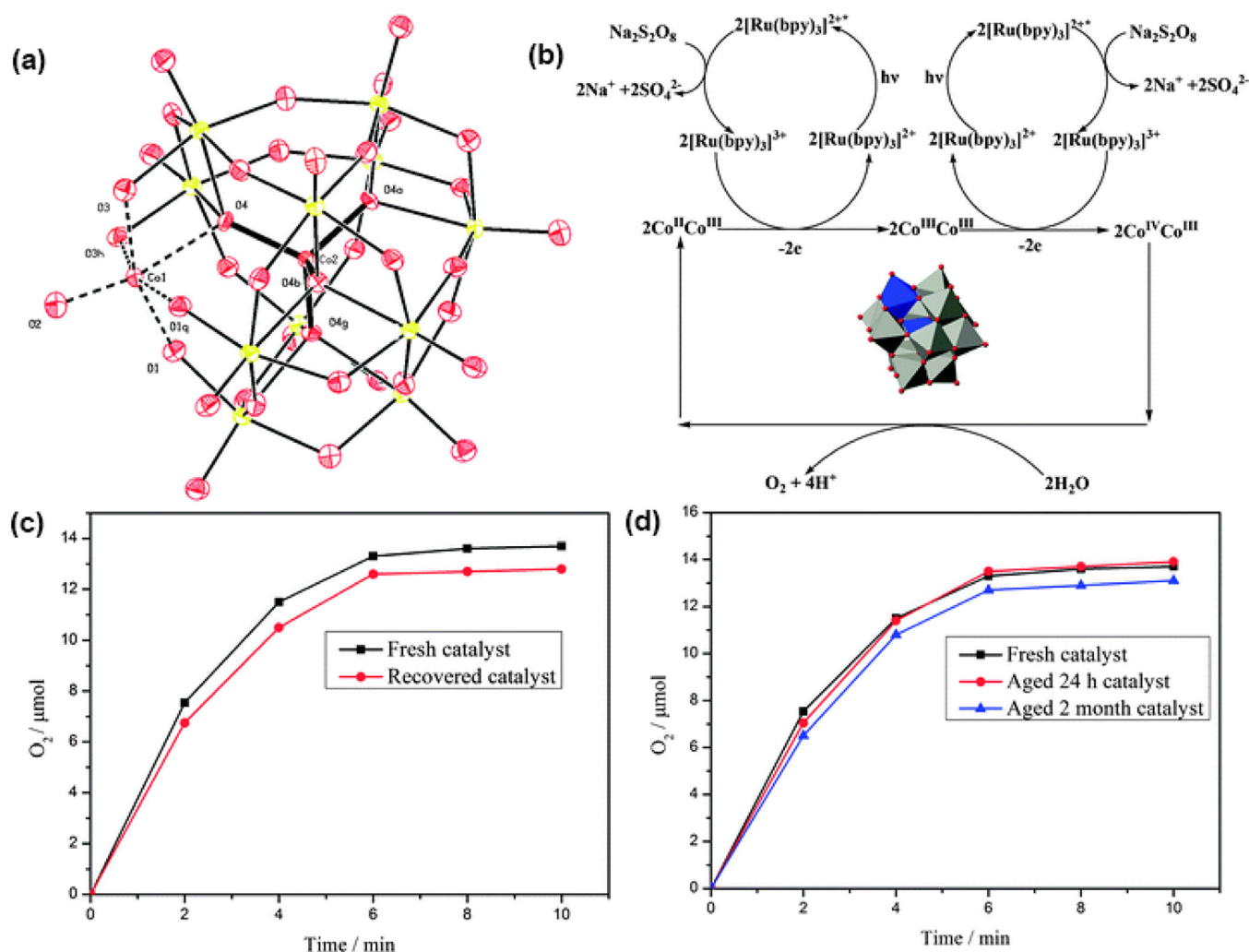


Fig. 18. (a) Thermal ellipsoid plot of the crystallographic structure of (1). The probability level is set to 50%. Potassium ions and water molecules have been omitted. (b) Photocatalytic water oxidation catalyzed by (1). (c) Kinetics of O_2 formation in the photocatalytic system using fresh (black) and recovered (red) (1). (d) Kinetics of O_2 formation in the photocatalytic system using 15 μM of fresh (black) and 24 h aged (1) (red). Kinetics of O_2 formation in the photocatalytic system using 2-month aged (1) (blue, initial concentration of (1) = 15 μM). Reproduced with permission.³¹ Copyright 2013, Royal Society of Chemistry. (For interpretation of the references to color in this figure legend, the reader is referred to the web version of this article.)

vanadium species to play the role of a water oxidation catalyst with synthesis of a mixed-valence $[(\text{V}^{\text{IV}}_5\text{V}^{\text{V}}_1\text{O}_7(\text{OCH}_3)_{12})^-]$ species, in which the catalytically active center was the polyoxometalated framework.¹⁵⁶ The photochemical quantum yield of 0.20 was calculated by using such a methoxo-POM cluster as the catalyst, using $[\text{Ru}(\text{bpy})_3]^{2+}$ as the photosensitizer, and $\text{Na}_2\text{S}_2\text{O}_8$ as the sacrificial electron acceptor, in mixed solvents at 450 nm excitation.

In natural oxygenic photosynthesis, generation of O_2 occurs at oxygen evolving complex (OEC) $\text{Mn}_4\text{O}_5\text{Ca}$ (a tetramanganese calcium oxo cluster) located within a large protein assembly, namely photosystem II (PS II).¹⁵⁷ The O–O bond was formed by the cooperation of a multi-redox $\text{Mn}^{\text{III}}/\text{Mn}^{\text{IV}}$ manifold that evolved through five electronic states (S_i , where $i = 0-4$). The researches towards synthesis of POM-based photocatalysts as OEC model have been proposed.^{32,37,158-160} In 2014, for the first time, Kortz, Bonchio and Scandola et al. proposed a photocatalytic WOC of tetramanganese-substituted tungstosilicate $[\text{Mn}^{\text{III}}_3\text{Mn}^{\text{IV}}\text{O}_3(\text{CH}_3\text{COO})_3(\text{A}-\alpha\text{-SiW}_9\text{O}_{34})]^{6-}$ (Mn_4POM) with mixed-valent $\text{Mn}^{\text{III}}_3\text{Mn}^{\text{IV}}\text{O}_3$ manganese oxo

core that mimicked the natural OEC in its reduced S_0 state.¹⁵⁸ The Mn_4 -OEC was anchored on the POM platform and combined with carboxylate bridges. The interplay of organic and inorganic ligands provided a coordination environment with both stability and flexibility to assist stepwise one-electron oxidation of the catalytic Mn_4 -OEC core and to access high-valent Mn states that were responsible for water oxidation. Photocatalytic oxygen evolution was achieved in a buffered medium (pH = 5) with a quantum efficiency of 1.7% with presence of $[\text{Ru}(\text{bpy})_3]^{2+}$ and $\text{S}_2\text{O}_8^{2-}$.

In 2014, Zhang, Lin and Wang et al. synthesized all-inorganic, abundant-metal-based, high nuclearity cobalt-phosphate (Co-Pi) molecular catalysts $[\{\text{Co}_4(\text{OH})_3(\text{PO}_4)_4(\text{SiW}_9\text{O}_{34})_4\}]^{32-}$, $[\{\text{Co}_4(\text{OH})_3(\text{PO}_4)_4(\text{GeW}_9\text{O}_{34})_4\}]^{32-}$, $[\{\text{Co}_4(\text{OH})_3(\text{PO}_4)_4(\text{PW}_9\text{O}_{34})_4\}]^{28-}$, and $[\{\text{Co}_4(\text{OH})_3(\text{PO}_4)_4(\text{AsW}_9\text{O}_{34})_4\}]^{28-}$ as highly effective photocatalytic WOCs.³² The prepared compounds were the first POM-based Co-Pi-cluster molecular catalysts for visible light-driven water oxidation. Additionally, the prepared clusters can serve as functional model of the OEC in PSII as the $\{\text{Co}_{16}(\text{PO}_4)_4\}$ cluster containing a

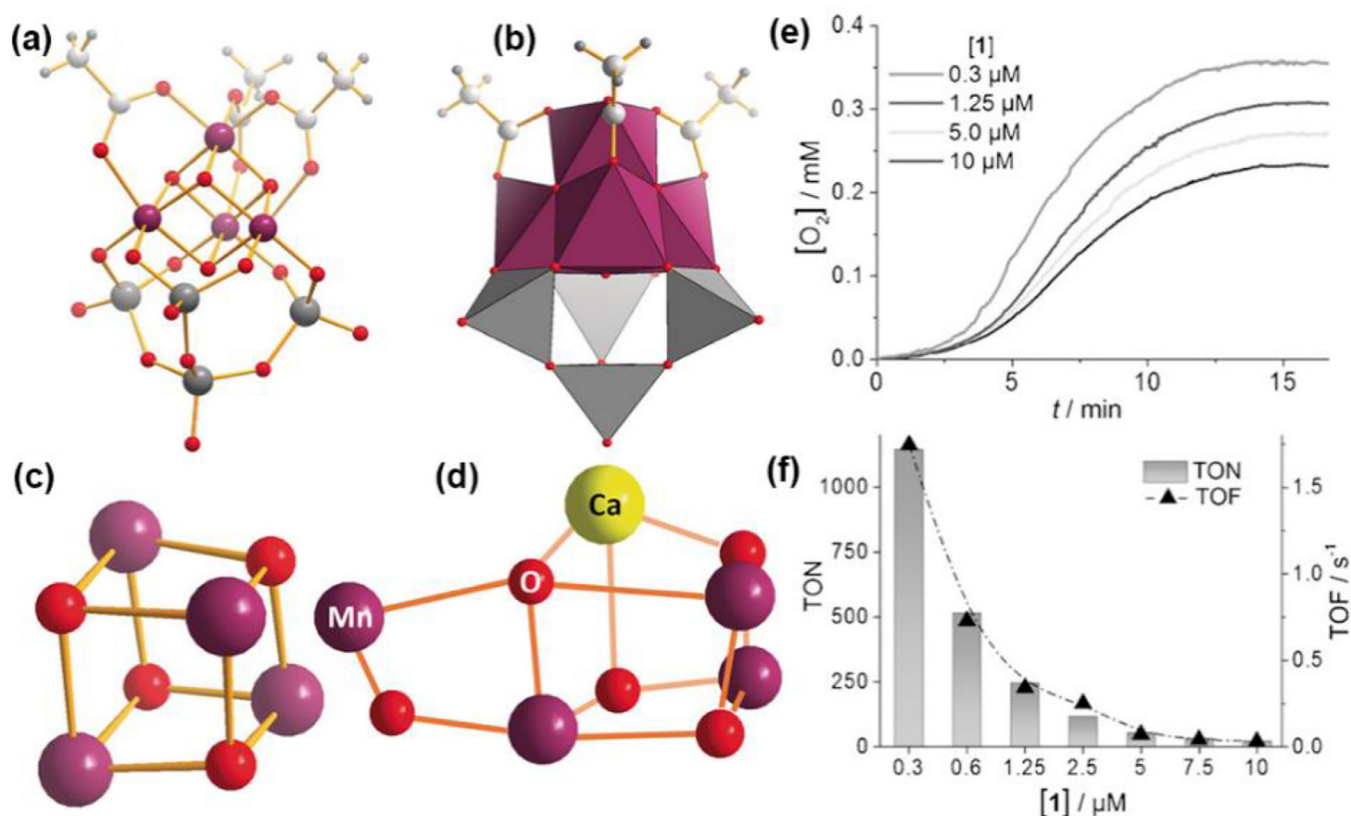


Fig. 19. Structure of the manganese vanadium oxide $[\text{Mn}_4\text{V}_4\text{O}_{17}(\text{OAc})_3]^{3-}$. (a) Ball-and-stick, (b) polyhedral representation, (c) the $[\text{Mn}_4\text{O}_4]^{6+}$ cubane core, and (d) the calcium manganese oxo core of the OEC.¹⁵⁷ Mn purple, V gray, Ca yellow, O red, C gray, H small, gray. (e) Visible-light-driven water oxidation with prepared cluster (0.3–10 μM) in the presence of $[\text{Ru}(\text{bpy})_3]^{2+}$ (1 mM) and $\text{S}_2\text{O}_8^{2-}$ (10 mM) in MeCN/ H_2O (9:1, v/v). (f) TON and TOF of the visible-light-driven water oxidation. Reproduced with permission.³⁷ Copyright 2016, Wiley-VCH. (For interpretation of the references to color in this figure legend, the reader is referred to the web version of this article.)

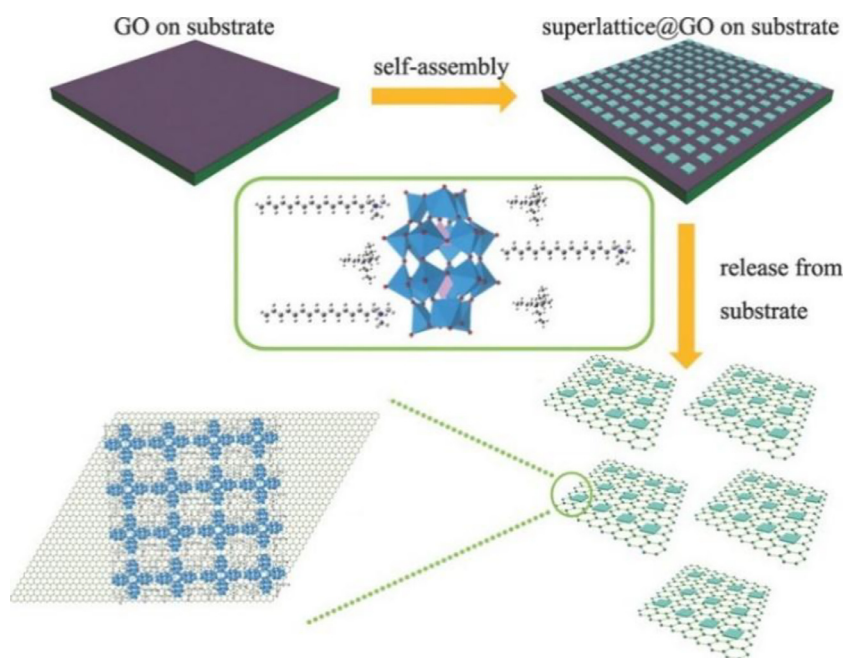
Co_4O_4 cubane is structurally analogous to the $[\text{Mn}_3\text{CaO}_4]$ core of the OEC in PSII. Then, in 2015, Wang's group reported the synthesis of POM-based nickel clusters, including $\text{Na}_{24}[\text{Ni}_{12}(\text{OH})_9(\text{CO}_3)_3(\text{PO}_4)(\text{SiW}_9\text{O}_{34})_3] \cdot 56\text{H}_2\text{O}$ (**1**), $\text{Na}_{25}[\text{Ni}_{13}(\text{H}_2\text{O})_3(\text{OH})_9(\text{PO}_4)_4(\text{SiW}_9\text{O}_{34})_3] \cdot 50\text{H}_2\text{O}$ (**2**), and $\text{Na}_{50}[\text{Ni}_{25}(\text{H}_2\text{O})_2(\text{OH})_{18}(\text{CO}_3)_2(\text{PO}_4)_6(\text{SiW}_9\text{O}_{34})_6] \cdot 85\text{H}_2\text{O}$ (**3**), for visible light-driven water oxidation.¹⁵⁹ The synthetic compounds possess central $\{\text{Ni}_{12}\}$ (for **1**), $\{\text{Ni}_{13}\}$ (for **2**) and $\{\text{Ni}_{25}\}$ (for **3**) cores encapsulated by the lacunary $\{\text{A}-\alpha\text{-SiW}_9\text{O}_{34}\}$ POM units and connected the inorganic $\{\text{PO}_4\}$ and/or $\{\text{CO}_3\}$ ligands. All three compounds containing $\{\text{Ni}_3\text{O}_3\}$ quasi-cubane or $\{\text{Ni}_4\text{O}_4\}$ cubane units, which are similar to the natural oxygen evolving center $\{\text{Mn}_4\text{O}_5\text{Ca}\}$ in PSII, showed excellent photocatalytic activities with high TON of 128.2 for **1**, 147.6 for **2**, and 204.5 for **3**, respectively.

In 2016, Streb et al. reported a synthetic OEC model based on a molecular manganese vanadium oxide cluster, $[\text{Mn}_4\text{V}_4\text{O}_{17}(\text{OAc})_3]^{3-}$.³⁷ The $[\text{Mn}_4\text{O}_4]^{6+}$ cubane core of the synthetic compound, which was stabilized by a tripodal $[\text{V}_4\text{O}_{13}]^{6-}$ polyoxovanadate and three acetate ligands as shown in Fig. 19a–c, catalyzed the homogeneous, visible-light-driven oxidation of water to molecular oxygen. Under visible-light irradiation, the cluster showed high WOC activity with the obtained TON of 1150 and TOF of 1.75 s^{-1} (Fig. 19f). Furthermore, this compound could serve as a model system for the OEC in photosystem II as it featured a mixed-valent manganese oxo cubane, $[\text{Mn}^{\text{III}}_2\text{Mn}^{\text{IV}}_2\text{O}_4]^{6+}$, corresponding to

the S_1 state of the Kok cycle. The higher oxidation states S_2 and S_3 were accessible by electrochemical oxidation.

The distinguish of dominant catalyst between homogeneous POM molecules and the corresponding metal ions/metal oxides have been achieved by the characterizations of dynamic light-scattering, UV–vis absorption, catalysts aged experiments, capillary electrophoretic measurements, etc.^{31,32,151,159,160–164} In 2017, Ding et al. proposed the preparation of an efficient WOC based on POM-based manganese clusters $[\text{Mn}_3(\text{H}_2\text{O})_3(\text{SbW}_9\text{O}_{33})_2]^{12-}$.¹⁶⁵ Together with multiple route experiments, implemented electrochemical impedance spectroscopy method was also introduced to confirm the differences in the electrocatalytic water oxidation properties between POM containing Mn and the equivalent $\text{Mn}^{2+}(\text{aq})$, which supported that the prepared Mn POM-based cluster was a homogeneous molecular dominant catalyst rather than Mn^{2+} ions (aq) or manganese oxide during the water oxidation process. Under optimum reaction conditions, a TON of 103 and $\text{TOF}_{\text{initial}}$ of 0.4 s^{-1} over the synthetic cluster were obtained for the photocatalytic water oxidation.

Weinstock et al. reported water-soluble complexes as WOC by using an oxidatively inert heteropolytungstate (POM) cluster anion $[\alpha\text{-PW}_{11}\text{O}_{39}\text{Fe}^{\text{III}}]^{4-}$ that could serve as a covalently attached oxo donor ligand for hematite Fe_2O_3 NCs.¹⁶⁶ The proposed complex composed of polyoxometalate (POM)-complexed hematite cores with 275 iron atoms is not only water-soluble but also inherently stable to oxidation and hydrolysis,



Scheme 4. Formation of monolayer superlattice on GO, with a building block in between. Reproduced with permission.¹⁶³ Copyright 2014, Wiley-VCH.

showing no decrease in activity for a week under turnover conditions. Solution-state methods to elucidate the mechanism of visible-light-driven water oxidation by freely diffusing nanocrystals of hematite α -Fe₂O₃ were proposed by investigation on solubility and stability of the synthesized complex. The catalytic oxygen evolution by prepared complex occurs by a chain mechanism, initiated by the rate-limiting capture of photoexcited electrons, which is different from the water oxidation at the conventional hematite photoanodes.

POM-based heterogeneous photocatalysts for water oxidation

Despite the promising features of reversible redox properties and stable structure, POMs are associated with certain drawbacks, such as solubility. As the homogenous catalysts are difficult to be recycled, the practical utilization is limited. Furthermore, the stability of these POMs under given set of experimental conditions is also an issue. To overcome these obstacles, some support materials, such as graphene, carbon nanotubes, MOFs *etc.* have been employed to immobilize POM into heterogeneous catalyst systems.^{167–170}

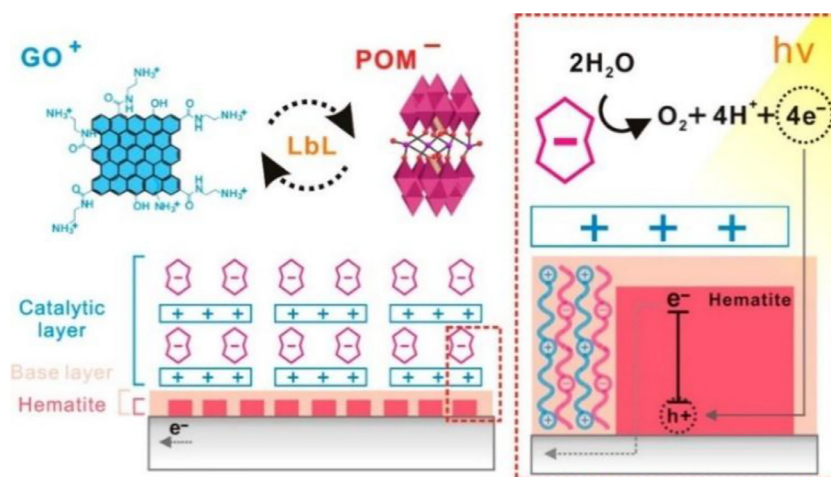
In accordance with the advantages that the POM clusters are usually in the range of 1–6 nm with single size distributions, and the solubility of POMs can be easily changed by surfactant encapsulation.^{171,172} Wang et al. reported the formation of a monolayer superlattice on graphene oxide (GO) with very high degrees of both translational and orientational order, obtained from the self-assembly of surfactant-encapsulated POMs by evaporation of solvents (Scheme 4).¹⁶³ (HDA)₃(TBA)₃P₂W₁₈O₆₂ clusters (HDA = hexadecyltrimethylammonium; TBA = tetrabutylammonium) were employed as building blocks. The synthesized superlattice@GO exhibited enhanced photoelectrochemical properties as well as excellent performance towards the reduction of hydrogen peroxide. Both excellent

properties can be attributed to the synergistic effects between the superlattice and GO.

Nadeem and Kögerler et al. reported a reproducible photocatalytic WOC with stable structure based on the encapsulation of cobalt-polyoxotungstates in MIL-100(Fe).¹⁶⁹ The POM-MOF composites of **Co2**@MIL-100(Fe) and **Co4**@MIL-100(Fe) were obtained successfully with two different cobalt-functionalized polyoxometalate anions, [Co^{II}Co^{III}W₁₁O₃₉(H₂O)]^{7–} (**Co2**) and [Co₄(PW₉O₃₄)₂(H₂O)₂]^{10–} (**Co4**), encapsulated in the MIL-100(Fe) MOF. The photocatalytic water oxidation ability of the synthesized POM-MOF composites investigated under the visible light irradiation revealed that the hybrid materials showed higher oxygen yield of 41% for **Co2**@MIL-100(Fe) and 72% for **Co4**@MIL-100(Fe) and TOFs of 0.53 s^{–1} for **Co2**@MIL-100(Fe) and 9.2 × 10^{–3} s^{–1} for **Co4**@MIL-100(Fe) compared to virgin **Co2** and **Co4**.

Inspired by the natural biological photosynthesis system, Kim and Ryu et al. developed an efficient water oxidation photoanode via tailored layer-by-layer assembly of graphene oxide (GO) nanosheets and cobalt polyoxometalate ([Co₄(H₂O)₂(PW₉O₃₄)₂]^{10–}, Co-POM) into a nacre-like multilayer architecture on hematite (Scheme 5).¹⁶¹ Owing to the enhanced charge transport and catalytic efficiency from the rational and precise assembly of GO and Co-POM, the catalytic multilayer electrode exhibited a higher photocurrent density and large cathodic shift in onset potential (~369 mV) at neutral pH conditions in contrast with the bare counterpart. Additionally, the pre-deposition of the polyelectrolyte base layer on hematite offered a crucial influence on photocatalytic performance by the tuning of surface dipole and flat band potential for efficient charge separation and injection.

More recently, Fontecave and Dolbecq et al. reported a noble-metal-free WOC based on hybrid framework composed of Co-POM ([Co₄(PW₉O₃₄)₂(H₂O)₂]^{10–}, P₂W₁₈Co₄) immobilized in a Zr(IV) porphyrinic MOF-545.¹⁷³ The POM located in the



Scheme 5. Schematic representation of LbL-assembled (GO/Co-POM)_n multilayers on a hematite electrode with a simplified charge transfer pathway. Reproduced with permission.¹⁶¹ Copyright 2019, American Chemical Society.

Table 2. Summary of POM-based catalysts in [Ru(bpy)₃]²⁺/Na₂S₂O₈ photocatalytic water oxidation systems reviewed in this work.

Catalyst	pH ^a	O ₂ yield (%)	TOF	TON	Ref.
[Co ₄ (H ₂ O) ₂ (PW ₉ O ₃₄) ₂] ¹⁰⁻	8.0	30	5 s ⁻¹	224	30
K ₇ [Co ^{III} Co ^{II} (H ₂ O)W ₁₁ O ₃₉]	9.0	30	0.5 s ⁻¹	361	31
[{Co ₄ (OH) ₃ (PO ₄) ₄ (GeW ₉ O ₃₄) ₄ }] ³²⁻	9.0	31	0.105 s ⁻¹	39	32
[Mn ₄ V ₄ O ₁₇ (OAc) ₃] ³⁻	^b	7.2	1.75 s ⁻¹	1150	37
[Co ₄ (H ₂ O) ₂ (α-PW ₉ O ₃₄) ₂] ¹⁰⁻	8.0	24.2	N/A	302	151
Na ₁₀ [Co ₄ (H ₂ O) ₂ (VW ₉ O ₃₄) ₂].35H ₂ O	9.0	59.4	2.2 × 10 ³ s ⁻¹	4210	152
K ₆ Na[{Ru ₃ O ₃ (H ₂ O)Cl ₂ }SiW ₉ O ₃₄].17H ₂ O	5.8	N/A	0.7 s ⁻¹	23	154
[{Co(H ₂ O) ₃ } ₂ {CoBi ₂ W ₁₉ O ₆₆ (OH) ₄ }] ¹⁰⁻	5.8	97	0.9 min ⁻¹	21	155
[Mn ^{III} ₃ Mn ^{IV} O ₃ (CH ₃ COO) ₃ (A-α-SiW ₉ O ₃₄)] ⁶⁻	5.2	3.7	0.71 × 10 ³ s ⁻¹	5.2	158
Na ₂₄ [Ni ₁₂ (OH) ₉ (CO ₃) ₃ (PO ₄)(SiW ₉ O ₃₄) ₃].56H ₂ O	9.0	15.1	0.20 s ⁻¹	128.2	159
Na ₂₅ [Ni ₁₃ (H ₂ O) ₃ (OH) ₉ (PO ₄) ₄ (SiW ₉ O ₃₄) ₃].50H ₂ O	9.0	15.5	0.25 s ⁻¹	147.6	159
Na ₅₀ [Ni ₂₅ (H ₂ O) ₂ (OH) ₁₈ (CO ₃) ₂ (PO ₄) ₆ (SiW ₉ O ₃₄) ₆].85H ₂ O	9.0	17.6	0.34 s ⁻¹	204.5	159
carbon nanodot/[Co ₄ (H ₂ O) ₂ (PW ₉ O ₃₄) ₂] ¹⁰⁻	7.0	N/A	N/A	552	164
[Mn ₃ (H ₂ O) ₃ (SbW ₉ O ₃₃) ₂] ¹²⁻	9.0	13.2	0.4 s ⁻¹	103	165
PW ₁₂ (Co ₃ O ₄) ₁₂	6.0	N/A	1.11 × 10 ⁻³ s ⁻¹	N/A	168
Co2@MIL-100(Fe)	9.0	41	0.53 s ⁻¹	257	169
Co4@MIL-100(Fe)	8.0	72	9.2 × 10 ⁻³ s ⁻¹	21	169

N/A These values were unavailable.

^a Borate buffer was used as reaction solution at pH 9.0 or 10.0, Na₂SiF₆ buffer was used for reaction solution at pH 5.8 or 6.0, and sodium phosphate buffer was used for reaction solution at pH 6.9 or 7.0.

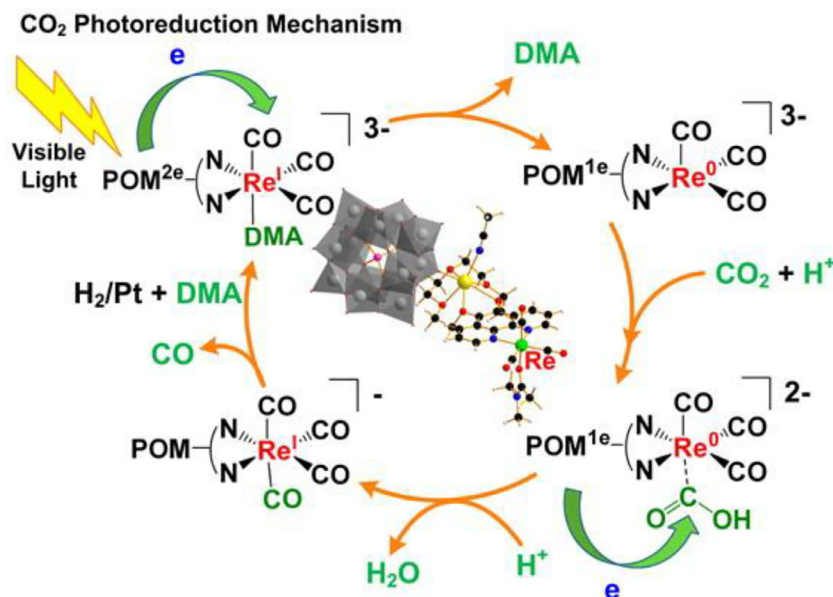
^b Mixed solution of MeCN/H₂O (9:1, v/v) was used as reaction solution.

vicinity of the Zr₆ clusters and porphyrin linkers constituting the MOF. Notably, the proposed composite is a typical example for the supramolecular heterogeneous photocatalytic system with the catalyst and the photosensitizer within the same porous solid material. The outstanding water oxidation activity of the P₂W₁₈Co₄@MOF-545 photosystem benefits from two main factors: (i) immobilization of the porphyrin as a ligand in the MOF increases its oxidizing power, and (ii) the confinement of POMs inside the pores of the MOF plays a key role in the stabilization of the cobalt POM's catalytic site while the POM-MOF interface provides key components (-OH, labile water molecules) relevant to the OER mechanism. Du and Liu et al. synthesized a high-nuclear {Cu₂₄(μ₃-Cl)₈(μ₄-Cl)₆}-based POM@MOF (**ZZULI-1**) as noble-metal-free photocatalyst for both H₂ and O₂ production.¹⁷⁴ **ZZULI-1** showed highly efficient photocatalytic H₂ evolution (6614 μmol g⁻¹ h⁻¹) and O₂ evolution (1032 μmol g⁻¹ calculated for the first 6 min). The

{Cu₂₄(μ₃-Cl)₈(μ₄-Cl)₆}-clusters and mixed POMs not only work as the active units for H₂ and O₂ production, respectively, but also improve the effective electron transfer between the photosensitizer and **ZZULI-1**. The summary of POM-based catalysts in [Ru(bpy)₃]²⁺/Na₂S₂O₈ photocatalytic water oxidation systems reviewed in this work is exhibited in Table 2.

POM-based photocatalysts for CO₂ reduction

The accomplishment of CO₂ reduction reaction through photocatalysis means that chemically inert CO₂ molecules adsorbed on the catalyst must undergo a proton-assisted multi-electron transfer process. It is a rather challenging task for catalyst design because of the uncontrollable multi-electron supply and complicated photocatalytic reaction mechanism.^{13,175} And the research on photocatalysis of CO₂ reduction reaction based on POM-based catalysts is still in its infancy. In 2010, Neumann and co-workers firstly reported a polyoxometalate of the Keggin structure



Scheme 6. Photoreduction mechanism of CO_2 to CO catalyzed by a $\text{Re}(\text{I})$ -POM hybrid Compound. Reproduced with permission.¹⁷⁸ Copyright 2016, American Chemical Society.

substituted with Ru^{III} , $\{(\text{C}_6\text{H}_{13})_4\text{N}\}_5[\text{Ru}^{\text{III}}(\text{H}_2\text{O})\text{SiW}_{11}\text{O}_{39}]$, catalyzed the photoreduction of CO_2 to CO .¹⁷⁶ Before their study, there were only several reports of polyoxometalates binding or coordinating CO_2 .¹⁶ It was demonstrated in their study that, with the coordination of CO_2 to Ru^{III} and Et_3N , the interaction of the nucleophilic O atom of CO_2 to Ru atom of the POM and the formation of a $\text{O}_2\text{C}-\text{NMe}$ zwitterion stabilize both Ru-O and C-N interactions and probably determine the promotional effect of an amine on the activation of CO_2 by $[\text{Ru}^{\text{III}}(\text{H}_2\text{O})\text{SiW}_{11}\text{O}_{39}]^{5-}$. The detailed mechanistic pathway for photoreduction of CO_2 was also predicted and provided, in which the POM took part in the activation of both CO_2 and Et_3N .

The sacrificial amine electron donors were used to afford the two electrons and two protons required by the photochemical reduction of CO_2 to CO . And it is usually difficult to avoid the use of organic amine as sacrificial agent. Thus, research works have been committed to avoid the utilization of amine donors. In the year of 2011, Neumann et al. proposed another research on the photoreduction of CO_2 to CO with H_2 as the reducing agent and a rhenium(I) Phenanthroline-POM $\text{Re}^{\text{I}}(\text{L})(\text{CO})_3\text{CH}_3\text{CN-MHPW}_{12}\text{O}_{40}$ ($\text{L} = 15\text{-crown-5-phenanthroline}$, $\text{M} = \text{Na}^+, \text{H}_3\text{O}^+$) hybrid as catalyst.¹⁷⁷ In the presence of Pt/C , the POM moiety in the prepared hybrid can oxidize H_2 to two protons and two electrons which, under visible light, can convert CO_2 into CO with H_2 as the reducing agent instead of the universally used amines. In 2016, Poblet and co-workers performed a detailed computational investigation on photoreduction mechanism of CO_2 to CO by the Re -organic hybrid POMs $\{\text{NaH}[\text{PW}_{12}\text{O}_{40}]^{3-}\text{Re}^{\text{I}}(\text{L})(\text{CO})_3\text{DMA}\}^{n-}$ ($\text{L} = 15\text{-crown-5-phenanthroline}$, $\text{DMA} = \text{N,N-dimethylacetamide}$) via DFT and TD-DFT calculations.¹⁷⁸ The proposed reaction mechanism, as shown in Scheme 6, can be divided into several steps, including photoexcitation and charge transfer, DMA release, CO_2 addition, protonation, and CO release and recoordination of DMA. The charge transfer states, POM to Re complex, are induced by metal-centered excitations occurring on the reduced POM. With one electron transferred to the organometallic unit from the

excited POM, the Re can bind and activate the CO_2 substrate. Subsequent steps involving protonation of CO_2 and CO release are thermodynamically favorable and are induced by a second electron transfer from the POM to the Re complex. In this system, the POM acts as photosensitizer, electron reservoir, as well as electron donor.

A concept towards the realization of a water-splitting reaction as the source of electrons and protons for CO_2 reduction is also induced. It means that such a polyoxometalate could, in principle, be an electron "shuttle" during water oxidation reaction that could produce electrons/protons and O_2 as well as CO_2 photoreduction catalyst. In 2017, Neumann and co-workers also found that the reduced acidic POM, $\text{H}_5\text{PW}_{12}\text{O}_{40}$, is a photoactive electron and proton donor with visible light through excitation of the intervalence charge-transfer band.¹⁷⁹ With the polyoxometalate linked to a dirhenium molecular catalyst, a cascade of transformations occurred where the polyoxometalate was electrochemically reduced at a relatively low negative potential. Under visible light or a red-LED, the photoelectrons from the POM transferred to the dirhenium catalyst for the selective reduction of CO_2 to CO . Almost at the same time, Roy et al. reported a softoxometalate based on a $\{[\text{K}_{6.5}\text{Cu}(\text{OH})_{8.5}(\text{H}_2\text{O})_{7.5}]_{0.5}[\text{K}_3\text{PW}_{12}\text{O}_{40}]\}$ metal oxide framework that was stable under reaction conditions and exhibited excellent performance to photochemical CO_2 reduction reaction in water with a TON of 613 and TOF of 47.15 h^{-1} .¹⁸⁰ During the reaction, water was oxidized to oxygen, while the electrons were released directly reducing CO_2 to formic acid without the addition of any photosensitizers or sacrificial electron donors. Also based on the strategy of utilizing released electrons from water oxidation to further reduce of CO_2 , in 2018, Roy and co-workers reported a giant polyoxometalate $\{\text{Mo}_{368}\}$ based homogeneous catalyst that efficiently reduced CO_2 to formic acid with a maximum TON of 27,666, a TOF of 4611 h^{-1} , an external quantum efficiency of 0.6% and excellent selectivity for formic acid production (95.73%).¹⁸¹ The $\{\text{Mo}_{368}\}$ is a photoactive material that absorbs UV-light ($\lambda = 373 \text{ nm}$) to generate holes (h^+) and electrons (e^-) in the system. The generated holes can oxidize

water to release electrons and protons which could further reduce CO₂ to formic acid.

For the practical utilization, the design of efficient heterogeneous catalysts is another major challenge in photocatalytic CO₂ reduction. In 2018, Liu et al. developed a visible light-driven hybrid photocatalyst Au@NENU-10, consisting of Au nanoparticles (NPs), Ti-substituted Keggin-Type POM [PTi₂W₁₀O₄₀]⁷⁻ (PTiW), and HKUST-1, for CO₂ photoreduction by a facile one-pot synthesis method.¹⁸² During the photocatalysis reaction, PTiW acted as both electron and proton reservoir, and the reactive active center was engaged into HKUST-1 to boost CO₂ reduction. HKUST-1 acted as a microreactor to concentrate CO₂ molecules, and Au NPs harvest visible light. Owing to the strong protonation of Ti=O and Ti-O-W, Au@NENU-10 showed high CO₂ reduction activity and selectivity under visible-light irradiation (> 420 nm) to the CO₂-to-CO conversion.

Wang and Sun et al. reported a noble-metal-free POM (Na₁₀Co₄(H₂O)₂(PW₉O₃₄)₂, **Co4**) with oxidative ability that were combined with g-C₃N₄ to form inexpensive hybrid materials (**Co4**@g-C₃N₄) with staggered band alignment. The obtained composited catalysts showed a higher activity of CO₂ reduction to CO than that of bare g-C₃N₄ with a highest yield reaching 107 μmol g⁻¹ h⁻¹ under visible-light irradiation (λ ≥ 420 nm) as well as high selectivity for CO production (94%). After 10 h of visible-light irradiation, the production of CO reached up to 896 μmol g⁻¹. Mechanistic analysis revealed the employment of **Co4** could facilitate the charge transfer of g-C₃N₄ as well as increased the surface catalytic oxidative ability.¹⁸³

The photocatalytic reduction of CO₂ to value-added CH₄ is promising but challenging research due to its necessary eight-electron transfer process. Recently, Lan and co-workers have reported an efficient photocatalytic CO₂-to-CH₄ reduction reaction for the first time in aqueous solution catalyzed by using two crystalline heterogeneous catalysts, NENU-605 and NENU-606, containing host inorganic polyoxometalate (POM) structures constructed with strong reductive {P₄Mo₆^V} units, homo/hetero transition metal ions (Mn^{II}/Co^{II}Mn^{II}) and alkali metal ions (K⁺ and/or Na⁺).³⁸ Notably, in the case of a photocatalytic reaction, the {P₄Mo₆^V} cluster containing six Mo^V atoms served as a multi-electron donor, the transition metal ions functioned as catalytically active sites for adsorbing and activating CO₂ molecules, and the presence of alkali metal ions assisted to capturing of more CO₂ (Fig. 20c). Additionally, as shown in Fig. 20b, NENU-606 containing hetero-metallic active sites finally exhibited high CH₄ generation selectivity of 85.5%.

More recently, Lan et al. have designed and synthesized a POMOF (NNU-29) with hydrophobic ligand and ε-{Zn₄P₄Mo₁₂O₄₀} cluster as a heterogeneous catalyst for photocatalytic reduction of CO₂.¹⁸⁴ The selective production of formic acid by NNU-29 under 16 h illumination in the water system is 97.9% under the hydrophobic group hindering the competitive reaction of hydrogen generation.

Very recently, Lan's group have presented two stable POM-grafted metalloporphyrin coordination frameworks (POMCFs, **NNU-13** and **NNU-14**) constructed with reductive Zn-ε-Keggin clusters and photosensitive TCPP linkers for high selective photo-reduce CO₂ into CH₄.¹⁸⁵ Notably, the introduction of Zn-ε-Keggin building blocks with strong reducing ability endows **NNU-13** and **NNU-14** facilitates the photocatalytic selectivity of CH₄ by theoretically delivering adequate electrons to accomplish the eight-electron reduction of the CO₂ molecule. To reveal the photo-excited charge carrier separation mechanism in these

porphyrin-based POMCFs catalytic systems, DFT calculation has been carried out. The partial density of states (PDOS) showed in Fig. 21 indicate that the photo-generated carriers of valence band (VB) and conduction band (CB) are mostly distributed on TCPP group and Zn-ε-Keggin cluster, respectively. Consequently, the photo-excited electrons more easily flow to POM port by efficient intercoupling between reductive Zn-ε-Keggin unit and TCPP linker. Assembling strong reducing component into visible-light sensitized photocatalyst architecture, can ignite research enthusiasm towards the construction of efficient POMCFs photocatalysts for highly selective reduction of CO₂ to CH₄ or other high-valued hydrocarbons. Thus, these POMCFs exhibit high photocatalytic CH₄ selectivity (> 96%) and activity that have far surpassed all the reported MCF-based photocatalysts.

POM-based photoelectrochemical catalysts

Due to the unique property that the POMs can multielectron redox reactions while their chemical structure keeps intact, they have been also widely used in the photoelectrochemical catalysis field, such as acting as electron transfer mediators to affect the photocurrent response of the photoanodes, and synergistically cooperating with semi-conductive photoanodes to achieve enhanced photoelectrochemical catalysis performance on organic pullet degradation or water splitting. The role of electron acceptors in semiconductor photocatalysis is critical in determining the overall photo-efficiencies, kinetics, and mechanisms. POMs can serve as electron acceptors and carriers in photoelectrochemical catalysis due to their excellent redox properties.^{186–188} Choi et al. investigated the behaviors of PW₁₂O₄₀³⁻/PW₁₂O₄₀⁴⁻ couple as electron transfer mediator in UV-illuminated suspensions of TiO₂ and Pt/TiO₂.¹⁸⁶ Although the POMs are less efficient compared with the conventional Fe³⁺/Fe²⁺ electron transfer mediator for the photocurrent generation in general, they have exhibited unique behaviors that are different from those of Fe³⁺.

By incorporating POMs into semi-conductive metal oxides can effectively increase the photocurrent response.^{189–194} Gao et al. synthesized a series of electrostatically self-assembled films by alternating adsorption of [P₂W₁₈M₄(H₂O)₂O₇₈]¹⁰⁻ (P₂W₁₈M₄, M = Ni, Cu, Zn) and a hemicyanine (E)-1,1'-(hexane-1,6-diyl)bis(4-(4-(dimethylamino)styryl)pyridinium) bromide (H⁶).¹⁸⁹ The (P₂W₁₈M₄/H₆)_n film-modified ITO electrodes generated stable cathodic photocurrents that could be efficiently tuned by changing the transition metal M in [P₂W₁₈M₄(H₂O)₂O₇₈]¹⁰⁻. Since P₂W₁₈M₄ acted as an electron shuttle, the energy level matching of ITO conduction band with LUMOs of [P₂W₁₈M₄(H₂O)₂O₇₈]¹⁰⁻ played a key role for photocurrent generation.

Xu et al. proposed a strategy to promote the photocurrent response of CdS via the photoinduced electron transfer from the CdS to POM (K₆P₂W₁₈O₆₂, P₂W₁₈).¹⁹⁰ The composite film of poly(allylamine hydrochloride)-modified CdS (CdS-PAH) and P₂W₁₈ prepared by the layer-by-layer (LBL) self-assembly method markedly enhanced the photocurrent response and power conversion efficiency in contrast with those of the single CdS-PAH film. Xie synthesized a polyoxophosphotungstate-titania/titanium (POW-TiO₂/Ti) hybrid electrode by encapsulating POW nanoaggregates into highly ordered TiO₂ nanotube array and studied its photoelectrocatalytic reactivities towards the degradation of an organic pullet (bisphenol A, BPA).¹⁹¹ Zhang et al. fabricated a graphene-CdS quantum dots-POM (rGO-CdS-H₂W₁₂) composite films by LBL assembly for the pollutant degradation.¹⁹² The photocurrent response of the rGO-CdS-

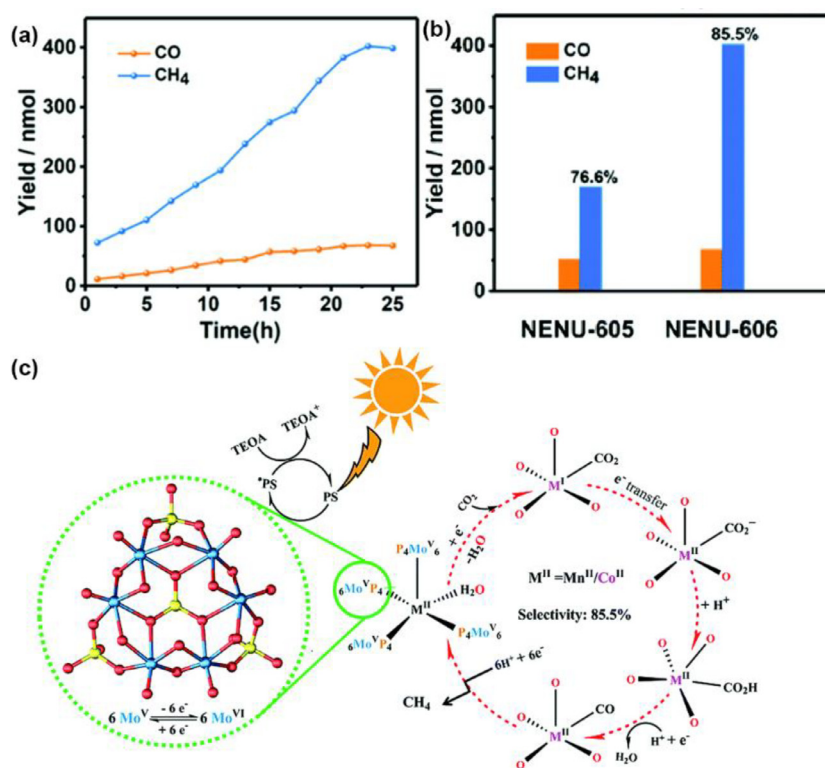


Fig. 20. Hetero-metallic active sites coupled with strongly reductive polyoxometalate for selective photocatalytic CO₂-to-CH₄ conversion in water. (a) Amounts of CH₄ and CO produced as a function of the time of visible-light irradiation using NENU-606, (b) total product yield and the selectivity of gaseous products in the photocatalytic CO₂ RR, and (c) proposed mechanism for the photocatalytic reduction of CO₂ to CH₄ using NENU-605 and NENU-606. Reproduced with permission.³⁸ Copyright 2019, Royal Society of Chemistry.

H₂W₁₂ composite film was enhanced five-fold compared with CdS film. The enhanced photoelectrochemical performance is attributed to the photoinduced electron transfer between CdS, H₂W₁₂ and rGO, which promotes the charge separation efficiency of CdS.

The hybrids composed of the semi-conductive metal oxides like TiO₂, WO₃, Fe₂O₃, *etc.* and POMs have been reported as efficient photoanodes for photoelectrochemical water oxidation,^{195–200} hydrogen evolution,²⁰¹ and water splitting.^{202–205} Ryu et al. successfully built a photoanode for solar water oxidation by depositing a thin film of diverse cationic polyelectrolytes and anionic POM water oxidation catalysts on the surface of various semi-conductive metal oxide photoelectrode materials (*e.g.* Fe₂O₃, BiVO₄ and TiO₂).²⁰⁵ It was demonstrated that the stability as well as photocatalytic properties of photoanodes could be significantly improved after the POM deposition, regardless of types of photoelectrodes and polyelectrolytes employed. Sun and Xu et al. proposed a non-precious ternary nanocomposite photocatalyst of TiO₂ nanotube/Co₉S₈/POM for photoelectrochemical water splitting.¹⁹⁶ In this proposed photoelectrochemical water oxidation system, the POM ((Bu₄N)₃PW₁₂O₄₀, PW₁₂) facilitated charge separation and Co₉S₈ acted as good electron transport mediator. The TiO₂/Co₉S₈/PW₁₂ composite photoanode exhibited an 8.5-fold and a 7-fold improvement of the photocurrent density at 1.23 V *vs.* RHE and the maximum photoconversion efficiency in the photoelectrochemical water oxidation, respectively, compared with the pristine TiO₂ nanotubes photoanode, which is mainly attributed to both the effective charge separation from PW₁₂ and the favorable electron transport from Co₉S₈. Furthermore, Sun and Xu et al. proposed

another investigation on POMs doping in BiVO₄ photoanodes for the enhancement of photoelectrocatalytic water oxidation properties of BiVO₄.¹⁹⁷ POMs-modified BiVO₄ exhibited different performance with different types and amounts of POMs. The BiVO₄/CoW₁₂ photoelectrode demonstrated the highest performance with 2.6-fold (at 0.7 V) increase in comparison with the pristine BiVO₄. The retarded electron-hole recombination and the facilitated charge separation and transfer by the incorporated POMs contributed to the improved photoelectrochemical performance.

More recently, Ryu and co-workers investigated the kinetics of photoelectrochemical water oxidation using a model photoanode BiVO₄ modified with various WOC including molecular POMs and the well-known WOCs like cobalt phosphate (CoPi) and NiOOH.¹⁹⁸ In particular, the BiVO₄ photoanodes were prepared using LBL strategy based on CMs in which polyelectrolytes and WOCs were assembled in a desired amount at a nanoscale precision. The EIS test results indicated that the separated charge carriers were efficiently transported to POM WOCs via a hopping mechanism due to the delicate architecture of the CMs. And the deposition of the CMs could efficiently improve the photoelectrochemical water oxidation performance.

Fabre and Cadot et al. recently reported a surface engineering method using POMs and conductive polymer modification for enhanced photoelectrochemical HER performance of MoS_x-based HER.²⁰¹ It was found that the covalent association between the {Mo₃S₄} core and the redox-active macrocyclic {P₈W₄₈} POM produced a striking synergistic effect featured by high HER performance, which was generated from the direct connection

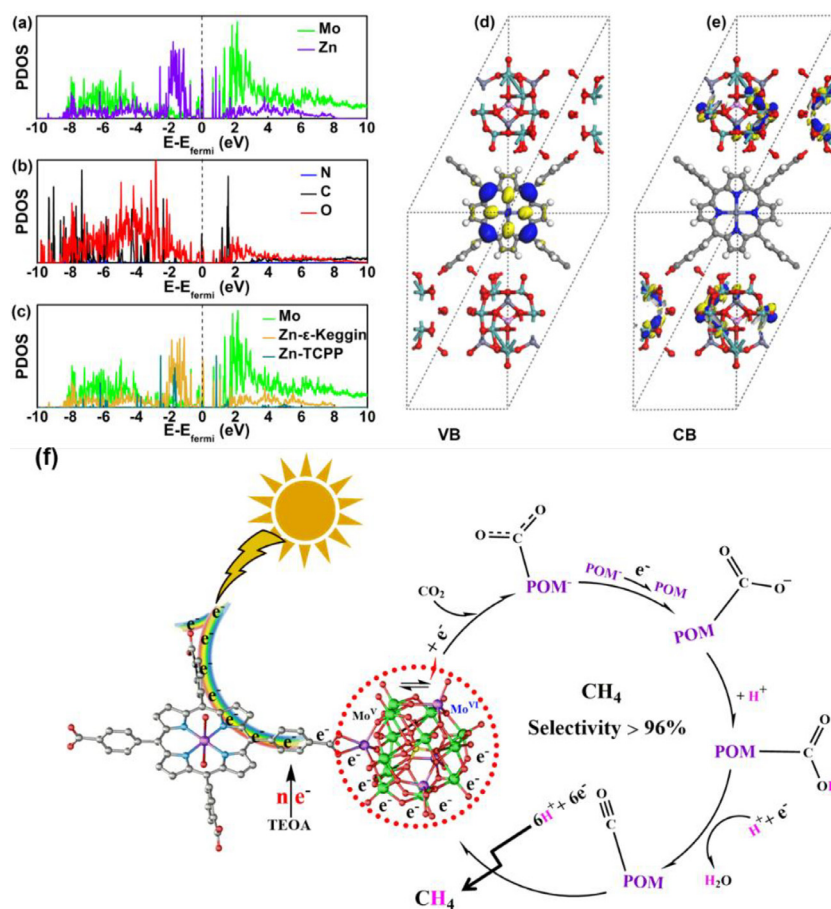


Fig. 21. Partial density of states (PDOS) of (a) Mo and total Zn atoms, (b) C, O and N atoms, (c) Mo atoms, Zn atoms in POMs and Zn atoms in TCPP. Partial charge density maps of (d) Valence band and (e) conduction band above the Fermi level for NNU-13. (f) Proposed mechanism for photocatalytic CO_2 reduction over POMCFs under visible-light irradiation. Reproduced with permission.¹⁸⁵ Copyright 2019, Oxford University Press.

between the $\{\text{Mo}_3\text{S}_4\}$ cluster and the toroidal $\{\text{P}_8\text{W}_{48}\}$ units. In addition, the electrostatic incorporation of the POM anion cocatalyst into a poly(3,4-ethylenedioxythiophene) (PEDOT) film was proved to be efficient and straightforward to durably retain the cocatalyst at the interface of a micropylamidal silicon (SimPy) photocathode. The thio-POM/PEDOT-modified photocathode could produce H_2 under 1 Sun illumination at a rate of *ca.* $100 \mu\text{mol cm}^{-2} \text{h}^{-1}$ at 0 V *vs.* RHE.

Solarska and co-workers reported a strategy based on bearing plasmonic Au nanoparticles with POM for enhanced water splitting at WO_3 film photoanodes.²⁰² The incorporated plasmonic Au NPs derivatized with $\text{H}_3\text{PMo}_{12}\text{O}_{40}$ species into WO_3 enhanced visible light conversion efficiency of WO_3 . Additionally, shielding the Au NPs with POMs was proven to be an effective means to avoid formation of recombination centers at the photoanode surface. Ryu et al. reported a solution processable bias-free photoelectrochemical cell for overall solar water splitting using a Cu_2O photocathode and a BiVO_4 photoanode modified with cationic polyelectrolyte and anionic molecular POM electrocatalysts through versatile layer-by-layer (LBL) assembly.²⁰³ The catalytic multi-layers (CMs) consisting of polyelectrolyte and anionic molecular POM catalysts facilitated charge transfer at the photo-electrode/electrolyte interface as well as suppressed the deactivation of photoelectrodes, especially a labile Cu_2O photocathode, by the formation of a protective coating layer.

An efficient and stable photoelectrochemical cell for unassisted solar water splitting without the use of toxic/hazardous chemicals and energetic processes was fabricated based on the proposed photoanodes.

Conclusions

The POM-based materials are emerging as one of the most promising photocatalysts for light-driven hydrogen production, water oxidation and CO_2 reduction due to their adjustable components, wide variety of redox metal centers and well-defined structure. Great progress has been made in these fields, such as the successful preparation of POM-based homogeneous molecular WOC catalysts, the strategy of trapping POMs into MOF structure to obtain effective heterogeneous light-driven catalysts, and the realization of a water-splitting reaction as the source of electrons and protons for CO_2 reduction process. However, the catalytic efficiencies of the currently reported photocatalysts for hydrogen production and water oxidation are still far from the requirement for the potential practical utilization. Therefore, the rational design of POM-based photocatalysts with high activity and stability should be conducted by taking insight into correlativity between the catalytic reactivity and the catalysts properties. And more robust synthetic methodologies will be vital for understanding the true active sites and the improvement of the heterogeneous water oxidation catalysts. The

POM-based catalysts for overall water splitting by photocatalysis are rarely reported, calling for more research work to be devoted. In addition, to obtain high-value multi-carbon products from CO₂ by photocatalytic reduction is one of most promising strategies for fuel and chemical production. The enhancement of the catalytic activity and selectivity of POM-based catalysts for CO₂ reduction via deeply studying the reaction routes and catalytic mechanisms is critical but rarely reported. More POM-based photocatalysts with well-defined structure need to be presented to act as typical models and give a picture on how to construct effective catalysts. Compared with the electrocatalysis process, photocatalytic reaction is more complicated since it usually involves co-catalysts or photosensitizers. Therefore, the achievement of simplification of the photocatalysis systems by developing multifunctional catalysts with single reduction product may be another challenge in this field. While there are some hurdles to overcome, more and more investigations show the advantages of POMs in the photocatalysis field and much more effort is needed to achieve photocatalytic processes with high efficiency.

■ POM-BASED ENERGY STORAGE AND CONVERSION DEVICES

The development of effective energy storage systems is another essential aspect to relief currently global energy situations. Electrochemical energy storage devices, including lithium/sodium ion battery, lithium sulfur battery, supercapacitors, and so on, have been proved to be promising alternative energy storage systems for daily life, especially Li-ion batteries and supercapacitors have been commercially utilized in practice.⁴ On account of the ability of POMs to undergo a large number of redox processes in a reversible fashion, POMs and their hybrids have been investigated as potential energy storage devices, including solid-state batteries (and battery electrodes) with Li⁺ and Na⁺ as charge carriers, and in redox supercapacitors.

POM-based rechargeable lithium ion batteries

Rechargeable lithium ion batteries (LIBs) are currently the dominant power source for portable electronic devices and electric vehicles, and for small-scale stationary energy storage.²⁰⁶ Owing to their multi-electron redox-chemistry, POM-based materials have been widely used for the construction of rechargeable Li-ion batteries. Herein, we have reviewed the research works reported from 2011 up to now, and give a complete summary on the POM-based materials using as lithium ion battery electrode materials, including POM, POM-carbon hybrids, POMOFs and so on.

POMs as electrode materials for lithium ion batteries

The first report on POM as component for rechargeable battery was focused on polyoxomolybdates.²⁰⁷ For the further application of POMs in Li-ion batteries, the structure and electronic state of POMs have been studied by *in-situ* X-ray absorption fine structure analyses to revealed their instinct redox properties in advance.^{208–210} In 2012, Yoshikawa and cooperators carried out *in operando* Mo K-edge X-ray absorption fine structure measurements on the rechargeable molecular cluster batteries (MCBs) of a Keggin-type POM, [PMo₁₂O₄₀]^{3−}, to revealed the evolution of the oxidation state and the local structure of Mo ions of the POM molecule in the battery reaction.²⁰⁸ As shown in Fig. 22, their study on X-ray absorption near-edge structure analyses suggested that all 12 Mo⁶⁺ ions in [PMo₁₂O₄₀]^{3−}

were reduced to Mo⁴⁺ with a reversible 24-electron redox during charging/discharging, which was account for the resulting experimental large capacity of *ca.* 270 Ah kg^{−1} in a voltage range between 4.0 to 1.5 V. Moreover, extended X-ray absorption fine structure analyses revealed the molecular structure of reductive state, [PMo₁₂O₄₀]^{27−}, was a slight shrinkage in molecular size from [PMo₁₂O₄₀]^{3−} and involved Mo⁴⁺ metal-metal-bonded triangles. The DFT calculations demonstrated that these triangles were formed because of the large number of additional electrons in the super-reduced state. Their research revealed the “electron sponge” behavior characteristic of POMs, indicating their potential to be promising cathode active materials for high-performance rechargeable batteries.

However, the [PMo₁₂O₄₀]^{3−} POMs have been proved to be unstable during the charging/discharging processes with capacities in excess of 200 mAh g^{−1} obtained after 10 cycles at a low current of 1 mA due to the limitation by the slow rate of charge/discharge.^{211,212} Due to the low atomic weight of Vanadium (50.96 g mol^{−1}) compared with the traditional POM metals Molybdenum (95.96 g mol^{−1}) and Tungsten (183.84 g mol^{−1}) which enables higher gravimetric energy densities, the polyoxovanadates (POVs) have been enormously investigated in rechargeable batteries. In 2015, Dong and Cronin et al. showed a vanadium-based POM (Li₇[V₁₅O₃₆(CO₃)]) as excellent cathode material candidates, exhibiting high capacities and rapid charging/discharging with a larger operating voltage than the POMs previously explored.²¹³ They found that the {V₁₅O₃₆} clusters containing the eight V^{IV} centers and seven V^V centers showed multielectron redox properties suitable for producing cathode materials. And the Li₇[V₁₅O₃₆(CO₃)] had a specific capacity of 250 mAh g^{−1}, energy densities and power densities of 1.5 kWh L^{−1} and 55 kW L^{−1} respectively in Li-based batteries. Zhang and Ueda et al. also developed a series of vanadium (V)-incorporated, inorganic POM-based open framework materials comprising ϵ -Keggin POM units with transition metal ion linkers via hydrothermal method for the Li-ion batteries cathode materials.²¹⁴ The content of the V introduced into the framework could be adjusted by initial V molar ratio in the precursor. After the 20th cycle of the charge-discharge process, the materials were transformed to the Li₂MoO₄ phase, which might be reason for the stable electrochemical performance of the V-incorporated sample. Then, Yoshikawa and Ueda et al. reported a microporous Mo-V-Bi oxide based cathode for Li battery and gave a detailed investigation by *operando* X-ray absorption fine structure to reveal the charging/discharging mechanism.²¹⁵ They proposed the strategy of incorporating a third metal ion in crystalline Mo-V complex oxides (**orth-MoVO**) to enhance the stability of the material and obtained a stable crystalline microporous complex metal oxide based on Mo, V, and Bi. The prepared Mo-V-Bi-O exhibits a high capacity of 380 Ah kg^{−1} as Li battery cathode. In 2018, Dong and Cronin et al. employed the previously reported {V₁₅O₃₆(CO₃)} as the active material in both the cathode and the anode in symmetrical Li-ion batteries to obtain the device with battery-like energy density and supercapacitor-like power density.²¹⁶ An ultrahigh specific power of 51.5 kW kg^{−1} at 100 A g^{−1} and a specific energy of 125 Wh kg^{−1} was achieved, along with a long cycling life (>500 cycles).

Additionally, the thermally dehydrated POVs have been used widely in Na-ion batteries.²¹⁷ However, more recently, in 2019, the study of Sterb et al. demonstrated that the prototype molecular vanadium oxide clusters, POVs, are unstable under typical battery electrode fabrication conditions, and even at moderate

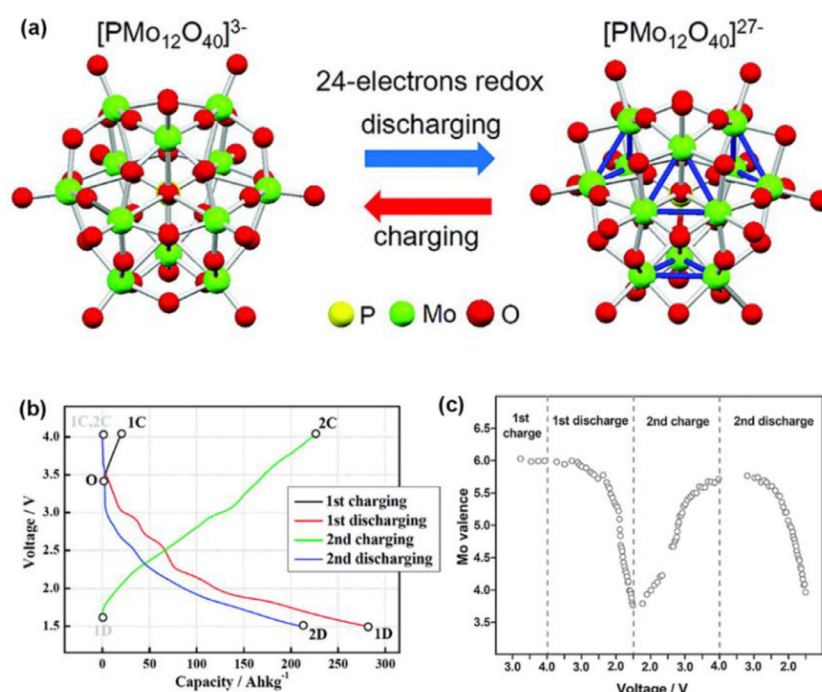


Fig. 22. (a) Schematic illustration of $[\text{PMo}_{12}\text{O}_{40}]^{3-}$ as “electron sponge”. (b) Charging and discharging curves of $\text{PMo}_{12}/\text{Li}$ MCBs during XAFS measurements. (c) Averaged Mo valence of PMo_{12} in the PMo_{12} MCBs as a function of the cell voltage (V). Reproduced with permission.²⁰⁸ Copyright 2012, American Chemical Society.

temperatures undergo irreversible structural reorganization into layered solid-state lithium vanadium oxide structures.²¹⁸ Therefore, the stabilization of molecular vanadium oxides clusters as active materials in lithium and sodium-ion batteries should be further investigated to explore the true performance of these molecular species as battery electrodes.

POMs-based composites as electrode materials for lithium ion batteries

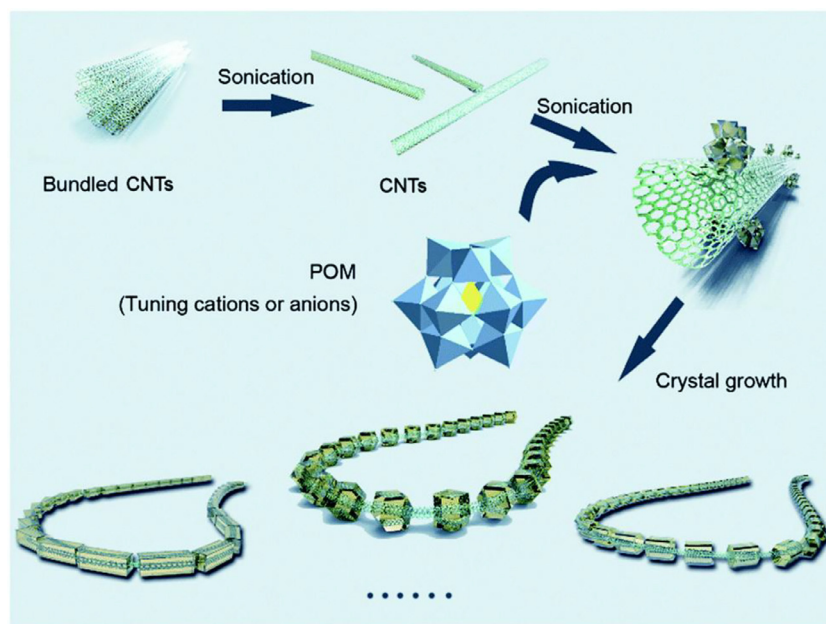
Although the well-defined structure and rich redox properties make the POMs as effective electrode materials, the stability and life-time of the POMs during charging and discharging processes, usually less than 100 cycles or tested at low current densities, still prohibits their further application. Additionally, the non-nanoscale uneven dispersion of the POM clusters results in the poor rate performance due to the sluggish electron transfer between the material and electrode. Therefore, a wisdom method of combining POMs with other materials that possess large surface area or porous structure, such as conductive matrix or MOF support, has been put forward to alleviate these issues.

The chemically modified nanocarbon materials with cationic functional groups could serve as substrate for the attachment of the anionic POM clusters via covalent interaction or electrostatic adsorption. In 2011, to achieve smooth electron transfer and quick lithium-ion diffusion, Yoshikawa and Awaga et al. developed a nanohybrid system with Keggin-type POM clusters ($\text{TBA}_3[\text{PMo}_{12}\text{O}_{40}]$, $\text{TBA} = [\text{N}(\text{CH}_2\text{CH}_2\text{CH}_2\text{CH}_3)_4]^+$) and single-wall carbon nanotubes (SWNTs) in which individual POM molecules were adsorbed onto the surfaces of SWNTs without chemical decomposition.²¹⁹ The hybrid material indicated a higher battery capacity and faster charging/discharging compared with those of the microcrystalline POMs. Then, they proposed other SWCNT/POM-based cathodes and further studied the

effects of the counter cations of the Keggin-POM on the nano-hybridization with SWNTs and on the battery performance.²²⁰

Song's group also have reported on a series of POM/carbon nanotube-based composites for the high-performance Li-ion battery anode materials.^{221–225} In 2013, the noncovalent sidewall functionalization of SWNTs by a covalently modified POM-pyrene hybrid (Py-SiW_{11}) was carried out.²²¹ The resulting SWNTs/ Py-SiW_{11} nanocomposite demonstrated that both SiW_{11} and pyrene moieties could interact with SWNTs without causing any chemical decomposition. And the sidewall defects of SWNTs by introducing Py-SiW_{11} , together with the highly conductive SWNTs shortened the diffusion length of lithium ions and led to the efficient electron and energy transfer between Py-SiW_{11} and SWNTs, making the composite a robust anode material for Li-ion battery. The SWNTs/ Py-SiW_{11} nanocomposite presented a high discharge capacity of 580 mAh g^{-1} after 100 cycles at 0.5 mA cm^{-2} . In 2016, Song and Streb et al. developed another sonication-driven strategy to obtain 1D periodically patterned POM/CNT composites (Scheme 7).²²⁵ The control over the amount, size and morphology of crystals deposited on CNTs was achieved by adjusting the experimental parameters of ultrasonication time and power intensity. Furthermore, the type of cation and anion deposited can also be varied by employing different POM salts. Taken as an example, the as-fabricated POM/CNTs composite of $\text{TBA-PMo}_{11}\text{V}/\text{CNTs}$ showed stable discharge capacities of 850 mA h g^{-1} at 0.5 mA cm^{-2} after 100 cycles.

With the high conductivity, large surface area, and the unique two-dimensional structure, graphene and its derivatives, like reduced graphene oxide (RGO) or graphene oxide (GO), have been used as matrix for supporting POM-based materials.^{226–229} In 2014, Yoshikawa and Awaga et al. studied the electrochemical properties of a nanohybrid system of POM and RGO, in which individual POM molecules were adsorbed on the RGO surfaces.



Scheme 7. Schematic representation of the ultrasonication-driven periodic patterning of POM nanocrystals on CNTs. Reproduced with permission.²²⁵ Copyright 2016, Royal Society of Chemistry.

Serving as cathode active material for molecular cluster battery, the POM/RGO hybrid exhibited a higher battery capacity than the POM/SWNT and the microcrystal POM.²²⁹ In 2016, Li and co-workers reported hybrids consisting of cluster like POM and EDA (ethylenediamine) decorated RGO as high-capacity and long-life Li-ion battery anodes (Fig. 23).²²⁶ The high loading and low solubility of the POMs were achieved by Al- or Si-driven polymerization and hybridization with positively charged graphene, which immobilized polyanions of POMs and improved their electric contact. The proposed Al-based POM composite (NAM-EDAG) for Li-storage achieved a high reversible capacity of 1000 mAh g⁻¹ and endured a long-term cycling with 1100 cycles at a high current density of 20 A g⁻¹ (Fig. 23d). And in 2018, Lan et al. proposed a “killing two birds with one stone” strategy of introducing ionic liquids (IL) for the fabrication of POMs/IL/RGO composite, in which the IL not only facilitated the formation of heterogeneous nanocrystalline composites but also acted as the template reagent to feature the morphology of homogeneous nanobelts on the RGO.²²⁷ The targeted composite Mn₃V₁₉-HIL/RGO-1 showed good cycling stability and the best ultrafast rate capabilities with capacities of 121 mA h g⁻¹ at 5 A g⁻¹ and 73 mA h g⁻¹ at 2 A g⁻¹ for lithium and sodium ion batteries, respectively.

Conductive polymers have been chosen for loading POMs as Li-ion batteries electrode materials as well due to their excellent conductivity and ease functionalization.^{230–232} In 1998, Gómez-Romero and co-worker synthesized hybrid materials based on a polyaniline (PANI) matrix with the phosphomolybdate anion (PMo₁₂) as the only doping species and explored their electrochemical properties as cathode for Li ion battery.²³³ In 2013, Paik and Kwon et al. prepared polyaniline/POM hybrid (PANI/PMo₁₂) nanofibers as cathode for Li-ion batteries by a facile interfacial polymerization method.²³² The fabricated nanofibers composing by phosphomolybdic acid polyanion, [PMo₁₂O₄₀]³⁻, and PANI matrix displayed a uniform diameter of 100 nm. The 1D structure could improve the utilization

of electrode materials and accommodate the volume change during cycling. The PANI/PMo₁₂ hybrid delivered better battery performance with a capacity of 183.4 mAh g⁻¹ at 0.1 C rate, cycling stability with 80.7% capacity retention after 50 cycles, and rate capability of 94.2 mAh g⁻¹ at 2 C rate, compared to polyaniline nanofibers and bulk polyaniline/polyoxometalate hybrid.

POMs are ideal building blocks as alternatives to metal ions for the construction of novel metal-organic frameworks (MOFs). POM-based MOF materials have attracted extensive interest due to their functional integrated and synergic effects.^{234,235} During the process of building MOF/POM hybrid, POMs usually act as anionic templates/structure-directing agents through host-guest supramolecular interactions.^{236,237} To improve the cycling performance of Li-ion battery anodes, in 2015, Yue and Dai et al. constructed the first POMOF anode of an extended 3D network architecture composed of flexible redox active POM clusters with redox active organic linkers.²³⁸ The architecture of the proposed POMOF anode with an intrinsic pore structure enables ion diffusion and the accommodation of large volume changes during cycling at relatively high current rates. Consequently, the POMOF anode showed an exceptional cycling stability of >500 times cycling at a current rate of 1.25 C with a well-maintained building units and local structure of this anode during lithiation and delithiation processing.

Sha and Jiang et al. fabricated POM based metal-carbene frameworks (POM-based MCFs) [Cu₁₀(H₃trz)₄(Htrz)₄](HPW₁₂O₄₀) (**1**) and [Cu₁₀(H₃trz)₄(Htrz)₄](H₂SiW₁₂O₄₀) (**2**) by a hydrothermal reaction between 1,2,4-triazole and Cu(CH₃COO)₂ with the saturated Keggin polyoxoanion [PW₁₂O₄₀]³⁻/[SiW₁₂O₄₀]⁴⁻ as a template.²³⁹ The as-prepared 3D POM-based MCFs showed good electrochemical performance in Li-ion batteries as anode materials, with first discharge capacities of ca. 1620 and 1245 mA h g⁻¹ for **1** and **2**, respectively, at a current density of 100 mA g⁻¹, and stabilized discharge capacities of ca. 570 mA h g⁻¹ for **1** and 426 mA h g⁻¹

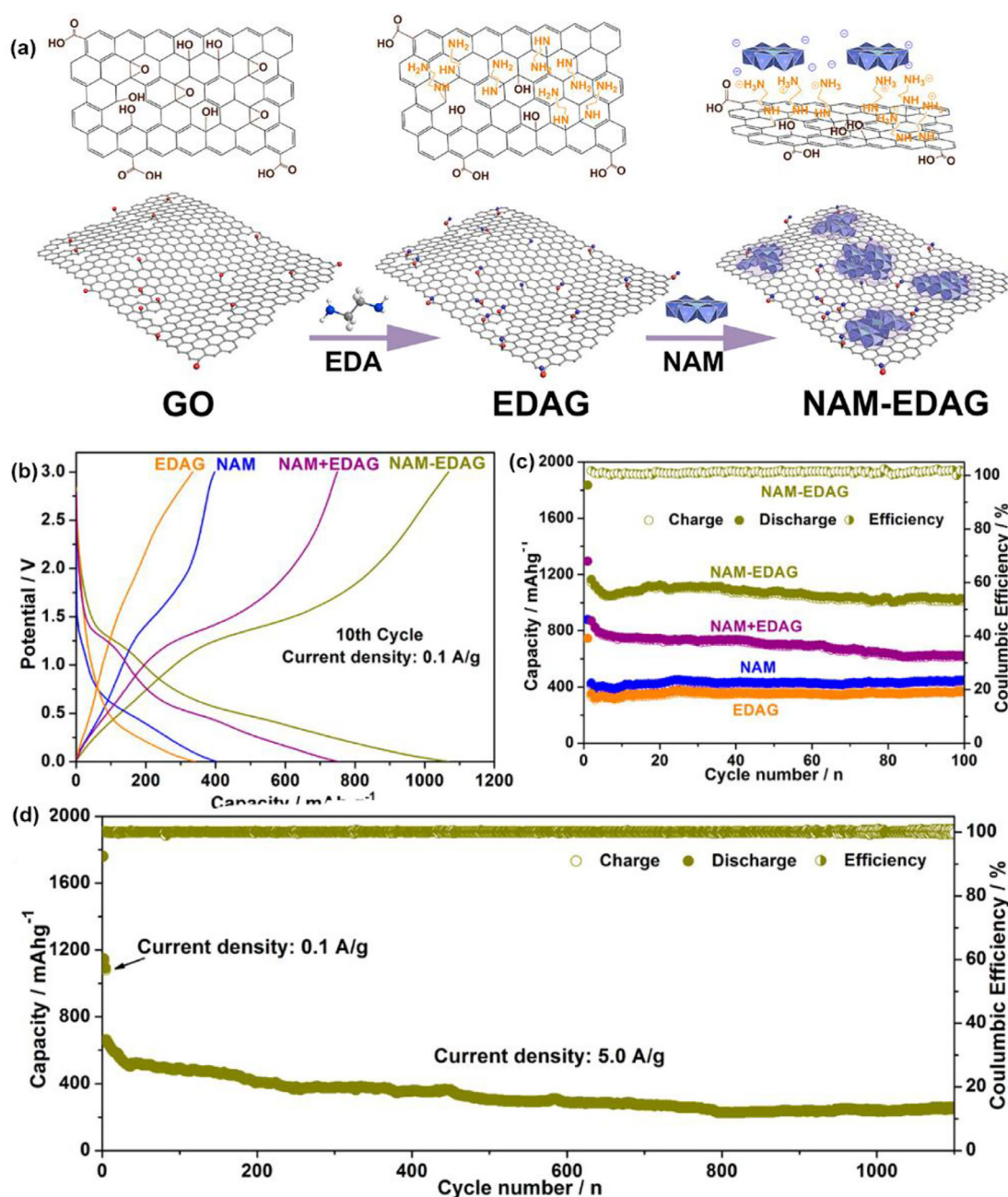


Fig. 23. (a) Preparation procedure of the NAM-EDAG composite. (b) NAM-EDAG anodes during the first ten cycles at 100 mA g^{-1} in a voltage range of 0–3 V. (c) Charge/discharge capacity and Coulombic efficiency of corresponding anodes as a function of cycle number at 100 mA g^{-1} . (d) Cycling performance of NAM-EDAG at 5.0 A g^{-1} after a few cycles at 100 mA g^{-1} . Reproduced with permission.²²⁶ Copyright 2016, American Chemical Society.

for 2 after 100 cycles. More recently, their group constructed a highly stable POM-containing nanocage based MOF (Zn-POMCF) by precisely choosing the suitable POMs as nodes and regulating the size of a metal-organic macrocycle through the surfactant-assisted method.²⁴⁰ Serving as an anode material for Li-ion battery, Zn-POMCF showed a capacity as high as 1294 mA h g^{-1} for the first discharge and a maintained capacity of 500 mA h g^{-1} after 200 cycles at a current density of 100 mA g^{-1} .

Lan's group has proposed several research works committing to the synthesis of POM-based MOF with high stability for Li-ion battery anode materials.^{241–246}

In 2017, Lan et al. reported on a POMOF, $[\text{PMo}^{\text{V}}_8\text{—Mo}^{\text{VI}}_4\text{O}_{37}(\text{OH})_3\text{Zn}_4][\text{TPT}]_5\cdot 2\text{TPT}\cdot 2\text{H}_2\text{O}$ (**NNU-11**, TPT = tris-(4-pyridyl)triazine), in which the Zn- ϵ -Keggin fragments were directly connected with TPT ligands generating 2D layers and further interdigitated with each other by π - π stacking interactions to pack into a 3D array.²⁴¹ The synthetic compound was highly stable in air, different organic solvents as well as aqueous solution from pH 1.0 to 11 due to the support by π - π stacking interactions. Employed as anode for Li-ion batteries, **NNU-11** showed excellent electrochemical performance due to the multi-electron redox property of POM units and the functionalization of MOFs, delivering a reversible

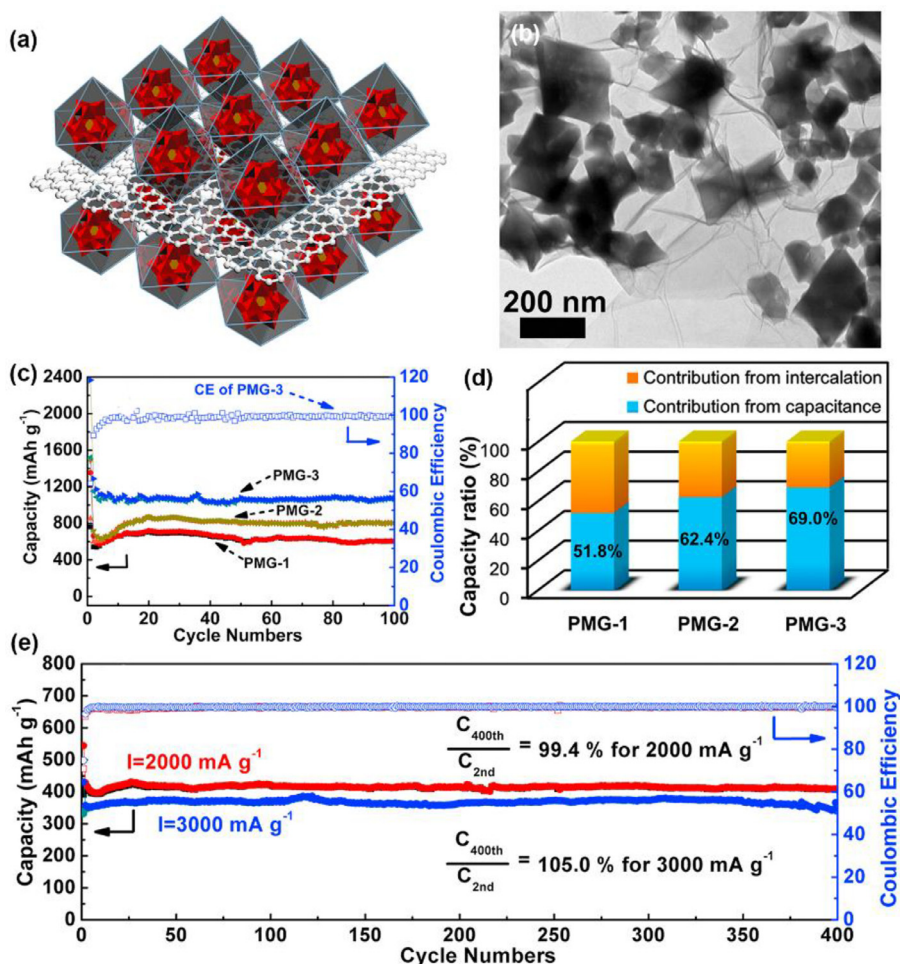


Fig. 24. (a) Schematic diagram of PMG nanocomposites, (b) TEM image of PMG-3, (c) cycling performance of PMG-1 to PMG-3 at a current density of 50 mA g⁻¹. (d) Comparison of capacity ratio for PMG nanocomposites (0.5 mV s⁻¹ sweep rate). The total capacity is separated into lithium intercalation and capacitive contributions. (e) Stability test of PMG-3 for 400 cycles at 2000 mA g⁻¹ and 3000 mA g⁻¹, respectively. Reproduced with permission.²⁴³ Copyright 2017, Elsevier.

capacity of 750 mA h g⁻¹ at f 50 mA g⁻¹ after 200 cycles along with good cycle stability and rate performance. Additionally, the employment of the POMOF crystalline structure model with intermolecular π - π stacking interactions to demonstrate the interesting behavior was demonstrated for the first time.

To further enhance the conductivity and stability of POMOF anode materials, Lan et al. prepared a POM-based MOF/reduced graphene oxide (PMG) nanocomposites for superior lithium storage (Fig. 24).²⁴³ H₃PMo₁₀V₂O₄₀ (PMo₁₀V₂) with stronger redox properties was adopted to increase the redox potential of the first electron transfer reaction, HKUST-1 was introduced to support the POM, and rGO was selected as substrate to prevent the nano-POMOFs particles from the agglomeration. Due to the synergic effect of POM, MOF, and rGO, the prepared composite showed ultra-stable electrochemical performance with a reversible capacity of 1075 mAh g⁻¹ maintained after 100 cycles, and negligible loss of capacity at 2000 and 3000 mA g⁻¹ for over 400 cycles as shown in Fig. 24c and e. In addition, the prepared PMG composite showed the cooperative capacity of battery-supercapacitor behavior for superior lithium storage and the contribution of lithium intercalation and capacitive was presented as well (Fig. 24d).

POMs-derived composites as electrode materials for lithium ion batteries

POMs are also promising precursors for the development of the Li-ion battery electrode materials because of their abundant transition metal species component.^{247–250} In 2016, Wang et al. reported the controlled synthesis of hierarchical MOF crystal nanotubes by using POMs as structural modulators during the nucleation and growth processes.²⁴⁸ The sodium phosphotungstate (Keggin-type POM, NaPW₁₂) was selected for preparation of MOF nanocrystals with the iron and cobalt ion as metallic nodes, 1,3,5-benzenetricarboxylic acid (H₃BTC) as the organic linker, and a N,N-dimethylformamide (DMF)/decanol mixture as the solvent, via a solvothermal process. A core-shell formation mechanism of the prepared Fe/Co-BTC nanotubes was proposed. And the POM was confirmed to be incorporated in the MOF structure with well-maintained component. By annealing the prepared Fe/Co-BTC, the obtained mixture of carbon, iron/cobalt oxide, and tungstates was adopted as a LIB anode material showing remarkable cycling stability. Chen and co-workers also used annealing treatment to obtain a MoO₂@C nano-octahedrons by using a POMOF as precursor.²⁴⁷ The annealing strategy ensured the *in-situ* formation of a porous carbon matrix that could increase active sites to store redox

ions and increase the ionic diffusivity of the encapsulated MoO_2 nanoparticles. The MoO_2/C composite delivered a reversible specific capacity of 1442 mA h g^{-1} after 50 cycles at 100 mA g^{-1} and $443.8 \text{ mA h g}^{-1}$ after 850 cycles at 1000 mA g^{-1} as an anode material for Li ion battery.

By the self-sulfuration and self-carbonization of POM $[\text{PMo}_{12}\text{O}_{40}]^{3-}$ complex with dithiooxamide (DTO) or L-cysteine via pyrolysis, Li et al. reported a $\text{MoS}_2\text{-C}$ composite with the MoS_2 nanobubbles conformally encapsulated by thin P, N-doped carbon layers.²⁵¹ The seamless welding between the carbon coating and the surrounding broader carbon substrate can effectively avoid the peel-off of MoS_2 active species and breakage of the conductive network. The reversible capacity of $\text{MoS}_2\text{-C}$ by pyrolyzing the POM-DTO chelate can reach $1500 \sim 2000 \text{ mAh g}^{-1}$ at $0.5 \sim 1 \text{ A g}^{-1}$ even after 700 cycles and be maintained around 1000 mAh g^{-1} under as high as $10 \sim 20 \text{ A g}^{-1}$, which is superior to most MoS_2 -based anodes for Li-storage performance. The summary of POM-based electrode materials for lithium ion batteries reviewed in this work is exhibited in Table 3.

POM-based supercapacitors

Supercapacitor, a typical high-power density device lying between the conventional capacitors and batteries, has become an indispensable auxiliary energy storage system in various fields, such as electrical vehicles and emergency energy supply equipment, among others.^{252–254} The supercapacitor electrode materials benefit from both electrical double layer capacitance (EDLC) and faradaic pseudocapacitance by electrolyte ions adsorption on the electrode surface and reversibly redox reactions of material, respectively. Owing to the well-defined structure, tunable redox properties, and excellent protonic conductivity, POM-based materials have become an inexpensive choice for the proton-insertion pseudocapacitance materials and have been demonstrated for the applications in supercapacitor electrodes.

In 1998, Goodenough et al. firstly introduced a Keggin-type heteropolyacid of 12-molybdophosphate as electrode material for an asymmetric electrochemical supercapacitor by using a proton-exchange membrane to prevent the dissolution of the reduced electrode.²⁵⁵ Although the proposed capacitor system did not show a satisfactory performance compared to the RuO_2 symmetric capacitor, this research opened a new chapter to optimize the voltage of supercapacitors by proper choice of two different transition metal oxides at the anode and cathode. After that, various strategies, including doping POM ions into the conductive polymers,^{256–259} designing the hybrids of POMs with nanocarbon additives,^{260–263} or adopting special electrolyte to stabilize the POMs,^{264,265} etc. have been proposed to develop efficient POM-based electrodes for supercapacitors.

POM/conductive polymer composites as supercapacitor electrodes

Because of their reversible redox chemistry and conductivity, good processability and reasonably low cost, conductive polymers are ideal candidates for POMs integration. The POM-modified conductive polymer composites attract much attention due to the homogeneous distribution of POM ions in the polymers which can enhance both the capacitance performance and the conductivity of the electrode.^{266–270} Freund et al. designed an asymmetric conducting polymer/polyoxometalate (POM) supercapacitor using polypyrrole (Ppy)/phosphomolybdic acid (PMA) and

poly(3,4-ethylenedioxythiophene) (PEDOT)/phosphotungstic acid (PTA) as electrode materials, which was a significant improvement over earlier symmetric systems that had PPy/PMA for both electrodes.²⁵⁷ However, the PPy/PMA//PEDOT/PTA system suffered from a drift of the absolute potential during long-term test due to the unstable structure of the fabricated POM-polymer composites. Lee et al. proposed another ordered POM-PPy nanopillar array with enhanced stability by soft lithography and subsequent electrodeposition.²⁵⁹ The as-prepared POM-PPy nanopillar films with unique structure exhibited superior electrochemical performances for pseudocapacitor and excellent cycle life of $\sim 100\%$ retention over 3500 cycles even when bent. Furthermore, Timo and co-workers took insight into tailoring the molecular-level linkage of charge transport parts and charge storage components via the study of POM-polymer systems.²⁵⁶ By systematically exploring the structural and electronic consequences of embedding a series of isostructural Lindqvist anions $[\text{V}_n\text{M}_{6-n}\text{O}_{19}]^{(2+n)-}$ ($= \{\text{V}_n\text{M}_{6-n}\}$, $\text{M} = \text{W(VI)}$ or Mo(VI) ; $n = 0, 1, 2$) in cationic PPy films, the electrochemical experiments together with the *in situ* (spectro-)electrochemistry and theoretical computations showed that a reductive electrochemical activation route of the Lindqvist-PPy composites could lead to significantly enhanced capacitance performance compared to the pure PPy.

The POM-based MOFs comprising merits of both components are promising candidates for supercapacitor electrodes. Lan et al. fabricated the first POMOF/conductive polymer symmetric supercapacitor device based on a NENU-5/PPy nanocomposite.²⁵⁸ The prepared POMOF, NENU-5, with the incorporation of PMo_{12} into MOF, can efficiently remain the electron storage ability of the PMo_{12} and simultaneously prevent its dissolution in electrolyte as well. Due to the good electroconductivity, appropriate surface area, porosity, and rich active sites, the NENU-5/PPy electrode delivered areal capacitance of 1879 mF cm^{-2} , excellent rate performance and long-term stability.

POM/carbon composites as supercapacitor electrodes

Expect for conductive polymers, the nanocarbon materials with high electrical conductivity, such as carbon nanotubes,^{271,272} activated carbon,^{273,274} graphene,²⁷⁵ and biomass derived carbon,²⁷⁶ are another vital kind of additives to improve the capacitive activity of POM-based electrodes. The synergy between carbon matrix with large surface area and POMs with facile redox process not only contributes both EDLC and pseudocapacitance to capacitive enhancement, but also leads to special properties of each part. Zhang et al. prepared a highly stable POM based hybrid of MoS/rGO .²⁶¹ The DFT calculations uncovered the affinity between MoS or its neutral form with graphene, which indicated that the strong interaction between them led to the coexistence of both redox activity and stability of the composites.

Gomez-Romero et al. proposed the researches on combination of Keggin-type POMs with several carbon-based materials for supercapacitor application. They developed PMo_{12} -adsorbed activated carbons as electrodes for supercapacitors for the first time.²⁷³ The presented hybrid combined double-layer capacitance and redox activity when applied in supercapacitor and showed much higher specific capacitance in contrast with the unmodified activated carbon. Another model composing of the rGO and PMo_{12} was subsequently developed for application in hybrid supercapacitors.²⁷⁵ The PMo_{12} nanoclusters homogeneously distributed on the rGO matrix after hydrothermal

Table 3. Summary of POM-based electrode materials for lithium ion batteries reviewed in this work.

Electrode Materials	Electrode	Initial Discharge Capacities of Active Materials	Rate Performance	Cycling Stability	Ref.
Li ₇ [V ₁₅ O ₃₆ (CO ₃)]	cathode	250 mA h g ⁻¹ @50 mA g ⁻¹	170 mA h g ⁻¹ @2 A g ⁻¹ , 140 mA h g ⁻¹ @10 A g ⁻¹	82%, 100 cycles@2 A g ⁻¹	213
Mo-V-Bi-O	cathode	380 A h kg ⁻¹ @1 mA cm ⁻²	380 A h kg ⁻¹ @1 mA cm ⁻² , 170 A h kg ⁻¹ @10 mA cm ⁻²	92%, 20 cycles@1 mA cm ⁻²	215
TBA ₃ [PMo ₁₂ O ₄₀]/SWNT	cathode	320 Ah kg ⁻¹ @1 mA g ⁻¹	N/A	94%, 10 cycles@1 mA g ⁻¹	219
SWNTs/Py-SiW ₁₁	anode	1570 mA h g ⁻¹ @0.5 mA cm ⁻²	920 mA h g ⁻¹ @0.05 mA cm ⁻² , 360 mA h g ⁻¹ @1 mA cm ⁻²	37%, 100 cycles@0.5 mA cm ⁻²	221
CNTs-SiW ₁₁	anode	1189 mA h g ⁻¹ @0.5 mA cm ⁻²	802 mA h g ⁻¹ @0.05 mA cm ⁻² , 584 mA h g ⁻¹ @1 mA cm ⁻²	55%, 100 cycles@0.5 mA cm ⁻²	222
Py-Anderson-CNT	anode	1899 mA h g ⁻¹ @0.5 mA cm ⁻²	1072 mA h g ⁻¹ @0.05 mA cm ⁻² , 480 mA h g ⁻¹ @1 mA cm ⁻²	35%, 100 cycles@0.5 mA cm ⁻²	223
SWNT/Anderson	anode	932 mA h g ⁻¹ @0.5 mA cm ⁻²	1351 mA h g ⁻¹ @0.05 mA cm ⁻² , 654 mA h g ⁻¹ @1 mA cm ⁻²	40%, 100 cycles@0.5 mA cm ⁻²	224
TBA-PMo ₁₁ V/CNTs	anode	3014 mA h g ⁻¹ @0.5 mA cm ⁻²	1532 mA h g ⁻¹ @0.05 mA cm ⁻² , 565 mA h g ⁻¹ @1 mA cm ⁻²	28%, 100 cycles@0.5 mA cm ⁻²	225
NAM-EDAG	anode	1835 mA h g ⁻¹ @100 mA g ⁻¹	1100 mA h g ⁻¹ @100 mA g ⁻¹ , 400 mA h g ⁻¹ @10 A g ⁻¹	35%, 1000 cycles@5 A g ⁻¹	226
Mn ₃ V ₁₉ -HIL/RGO	cathode	214 mA h g ⁻¹ @100 mA g ⁻¹	210 mA h g ⁻¹ @100 mA g ⁻¹ , 121 mA h g ⁻¹ @5 A g ⁻¹	89%, 100 cycles@100 mA g ⁻¹	227
EMI-Mo ₇₂ V ₃₀ @rGO	anode	1145 mA h g ⁻¹ @100 mA g ⁻¹	1150 mA h g ⁻¹ @100 mA g ⁻¹ , 591 mA h g ⁻¹ @2 A g ⁻¹	100%, 500 cycles@2 A g ⁻¹	228
PMo ₁₀ V ₂ /PDA	anode	915 mA h g ⁻¹ @100 mA g ⁻¹	996 mA h g ⁻¹ @20 mA g ⁻¹ , 560 mA h g ⁻¹ @2 A g ⁻¹	93%, 300 cycles@1 A g ⁻¹	230
PANI/PMo ₁₂ nanofiber	cathode	183.4 mA h g ⁻¹ @0.1 C	183 mA h g ⁻¹ @0.1 C, 94 mA h g ⁻¹ @2 C	81%, 50 cycles@0.1 C	232
POMOF-1	anode	1525 mA h g ⁻¹ @0.25 C	1525 mA h g ⁻¹ @0.25 C, 1421 mA h g ⁻¹ @1.25 C	46%, 500 cycles@1.25 C	238
[Cu ₁₀ (H ₃ trz) ₄ (Htrz) ₄](HPW ₁₂ O ₄₀)	anode	1620 mA h g ⁻¹ @100 mA g ⁻¹	553 mA h g ⁻¹ @100 mA g ⁻¹ , 298 mA h g ⁻¹ @1 A g ⁻¹	68%, 100 cycles@100 mA g ⁻¹	239
[Zn ₁₂ (trz) ₁₂ (OH) ₈][VW ₁₂ O ₄₀]-4H ₂ O	anode	1294 mA h g ⁻¹ @100 mA g ⁻¹	480 mA h g ⁻¹ @50 mA g ⁻¹ , 335 mA h g ⁻¹ @1 A g ⁻¹	42%, 200 cycles@100 mA g ⁻¹	240
NNU-11	anode	1322 mA h g ⁻¹ @50 mA g ⁻¹	N/A	100%, 400 cycles@500 mA g ⁻¹	241
NENU-507	anode	1008 mA h g ⁻¹ @100 mA g ⁻¹	1024 mA h g ⁻¹ @50 mA g ⁻¹ , 480 mA h g ⁻¹ @500 mA g ⁻¹	97%, 100 cycles@100 mA g ⁻¹	242
PMG-3	anode	2400 mA h g ⁻¹ @50 mA g ⁻¹	1088 mA h g ⁻¹ @50 mA g ⁻¹ , 428 mA h g ⁻¹ @2 A g ⁻¹	105%, 400 cycles@3 A g ⁻¹	243
[Ag ₅ (trz) ₆][H ₅ SiMo ₁₂ O ₄₀]	anode	1452 mA h g ⁻¹ @100 mA g ⁻¹	640 mA h g ⁻¹ @100 mA g ⁻¹ , 370 mA h g ⁻¹ @1 A g ⁻¹	63%, 100 cycles@100 mA g ⁻¹	244
HP-NENU-5/CC	anode	1723 mA h g ⁻¹ @200 mA g ⁻¹	1723 mA h g ⁻¹ @200 mA g ⁻¹ , 1072 mA h g ⁻¹ @1 A g ⁻¹	99%, 400 cycles@1 A g ⁻¹	245
PMo ₁₀ V ₂ -ILs@MIL-100	anode	1666 mA h g ⁻¹ @100 mA g ⁻¹	1033 mA h g ⁻¹ @100 mA g ⁻¹ , 348 mA h g ⁻¹ @3 A g ⁻¹	95%, 400 cycles@1 A g ⁻¹	246
MoO ₂ @C	anode	2937 mA h g ⁻¹ @100 mA g ⁻¹	1450 mA h g ⁻¹ @50 mA g ⁻¹ , 543 mA h g ⁻¹ @1 A g ⁻¹	90%, 50 cycles@100 mA g ⁻¹	247
MoS ₂ -C	anode	2400 mA h g ⁻¹ @500 mA g ⁻¹	1200 mA h g ⁻¹ @5 A g ⁻¹ , 900 mA h g ⁻¹ @20 A g ⁻¹	113%, 1750 cycles@5 A g ⁻¹	251
N/A These values were unavailable.					

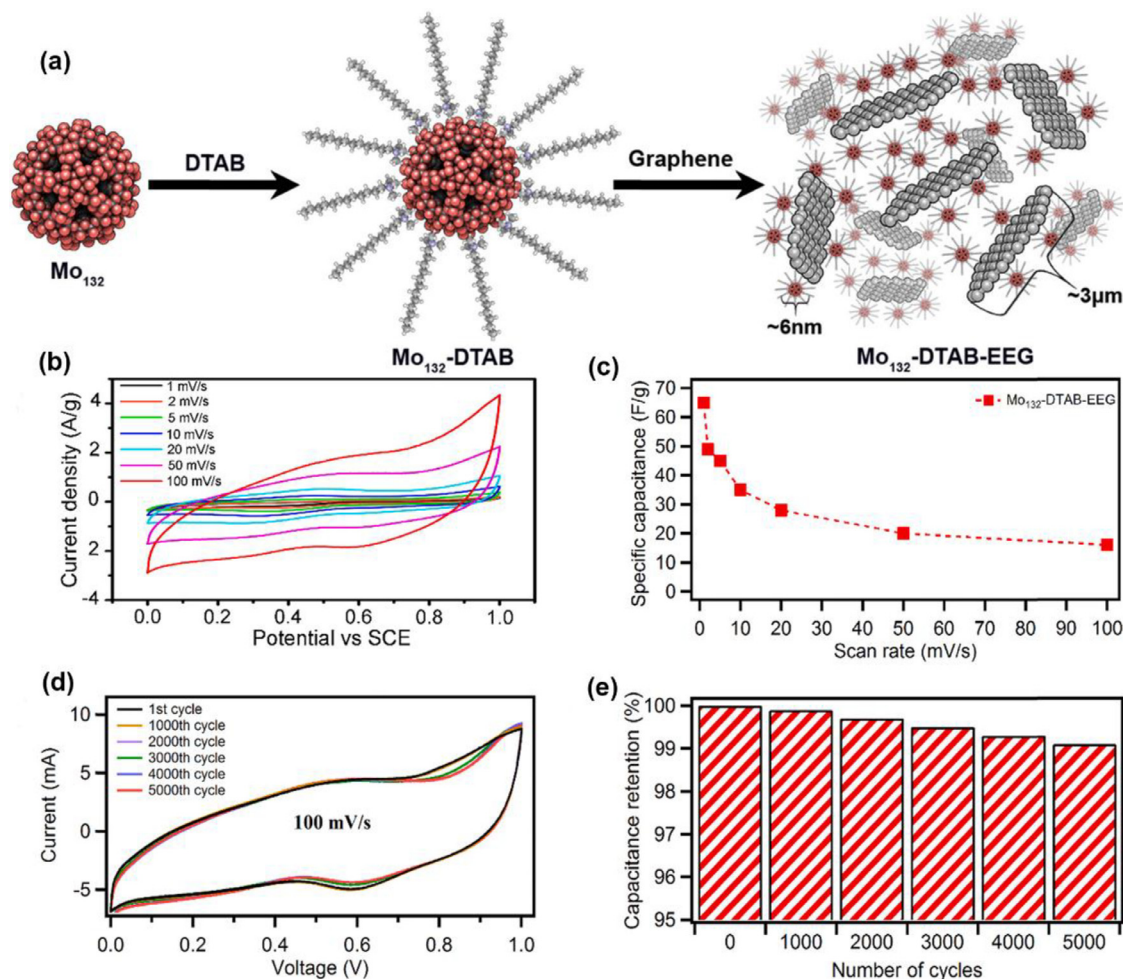


Fig. 25. (a) Schematic illustration of the formation of Mo₁₃₂-DTAB-EEG hybrid material. (b) CV curves of Mo₁₃₂-DTAB-EEG. (c) Specific capacitance vs. scan rate for Mo₁₃₂-DTAB-EEG; (d-e) Electrochemical cycling stability of Mo₁₃₂-DTAB-EEG, CV curves and capacitance retention. Reproduced with permission.²⁶² Copyright 2019, Elsevier.

reaction and the composite exhibited a superior capacitance of 276 F g⁻¹ with a small decrease of 4% after 10,000 cycles. To extend the operating voltage boundary and enhance the energy density of the device, an asymmetric supercapacitor based on rGO with different POMs as positive and negative electrodes was prepared.²⁷⁷ The designed rGO-PMo₁₂//rGO-PW₁₂ asymmetric cell could be cycled successfully in a wide voltage window up to 1.6 V with an excellent energy density of 39 Wh kg⁻¹ at a power density of 658 W kg⁻¹.

Besides the classic Keggin-type POMs have been intensively investigated as the electrode materials for supercapacitors, the other kinds of POMs are far from discussed. Recently, a Dawson-type POM, P₂Mo₁₈, a kind of high proton conductor with an excellent and reversible redox property, was introduced to develop supercapacitor electrode by Wang et al.²⁷⁸ The synthesized activated carbon/P₂Mo₁₈ composite showed a specific capacitance of 275 F g⁻¹ at a high current density of 6 A g⁻¹ and a remarkable rate capability (89%) with current density increasing from 2 to 6 A g⁻¹. Very lately, a porous 3D architecture based on dodecyltrimethylammonium bromide (DTAB) modified Keplerate type POM (Mo₁₃₂)/electrochemically exfoliated graphene (EEG) nanosheets was produced by Pakulski et al. for supercapacitors, as shown in Fig. 25a.²⁶² Compared to other hybrid POM/carbon-based systems, the strong non-covalent

interactions between Keplerate type polyoxometalate Mo₁₃₂-DTAB and graphene surface offered higher stability that the electrode retained 99% of its initial capacitance after 5000 cycles at different current densities (Fig. 25d-e).

For the further application of POM-based electrode materials, the high solubility of POMs in traditional aqueous electrolytes that may lead to rapid capacity fading should be taken into consideration as well. Instead of the aqueous sulfuric acid solutions, Yushin et al. firstly demonstrated the use of aqueous solutions of protic ionic liquids (P-IL) as electrolyte for the construction of the POM/carbon-based supercapacitors.²⁶⁵ The POM-infiltrated activated carbon composites showed virtually no decrease in capacitance during 10,000 cycles in P-IL comprising aqueous electrolytes. Additionally, Lan's group put forward to a strategy of encapsulating ionic liquids (ILs) into POMOFs to fabricate a series of ILs-functionalized POMOF crystals to avoid the leaching of POM as well as enhance the conductivity of the MOF substrate, which proposed a new strategy to improve the conductivity of MOFs and POMOFs for energy storage electrodes.²⁴⁶

All-solid-state supercapacitor with gel-electrolyte is much safer configuration for practical utilization. Lan et al. presented a polypyrrole-polyoxometalate/reduced graphene oxide ternary nanohybrids (PPy-PMo₁₂/rGO TNHs) for flexible all-solid-state

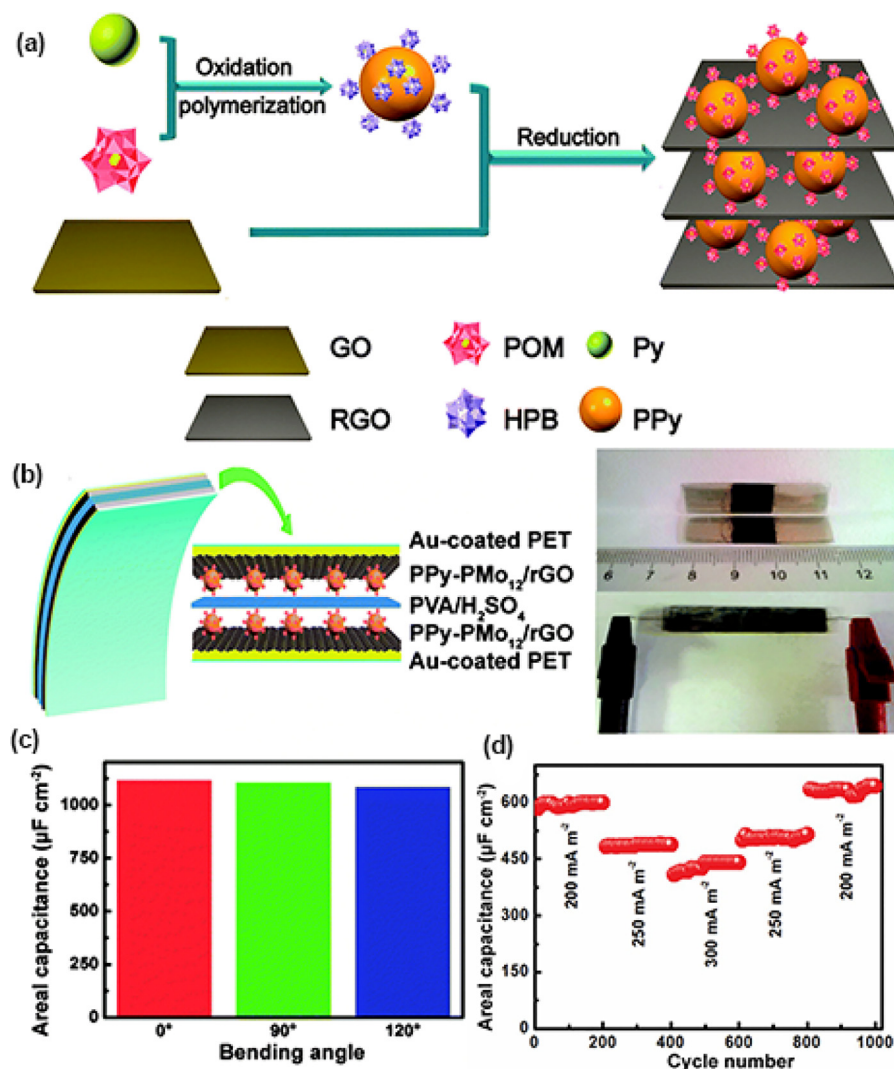


Fig. 26. (a) The schematic diagram for formation of PPy-PMo₁₂/rGO TNHs. (b) Schematic diagrams (left) of the PPG-SSCs and photographs (right) of the two electrodes for the PPG-SSCs. (c) Specific capacitances of the device by bending at different angles. (d) Cycling performance of PPG-SSCs measured by progressively varying the current density. Reproduced with permission.²⁷⁹ Copyright 2015, Royal Society of Chemistry. (For interpretation of the references to color in this figure legend, the reader is referred to the web version of this article.)

supercapacitors.²⁷⁹ For the hybrid syntheses as shown in Fig. 26a, a facile one-pot “redox relay” strategy was proposed for the first time that the adopted POM (PMo₁₂) acted as the oxidant to the polymerization of pyrrole monomer and the corresponding reductive product of heteropoly blue (HPB) reduced the GO simultaneously. Due to the pseudocapacitive activity of PPy and PMo₁₂, together with the conductive rGO substrate, the fabricated all-solid-state device exhibited excellent a high areal specific capacitance of 2.61 mF cm⁻² as well as excellent rate capacity and long-term stability even under bending (Fig. 26). Another rGO-PMo₁₂ based all-solid-state symmetric supercapacitor was fabricated with a hydroquinone doped hybrid gel-electrolyte by Dubal and co-workers.²⁸⁰ By doping redox-active species (hydroquinone) into the PVA/H₂SO₄ gel-electrolyte, the fabricated all-solid-state device exhibits intense redox peaks with a higher capacity as a result of the additional protons introduced by hydroquinone/quinone couples that provided more reaction sites for fast and reversible redox reactions. An excellent increase in the energy density of 1.7 mWh cm⁻³ with the redox-active electrolyte was achieved.

Ma and Pang et al. devoted their researches to synthesize POM-based coordination polymers for supercapacitor electrodes. The prepared polymers with well-designed structures showed excellent pseudocapacitive performance. However, the stabilities (capacitances usually decreased to ~ 85% after 1000 cycles) of these coordination polymers are still far from enough for the further utilization in devices.^{281,282}

Laskin and co-workers have studied the effect of electrode-electrolyte interfaces (EEI) on the POM-based supercapacitor performance.²⁸³ It was found that the electrodes prepared with conventional preparation techniques involving inactive counter ions at EEI would lead to aggregation, which was largely responsible for the reduced performance of POM-based supercapacitors. Thus, they proposed the ion soft landing (SL) deposition to achieve substantially high performance and long-term stability EEI prepared with highly dispersed discrete redox-active cluster POM anions (50 ng of pure ~ 0.75 nm size PMo₁₂O₄₀³⁻ on 25 μg (~ 0.2 wt%) carbon nanotube (CNT) electrodes) by complete elimination of strongly coordinating non-redox species.

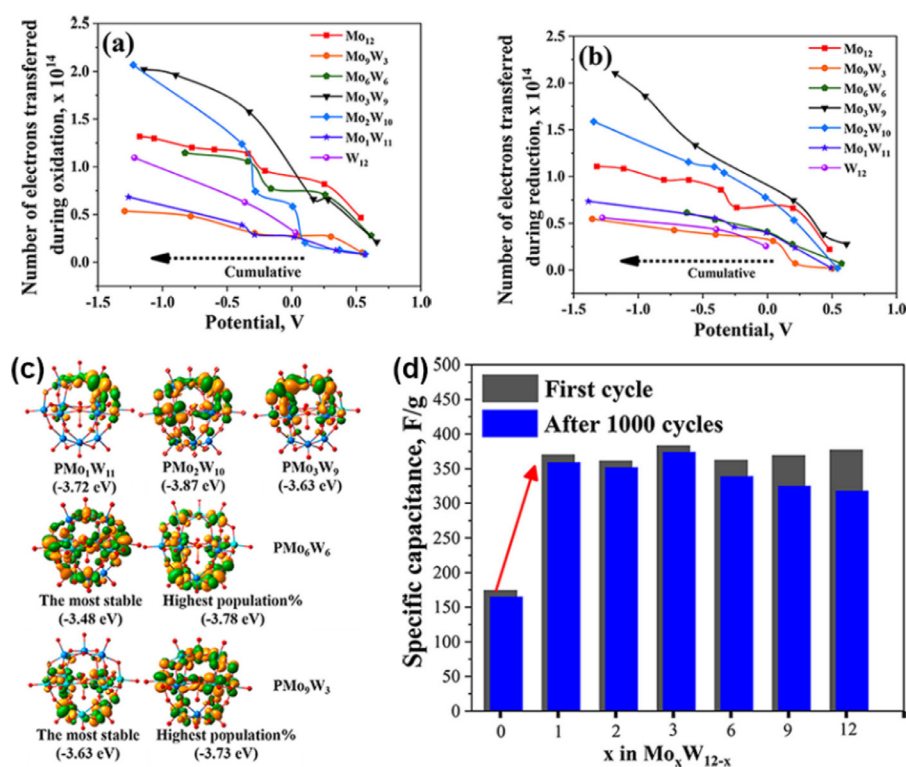


Fig. 27. Cumulative number of electrons transferred during (a) oxidation and (b) reduction scans of a range of soft landed mixed-addenda POM anions on the *in situ* electrochemical cell. (c) 3D representation of the LUMOs calculated for the mixed addenda POM anions (Mo_xW_{12-x}, $x = 1, 2, 3, 6$, and 9). (d) Comparison of the total specific capacitance before (black bars) and after (blue bars) 1000 charging/discharging cycles performed between 0 and 1 V at a rate of 8 A g⁻¹ observed with redox supercapacitor devices containing a range of soft landed mixed-addenda POM anions. The total number of POM soft landed in each case is 1×10^{14} ions. Reproduced with permission.²⁸⁴ Copyright 2019, American Chemical Society. (For interpretation of the references to color in this figure legend, the reader is referred to the web version of this article.)

SL of only small amounts of redox-active species resulted in dramatically enhanced total specific capacitance and superior long-term stability of carbon-based electrodes. More recently, Poblet and Laskin et al. deeply study the effect of “atom-by-atom” metal substitution on the supercapacitor activity and stability of well-defined redox-active anions, PMo_xW_{12-x}O₄₀³⁻ (Mo_xW_{12-x}POM, $x = 0, 1, 2, 3, 6, 9$, or 12) at nanostructured ionic liquid EEL.²⁸⁴ The combination of the *in-situ* electrochemical cell, ion soft landing, and DFT calculations were used to examine and model the electrochemical properties of mass-selected POM anions. Theoretical calculations showed a single substitution of a W atom by Mo was enough to substantially alter the electronic structure of Keggin W₁₂POM, resulted in a dramatic increase in the first redox potential. *In-situ* electrochemical measurements showed that Mo₃W₉ has the highest redox potential and transfers the largest number of electrons, as shown in Fig. 27a and b. And hybridized with functional CNT electrodes, Mo₃W₉ showed higher specific capacitance and capacity retention compared with other mixed addenda POM species as displayed in Fig. 27d. The summary of POM-based electrode materials for supercapacitors reviewed in this work is exhibited in Table 4.

POM-based materials for other rechargeable batteries

The POM-based materials are also investigated as functional components for sodium ion batteries,^{285,286} lithium sulfur batteries,^{287–289} lithium oxygen batteries,²⁹⁰ redox flow batteries,^{291–293} and electrolyte for batteries.^{294–296}

In 2017, Fan, Huang, and Shen et al. reported an earth-abundant, environmentally friendly and safe POM compound, Na₂H₈[MnV₁₃O₃₈] (NMV), for providing efficient Na⁺ storage sites in Na-ion batteries.²⁸⁵ The “electron/Na-ion sponge” electrochemical behaviors with 11 electrons/Na⁺ acceptability per mole of NMV cathode contributed to the high capacity. Additionally, first-principle calculations demonstrated the NMV exhibited a “ion sponge” feature that a super-reduced state of [MnV₁₃O₃₈]²⁰⁻ could form with slightly expanded size (*ca.* 7.5%) upon Na⁺ insertion compared to the original [MnV₁₃O₃₈]⁹⁻, which ensured the good cycling stability. Consequently, by coating NMV nanoplates with graphene to form a robust composite material, Na₂H₈[MnV₁₃O₃₈]/G exhibited a high specific capacity of 190 mA h g⁻¹ at 0.1 C, associating with a good rate capability (130 mA h g⁻¹ at 1 C) and a good capacity retention of 81% at 0.2 C. In 2018, Chen et al. synthesized vanadium-based POMs, Na₇[H₂PV₁₄O₄₂]·*n*H₂O ($n = 15–24$), by a facile aqueous solution procedure.²⁸⁶ Introduced as anode material for Na⁺ batteries, the Na₇[H₂PV₁₄O₄₂] exhibited a reversible capacity of 322 mA h g⁻¹ at 25 mA g⁻¹ with capacity retention of 87% after 120 cycles. The *ex-situ* XPS and *in-situ* synchrotron XANES measurements reveal the high capacity originated from the redox reactions of vanadium (average valence from V⁵⁺ to V^{3.7+}) accompanied by the insertion/extraction of Na ions between the polyanions and adsorption/desorption of Na ions on the surface of the polyanions.

More recently, the POM-based materials have been tried to act as cathodic materials or separators to reduce the active

Table 4. Summary of POM-based electrode materials for supercapacitors reviewed in this work.

Electrode Materials	Electrolyte	Specific Capacitance of Active Materials	Energy Density of devices	Retention and Cycling Number	Ref.
PMo ₁₂	5.3 M H ₂ SO ₄	112 F g ⁻¹	36 J g ⁻¹	N/A	255
{VW ₅ }-PPy	0.1 M nBu ₄ NBF ₄	38 F g ⁻¹ @50 mV s ⁻¹	N/A	90%, 1000@50 mV s ⁻¹	256
PPy/PMA	0.5 M H ₂ SO ₄	31 F g ⁻¹	4 Wh kg ⁻¹ @103 W kg ⁻¹	N/A	257
NENU-5/PPy	3 M KCl	5.1 F cm ⁻² @0.5 mA cm ⁻²	0.32 mWhcm ⁻² @6.4mWcm ⁻²	50%, 300@0.5 mA cm ⁻²	258
POM-PPy/nanopillar	0.05 M H ₂ SO ₄	79 mFcm ⁻² @1 mAcm ⁻²	N/A	100%, 3500@1 mAcm ⁻²	259
{Mo ₁₃₂ }-rGO	1 M Li ₂ SO ₄	617.3 F g ⁻¹ @5 A g ⁻¹	31.6 Wh kg ⁻¹ @207.7 W kg ⁻¹	67%, 3000@5 A g ⁻¹	260
MoS/rGO/CC	0.5 M H ₂ SO ₄	870 F g ⁻¹ @10 mV s ⁻¹	N/A	100%, 5000@100 mV s ⁻¹	261
Mo ₁₃₂ -DTAB-EEG	1 M H ₂ SO ₄	65 F g ⁻¹ @1 mV s ⁻¹	N/A	99%, 5000@100 mV s ⁻¹	262
[Ru(bpy) ₃] _{3.33} PMo ₁₈ O ₆₂ ·mH ₂ O	PBS 7.0	125 F g ⁻¹ @0.2 A g ⁻¹	3.5Whkg ⁻¹ @0.16 kW kg ⁻¹	87%, 500@0.3 A g ⁻¹	264
AC@PMo ₁₂	1M[Bmim]HSO ₄	230 F g ⁻¹ @1 mV s ⁻¹	N/A	100%, 3000@10 A g ⁻¹	265
PMo/PW-MWCNTs	1 M H ₂ SO ₄	92.7 Fcm ⁻³ @0.1Vs ⁻¹	N/A	92%, 2000	271
PMo ₁₂ -AC	1 M H ₂ SO ₄	183 F g ⁻¹ @2 A g ⁻¹	N/A	91%, 8000@1.6 A g ⁻¹	273
AC-PW ₁₂	1 M H ₂ SO ₄	254 F g ⁻¹ @10 mV s ⁻¹	4.96Whkg ⁻¹ @115kWkg ⁻¹	98%, 30,000@6 A g ⁻¹	274
HT-RGO-PMo ₁₂	1 M H ₂ SO ₄	276 F g ⁻¹ @10 mV s ⁻¹	4.3 Wh kg ⁻¹ @30 kW kg ⁻¹	96%, 10,000@1 A g ⁻¹	275
Pinecone AC/PMo ₁₂ O ₄₀	1 M H ₂ SO ₄	1.19 F cm ⁻² @10 mV s ⁻¹	N/A	91%, 5000@50 mV s ⁻¹	276
rGO-PW ₁₂	1 M H ₂ SO ₄	369 mF cm ⁻² @5 mA cm ⁻²	39 Wh kg ⁻¹ @658 W kg ⁻¹	95%, 2000@10 mAcm ⁻²	277
AC/P ₂ Mo ₁₈	1 M H ₂ SO ₄	275 Fg ⁻¹ @6 Ag ⁻¹	N/A	70%, 2000@6 A g ⁻¹	278
PPy-PMo ₁₂ /rGO	1 M H ₂ SO ₄	295 F g ⁻¹ @1 A g ⁻¹	N/A	60%,1200@200 mAcm ⁻²	279
rGO-PMo ₁₂	HQ-PVA/H ₂ SO ₄	5.3 Fcm ⁻³ @2 mA cm ⁻²	17.2Whkg ⁻¹ @127 W kg ⁻¹	86%, 5000@12.7 mAcm ⁻²	280
[Ag ₅ (brtmb) ₄][VW ₁₀ V ₂ O ₄₀]	1 M H ₂ SO ₄	206 F g ⁻¹ @110 A g ⁻¹	N/A	81.7%, 1000	281
[Cu ^I (btx)] ₄ [SiW ₁₂ O ₄₀]	1 M H ₂ SO ₄	110.3 F g ⁻¹ @3 A g ⁻¹	N/A	87%, 1000@18 A g ⁻¹	282
N/A These values were unavailable.					

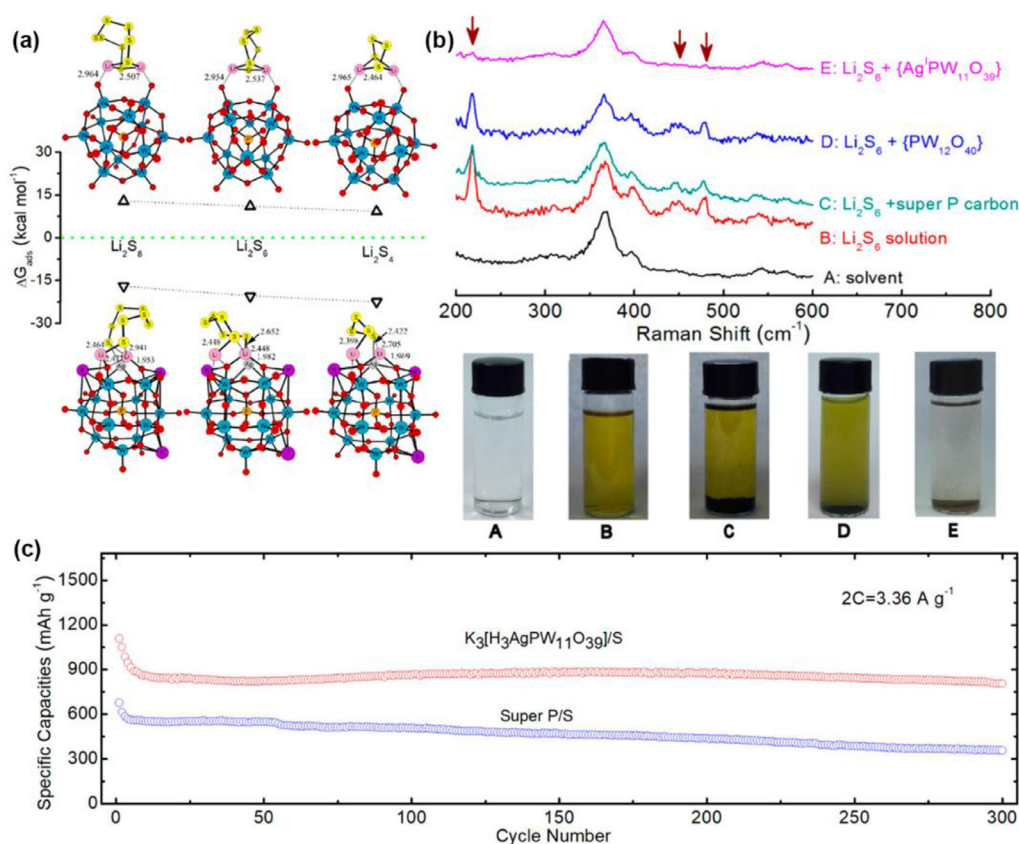


Fig. 28. (a) Calculated differences of adsorption free energy, ΔG_{ads} , and optimized structures for Li_2S_n species ($n = 8, 6, 4$) binding with $\{\text{PW}_{12}\text{O}_{40}\}$ and $\{\text{K}_3\text{AgPW}_{11}\text{O}_{39}\}$ clusters, respectively. $\{\text{PW}_{12}\text{O}_{40}\}$ is adopted as a control example to explore the role of the Ag ion. Bond lengths are given in Å. Atoms: (red, oxygen; blue, tungsten; yellow, sulfur; pink, lithium; purple, potassium; gray, silver; and orange, phosphorus). (b) Raman spectra and their corresponding photographs. And (c) long battery cycling of $\text{AgPW}_{11}/\text{S}$ cathode and super P carbon/S at a higher rate of 2 C. Reproduced with permission.²⁸⁹ Copyright 2018, American Chemical Society. (For interpretation of the references to color in this figure legend, the reader is referred to the web version of this article.)

lithium polysulfide in lithium sulfur batteries.^{287–289} In 2018, Cronin and Dong et al. employed the Ag (I)-substituted Keggin POMs as cathode materials for rechargeable Li-S batteries.²⁸⁹ The proposed $\text{K}_3[\text{H}_3\text{AgPW}_{11}\text{O}_{39}]$ (AgPW_{11}) was put forward as a bifunctional Lewis acidic and basic catalyst to stabilize Li_2S_n so that reversible redox reactions in S-based electrodes would be possible. As shown in Fig. 28a and b, DFT calculation investigation together with the Raman spectra have suggested that the Ag(I) ion can act as a Lewis acid site to further enhance the adsorption of the S-moieties, resulting in an energetically favorable adsorption of soluble Li_2S_n on the $\{\text{K}_3\text{AgPW}_{11}\text{O}_{39}\}$ cluster. Using the $\text{AgPW}_{11}/\text{S}$ composite as electrode materials for Li-S batteries, a high S utilization of 94% and a coulometric capacity of 1580 mAh g^{-1} have been achieved. Furthermore, the composite electrode showed a highly stable battery performance with a capacity around 810 mAh g^{-1} at 2 C during 300 cycling with an active S mass loading of 1.5 mg cm^{-2} (Fig. 28c).

Su and Qin et al. have fabricated a polypropylene (PP) matrix layer and Keggin-type POM $[\text{PW}_{12}\text{O}_{40}]^{3-}$ /super P carbon ($\text{PW}_{12}/\text{Super P}$) composite retarding layer as functional separator in Li-S batteries.²⁸⁸ By utilizing the Coulombic repulsion between POM polyanion and polysulfides anion, the polysulfides could be blocked to reduce the “shuttle” phenomenon. With the introduction of the $\text{PW}_{12}/\text{Super P}$ composite, the capacity of the

assembled Li-S batteries was improved by 41% after 120 cycles compared to the ones using PP matrix separator.

Inspired by the natural oxygen-evolving complex, Ryu and co-workers reported the use of cobalt-based POMs ($[\text{Co}_4(\text{H}_2\text{O})_2(\text{PW}_9\text{O}_{34})_2]^{10-}$, Co-POM) with an oxo-bridged tetracobalt active site as an efficient and stable redox catalyst for Li-O₂ batteries.²⁹⁰ The proposed Co-POM exhibits catalytic activity for both oxygen evolution and reduction reactions (OER and ORR, respectively) under a certain condition when it forms a stable dispersion of molecular aggregates. As a result, the Li-O₂ cells facilitated by Co-POM redox reactions successfully achieve improved efficiency of ~ 100% after 40 cycles in both diethylene glycol dimethyl ether (DEGDME) and tetraethylene glycol dimethyl ether (TEGDME) electrolytes. In addition, it was demonstrated that the POM molecules should be dispersed in the electrolyte, instead of using dissolution, to offer catalytic activity, and the redox characteristics of POM molecules can be tuned off by light emission, enabling the catalyst to be switched off.

POMs are one of the promising compounds for electricity carriers in redox flow batteries because of their highly stable redox cycles. In 2018, Stimming and co-workers investigated polyoxometalates (POMs), $[\text{SiW}_{12}\text{O}_{40}]^{4-}$ and $[\text{PV}_{14}\text{O}_{42}]^{9-}$, as nano-sized electron shuttles that showed fast redox kinetics (electron transfer constant of $\sim 10^{-2} \text{ cm s}^{-1}$ for $[\text{SiW}_{12}\text{O}_{40}]^{4-}$),

enabled high power densities redox flow batteries.²⁹² In flow battery studies, the theoretical capacity (10.7 Ah L^{-1}) could be achieved under operating conditions, and the cell was cycled for 14 days with current densities in the range of 30 to 60 mA cm^{-2} (155 cycles) with Coulombic efficiencies of $\sim 94\%$ during cycling. Abouzari-Lotf et al. developed a phosphotungstic acid (PWA)-carbon nanofiber electrode exhibiting excellent stability in vanadium electrolyte and battery cycling for redox flow batteries.²⁹¹ The vanadium redox flow battery demonstrated energy efficiency of above 83% that was substantially higher than that of pristine carbon felt (71.4%). In addition, Matson and co-workers reported a series of polyoxovanadium clusters, $[\text{V}_6\text{O}_7(\text{OR})_{12}]$ ($\text{R} = \text{CH}_3; \text{C}_2\text{H}_5$), with respect to their performance as charge carriers for nonaqueous redox flow batteries.²⁹³ The incorporation of one $[\text{TiV}_5(\text{OCH}_3)_{13}]$ or two $[\text{Ti}_2\text{V}_4(\text{OCH}_3)_{14}]$ titanium ions within the Lindqvist core significantly increased the cell voltage of the system from 1.60 V, to 2.30 and 2.74 V, respectively.

Employing a thermally-stable inorganic POM and a structurally-flexible organic moiety to construct inorganic-organic hybrid materials is a promising strategy to obtain efficient electrolyte. Thangadurai et al. prepared hybrid gel electrolytes derived from synergetic self-assembling of inorganic polyoxometalates (POMs) and organic ionic liquid (IL) components by using Keggin-type $\{\text{PMo}_{11}\text{VO}_{40}\}^{4-}$ and $\{\text{PW}_{11}\text{MoO}_{40}\}^{3-}$, and ionic liquid N-methyl imidazolium-1-(3-sulfonic group) propyl (MIMPS).²⁹⁶ Ionic conductivity (σ) of $\sim 0.1 \text{ S cm}^{-1}$ under ambient conduction was observed at 93°C for $[\text{MIMPS}]_4\text{PMo}_{11}\text{VO}_{40}$ (IL- PMo_{11}V) and $[\text{MIMPS}]_3\text{PW}_{11}\text{MoO}_{40}$ (IL- PW_{11}Mo) hybrid gels. The electrochemical stability windows (ESW) of IL- PMo_{11}V and IL- PW_{11}Mo reach to about 2 and 4 V, respectively, at room temperature. Additionally, Ito and Nagase et al. reported on a new type electrolyte of inorganic-organic hybrid MAImC1- PW_{12} by hybridizing ionic liquid imidazolium cations having polymerizable methacryl group (MAImC1) with heteropolyanions of $[\text{PW}_{12}\text{O}_{40}]^{3-}$ (PW_{12}).²⁹⁵ The MAImC1- PW_{12} was obtained as single crystals and was polymerized by a radical polymerization using AIBN as an initiator. The as-prepared polymer exhibited conductivity of $10^{-4} \text{ S cm}^{-1}$ order under humidified conditions at 313 K.

In 2018, Symes and Cronin et al. presented a polyoxoanion, $[\text{P}_2\text{W}_{18}\text{O}_{62}]^{6-}$, which can be reversibly reduced and protonated by 18 electrons/ H^+ per anion in aqueous solution, and that can act as a high-performance redox flow battery electrolyte.²⁹⁴ A practical discharged energy density of 225 Wh L^{-1} was achieved by the POM-based redox flow batteries with an open-circuit voltage of 1.25 V and an energy efficiency of 76% at room temperature at 0.5 M. Additionally, when extrapolating to the limits of the solubility of this POMs of 1.9 M L^{-1} in aqueous solution, an effective storage potential of $34.2 \text{ g H}_2 \text{ L}^{-1}$ could be achieved, which would yield a flow battery with an energy density breaking the 1000 Wh L^{-1} barrier.

POM-based materials for proton-exchange membrane fuel cell

Proton-exchange membrane fuel cells (PEMFCs), a kind of electrochemical conversion devices that utilize fuel supply (e.g. hydrogen, natural gas, or methanol) and an oxidant (e.g. oxygen, air, or hydrogen peroxide) to output electricity, have become a popular replacement for conventional energy supply systems and attracted extraordinary attention due to their high power

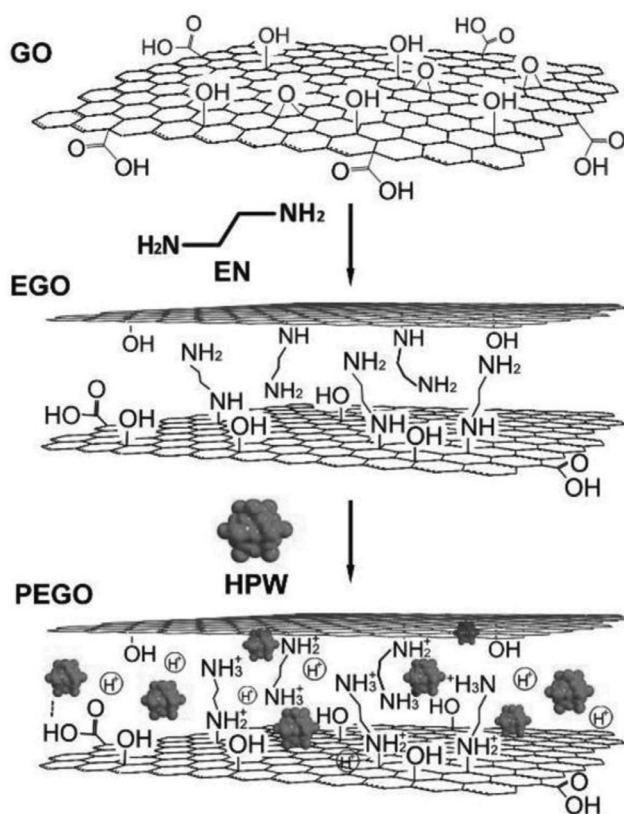


Fig. 29. Schematic diagram of the synthesis process of PEGO. Reproduced with permission.³⁰¹ Copyright 2015, Wiley-VCH.

density and low pollute emission.^{42,297} However, the high cost and limited thermal stability under high working temperature of the currently utilized Nafion or Nafion-like polymer based proton-exchange membranes call for promising alternatives with high protonic conductivity and stability.²⁹⁸ POMs that have unique ionic structure composed by the basic structural units of polyanions and the fairly mobile counter-cations (e.g. H^+ , H_3O^+ , or H_5O_2^+),²⁹⁹ exhibit excellent protonic conductivity and are expected to have great potential for the high performance proton-exchange membranes in fuel cells.

Liu's group have reported several researches for the investigation on the proton conductivity of POM-based materials.^{299–302} In 2014, Liu et al. prepared a 3D inorganic-organic hybrid proton conductor based on Anderson POM, $[\text{Sm}(\text{H}_2\text{O})_5(\text{CO}_2\text{CH}_2\text{NH}_3)_2][\text{Al}(\text{OH})_6\text{Mo}_6\text{O}_{18}] \cdot 10\text{H}_2\text{O}$.³⁰⁰ The unique 3D supramolecular network structure formed by the polyanions $[\text{AlMo}_6]$ and the coordination cations ($[\text{Sm}(\text{H}_2\text{O})_5(\text{gly})_2]^{3+}$) contains 1D channels that are water-filled with a high water content. The as-prepared ionic network revealed an excellent conductivity of $4.53 \times 10^{-3} \text{ S cm}^{-1}$ at 80°C under 95% relative humidity (RH).

In 2015, to overcome the water-soluble and limited machinability of POMs and make full use of their proton conductivity, Luo and Liu et al. proposed a strategy of introducing POMs into the interlayer space of graphene oxide (GO) sheets to obtain a POM-modified sponge-like GO monolith (PEGO) (Fig. 29).³⁰¹ The ethylenediamine with flexible chain structure and amino hydrogen bond acceptor was employed to substitute the unstable epoxy groups on GO surfaces. Due to the employed HWP (phosphotungstic acid, $\text{H}_3\text{PW}_{12}\text{O}_{40} \cdot 28\text{H}_2\text{O}$) POM and

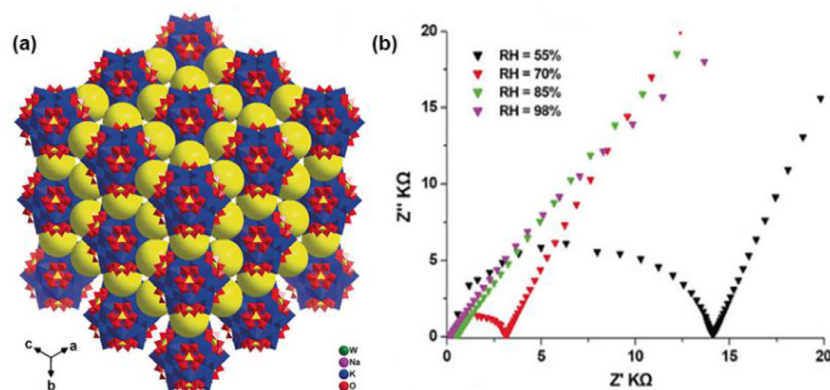


Fig. 30. (a) View of 3D structure of $\text{H}_{14}[\text{Na}_6(\text{H}_2\text{O})_{12}]_4\text{-}[\text{K}_{42}\text{Ge}_8\text{W}_{72}\text{O}_{272}(\text{H}_2\text{O})_{60}]\cdot\text{solvent}$ with large voids. (b) Nyquist plot under $T = 30^\circ\text{C}$. Reproduced with permission.³⁰³ Copyright 2018, Wiley-VCH.

the ethylenediamine, PEGO showed high proton conductivity of $1.02 \times 10^{-2} \text{ S cm}^{-1}$ at 60% relative humidity and excellent long-term stability. In 2017, Liu and co-workers proposed another method to introduce POM into MOFs for high protonic conduction network.³⁰² Two types of hydrogen bond networks were constructed by situating HPWs in the different targeting pores of MIL-101. The one with linear pathways exhibited about 2.1 times faster proton diffusion rates in contrast with the one with zigzag pathways. Further modification of an HPW-impregnated MIL-101 with flexible polyamine resulted in a conductivity of $1.52 \times 10^{-2} \text{ S cm}^{-1}$.

In 2018, Zheng et al. synthesized giant ionic alkali-metal-POM composite cluster $\{\text{K}_{42}\text{Ge}_8\text{W}_{72}\text{O}_{272}(\text{H}_2\text{O})_{60}\}$ by using high-negative and high-symmetry lacunary POMs.³⁰³ When linked by another kind of alkali metal ions Na^+ , the as-prepared giant clusters form an amazing three-dimensional all-inorganic ionic porous framework with high chemical stability, proton conductivity, and water vapor adsorption. As shown in Fig. 30b, the Nyquist plot of 3D structural $\text{H}_{14}[\text{Na}_6(\text{H}_2\text{O})_{12}]_4\text{-}[\text{K}_{42}\text{Ge}_8\text{W}_{72}\text{O}_{272}(\text{H}_2\text{O})_{60}]\cdot\text{solvent}$ showed that with the RH increased from 55% to 98%, the proton conductivity increased from $4.3 \times 10^{-5} \text{ S cm}^{-1}$ to $3.3 \times 10^{-3} \text{ S cm}^{-1}$, indicating an excellent protonic conduction performance. More recently, Das et al. reported metal-hydrogen-bonded organic frameworks (MHOs) based on $[\text{Ni}(\text{Imdz})_6]^{2+}$ and arene disulfonates or dicarboxylate for protonic conductors.³⁰⁴ The presence of an ionic backbone with charge assisted H-bonds, coupled with amphiprotic imidazoles made these MHOs protonic conductors, exhibiting conduction values of 0.75×10^{-3} , 3.5×10^{-4} and $0.97 \times 10^{-3} \text{ S cm}^{-1}$, respectively, at 80°C and 98% RH. Khashab and co-workers obtained two “metal-oxo cluster within cluster” assemblies, $\{[\text{Na}(\text{NO}_3)(\text{H}_2\text{O})_4][\text{Al}_{16}(\text{OH})_{24}(\text{H}_2\text{O})_8(\text{P}_8\text{W}_{48}\text{O}_{184})]\}^{16-}$ (**1**) and $[\text{Ga}_{16}(\text{OH})_{32}(\text{P}_8\text{W}_{48}\text{O}_{184})]^{24-}$ (**2**), via a facile solution reaction of $\text{Al}^{\text{III}}/\text{Ga}^{\text{III}}$ ions as guests with the super-lacunary P_8W_{48} as host.³⁰⁵ The Lewis acid functionalized polyanion (**1**) exhibited an exceptional proton conductivity of $4.5 \times 10^{-2} \text{ S cm}^{-1}$ (85°C , 70% RH).

Conclusions

POMs are favorable to the energy storage devices like lithium ion batteries and pseudocapacitors where energy storage and release is based on chemical redox reactions, due to their “electron

sponge” feature based on the instinct redox properties. For lithium ion batteries and supercapacitor applications, POMs and their composites with carbon or conductive polymers as electrode materials and electrolytes have been reported. The hybrid of POM and conductive matrix is beneficial to making POMs perform redox properties as well as enhance the conductivity of materials. However, there is still a long way to go towards their industrialization in energy storage devices due to the limited capacitance and long-term stability. In addition, expect for improving the electrode performance, the explanation of the electrochemical behavior based on the properties of electrode materials, such as the components and architecture, should be considered as well to give an instruction on how to construct effective electrode materials. The further research works of POM-based materials in this field can be conducted along the directions as following. Firstly, to make full use of the redox capacity of POMs, the conductive substrates are still necessary as the conductivity between POM clusters is negligible. Thus, the structure and surface properties of the conductive supports as well as the interaction between the POMs and the support should be taken into consideration and deeply studied for the rational design of the electrode materials. Secondly, the POMOFs combined the advantages of both redox-active POMs and porous MOFs are promising platforms to construct electrode materials with high capacitive activity and versatile ion channels. However, the performance of currently reported POMOF-based electrode materials is still far from enough due to the limited conductivity. The development of POMOFs with improved conductivity that may provide both fast electron transfer pathway and ion channels is demanding. Thirdly, the component optimization of POM clusters is significant to control their instinct redox properties. The currently reported research is almost exclusively focused on the prototype Keggin and Dawson anions. The utilization of other accessible POM anions and the development of novel POMs are also of great importance. The precise adjustment on the structure of POMs may lead to different redox properties, which gives tremendous opportunities to get novel electrode materials with high capacitive activities. In addition to batteries and supercapacitors, fuel cells are much more attractive due to their high-power density. The investigation on POMs used in the proton-exchange membrane fuel cell is of remarkable significance. The corresponding investigation is still ongoing.

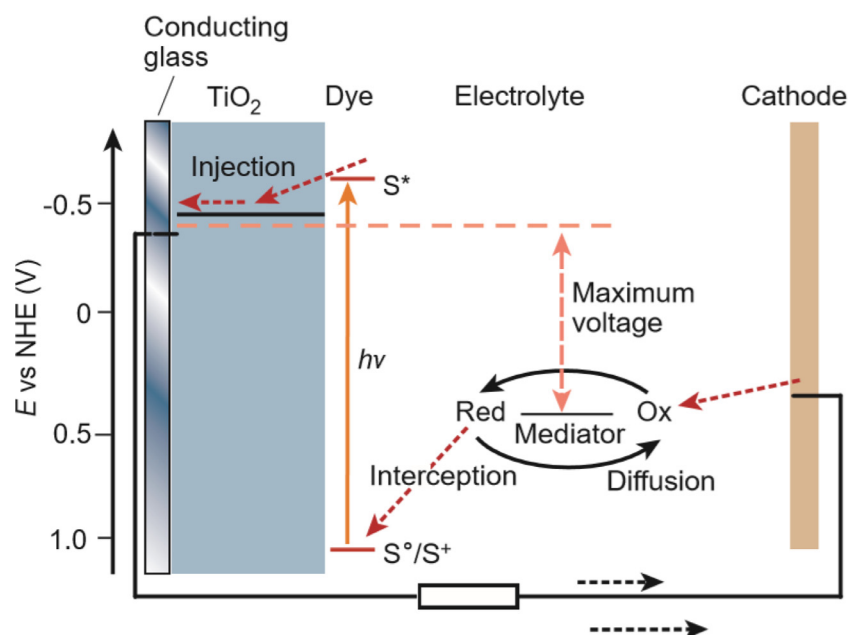


Fig. 31. Schematic operation of the dye-sensitized electrochemical photovoltaic cell. Reproduced with permission.⁴² Copyright 2013, Royal Society of Chemistry.

■ POM-BASED MATERIALS FOR DYE-SENSITIZED SOLAR CELLS

Solar cells are a kind of significant device to realize the conversion from solar energy resources to electricity energy and thus become one of the most direct and essential options for sustainable development in the world. Dye-sensitized solar cells (DSSCs), the third generation of photovoltaic cells, attract increasing attention due to the low cost, easy fabricating process, controllable optical properties, and higher photoelectric conversion efficiency (the new record of PCE is 13.6% and the corresponding independent certified PCE reaches 12.4%).^{306,307} According to the working mechanism of the DSSC displayed in Fig. 31, it could be seen that DSSC performs based on a semiconductor formed between a photo-sensitized anode and an electrolyte. The semiconducting material, dye and electrolyte are the main significant components in solar cells.

As a kind of molecular inorganic quasi-semiconductors, POMs have been widely reported both theoretically and experimentally for the application in different parts of DSSC owing to their excellent redox ability, good photosensitivity and electron acceptability.³⁰⁸ The electron-hole recombination on the TiO_2 /dye/electrolyte interface is one of the main obstacles to the enhancement of DSSC photoelectric conversion efficiency (PCE). By utilizing the superior electron acceptability of POMs, photo-generated electrons in the conductive band of semiconductor could be captured by POMs and thus facilitate the transfer of photo-generated carriers, which enhances the photoanode and improves the PCE of the DSSCs.

Wang's group has carried out several research studies on DSSCs using POMs as electron acceptors. In 2013, they reported a Keplerate-type POM $[\text{K}_{20}\{\text{W}_5\text{O}_{21}(\text{SO}_4)\}_{12}(\text{VO})_{30}(\text{SO}_4)(\text{H}_2\text{O})_{63}]^{18-}\{\text{W}_{72}\text{V}_{30}\}$ acting as alternative to the conventional electron acceptor fullerene in a polymer photovoltaic system.³⁰⁹ Then, in 2016, they proposed four kind of metal oxide semiconductor based photoelectrodes by bonding a Keplerate-type POM

$(\text{NH}_4)_{42}[\text{Mo}^{\text{VI}}_{72}\text{Mo}^{\text{V}}_{60}\text{O}_{372}(\text{CH}_3\text{COO})_{30}(\text{H}_2\text{O})_{72}] \{\text{Mo}_{132}\}$ with TiO_2 , SnO_2 , WO_3 , and ZnO .³¹⁰ As shown in Fig. 32, the intensity of photocurrent response of the $\{\text{Mo}_{132}\}/\text{TiO}_2$ was 4 times higher than that of pristine TiO_2 , suggesting the photo-induced electrons were accepted by the introduced $\{\text{Mo}_{132}\}$. According to the scheme displayed in Fig. 32b, the LUMO energy level of $\{\text{Mo}_{132}\}$ was lower than the conductive band of TiO_2 , making it possible for $\{\text{Mo}_{132}\}$ to accept electrons from TiO_2 and thus achieving a favorable exothermic process.

To further enhance the efficiency of DSSCs, Wang and co-workers also have developed strategies to prevent the aggregation of POMs and expose more active sites.^{311–313} For example, they prepared a highly dispersive and small-sized $\text{K}_6\text{CoW}_{12}\text{O}_{40}$ nanoparticles supported on TiO_2 nanosheets by using MIL-101 as a protective cover to prevent POM agglomeration. And the MOF could be broken by a further calcination step.³¹¹ Additionally, they proposed that when breaking POM-based MOFs, high loading amounts of nanosized POM clusters could be obtained.³¹² By annealing POM-based MOFs $[\text{Ni}(\text{bpp})(\text{H}_2\text{O})_2]_3[\text{P}_2\text{W}_{18}\text{O}_{62}] \cdot 24\text{H}_2\text{O}$ ($\text{bpp} = 1,3$ -bis(4-pyridyl)propane) or $\text{H}_6[\text{Cu}_3(\text{H}_2\text{O})_6(\text{P}_2\text{W}_{18}\text{O}_{62})_2(3\text{-dppe})_6] \cdot 28\text{H}_2\text{O}$ ($3\text{-dppe} = \text{N,N}'$ -bis(3-pyridinecarboxamide)-1,2-ethane), highly dispersed and small-sized $\text{P}_2\text{W}_{18}\text{O}_{62}^{6-}$ (P_2W_{18}) with a diameter of approximately 1 nm could be prepared on the TiO_2 support with a loading amount as high as 75.67 wt%. The highly dispersed P_2W_{18} nanoparticles could provide uniform sites and surface areas, resulting in an enhanced DSSC PCE of up to 7.56%, which is 26% higher than the pure TiO_2 based photoanodes. In addition, some other researches on POMs assembled onto metal oxide semiconductor photoanodes of DSSCs as electron acceptors have been reported as well.^{314–318}

Another utilization of POMs in DSSCs is serving as sensitizers or co-sensitizers owing to their tunable energy band structure and excellent photosensitivity.^{319–321} The adjustment of energy level of POMs is playing key roles in their application for DSSCs.

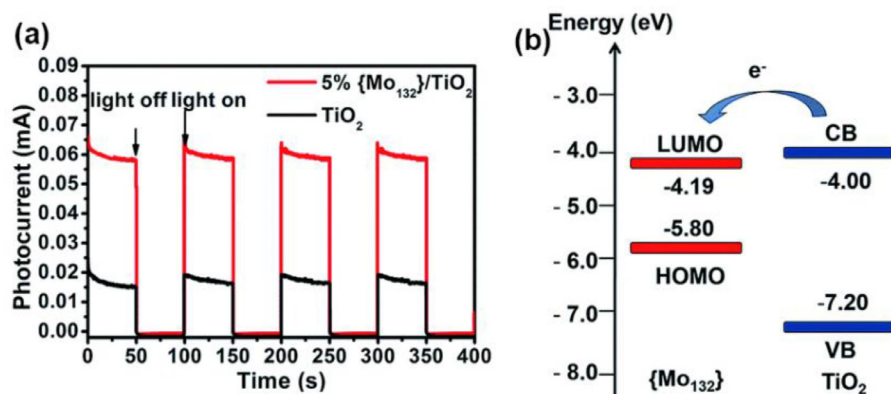


Fig. 32. (a) Photocurrent responses with on-off light illumination under the simulated AM 1.5 illumination at 100 mW cm^{-2} . (b) Energy levels of TiO_2 and $\{\text{Mo}_{132}\}$. Reproduced with permission.³¹⁰ Copyright 2016, Royal Society of Chemistry.

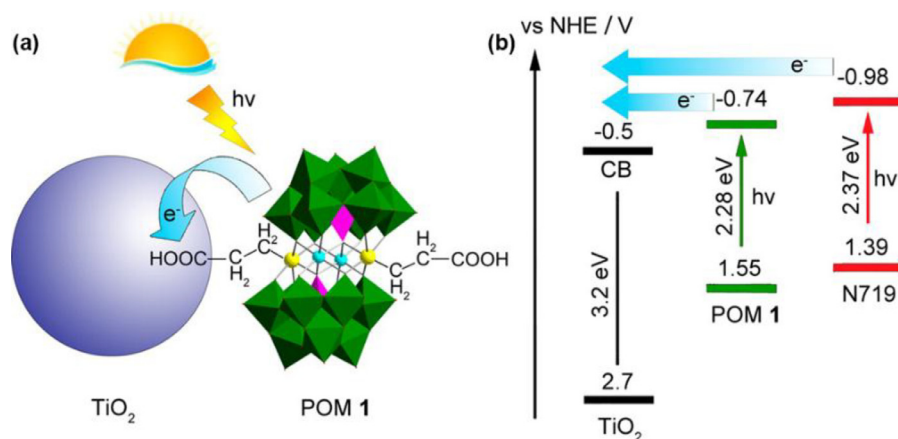


Fig. 33. Schematic diagram of (a) a $\text{GeW}_9\text{-Mn-SnR}$ POM as a cosensitizer; (b) schematic energy level of POM and TiO_2 . Reproduced with permission.³²⁰ Copyright 2014, American Chemical Society.

Lots of reported research works have demonstrated that the adjustment to the band gaps of POMs can be tuned by changing their structures and compositions. Several possible aspects that should possibly been taken into consideration for tuning the energy level regulation of POMs have been summarized by Chen and Wang et al. and shown as follow.³⁰⁸ (i) The introduction of transition metal atoms into POMs could lower the band gap. (ii) W-based POMs usually have larger E_g and higher LUMO energy levels than the Mo-based series with the similar structures and central atoms. (iii) A decreased saturation of POMs leads to an increase in band gaps. And the LUMO energy levels of POMs are affected by the central atoms and coordinated atoms. (iv) The smaller oxidation number of the central atom may lead to higher LUMO energy levels for POMs when the structures and coordinated atoms are both same. (v) POMs usually possess larger band gaps and lower LUMO energy levels than those of TiO_2 .

Zhang, Chen and Wang et al. reported a sandwich-type POM, $[\text{C}-(\text{NH}_2)_3]_{10}[\text{Mn}_2\{\text{Sn}(\text{CH}_2)_2\text{COOH}\}_2(\text{B}-\alpha\text{-GeW}_9\text{O}_{34})_2] \cdot 8\text{H}_2\text{O}$ ($\text{GeW}_9\text{-Mn-SnR}$) that was synthesized in aqueous solution and applied in DSSC.³²⁰ The functionalization of exposed carboxyl group of the $\text{GeW}_9\text{-Mn-SnR}$ is favorable to its adsorption on TiO_2 surface (Fig. 33a). The photosensitivity of $\text{GeW}_9\text{-Mn-SnR}$ has been characterized by fluorescence

spectrum, surface photovoltage spectrum, electrochemical method, and solid diffuse spectrum. As shown in Fig. 33b, the schematic illustration indicates that $\text{GeW}_9\text{-Mn-SnR}$ exhibits essential feasibility to be a dye for photovoltaic cell due to the energy levels of $\text{GeW}_9\text{-Mn-SnR}$, N719 and TiO_2 . When employed to assemble a cosensitized solar cell, the $\text{GeW}_9\text{-Mn-SnR}/\text{TiO}_2$ electrode with additionally adsorbing N719 dyes showed an enhanced efficiency that is 19.4% higher than that of single N719 sensitization. Then, they studied the POM compound $\text{K}_6\text{H}_4[\alpha\text{-SiW}_9\text{O}_{37}\text{Co}_3(\text{H}_2\text{O})_3] \cdot 17\text{H}_2\text{O}$ (SiW_9Co_3) that has a small band gap of 2.23 eV and relatively high LUMO level of -0.63 V vs. NHE .³¹⁵ The nanocomposite film of $\{\text{TiO}_2/\text{SiW}_9\text{Co}_3\}_3$ showed a power conversion efficiency increased from 6.79% to 8.53%.

More recently, Zhu and Wang et al. have developed a strategy based on vacuum thermal evaporation solid-phase reduction and layer-by-layer self-assembly to prepare Keggin HPBs nanocomposite ($\{\text{PW}_{12}\}_6\text{-Al}$ (HPB)) thin films with long-term stability (Fig. 34a).³²² The as fabricated HPBs show wide visible light absorption and high exciton dissociation efficiency, which improves the photoresponse of TiO_2 as well as generate high photocurrent. As shown in Fig. 34b, an obvious higher photocurrent response of the $\{\text{TiO}_2\}_5/\{\text{PW}_{12}\}_6\text{-Al}$ (HPB) film ($1.7 \mu\text{A}$) is obtained compared with that of $\{\text{TiO}_2\}_5/\{\text{PW}_{12}\}_6$ film. Furthermore,

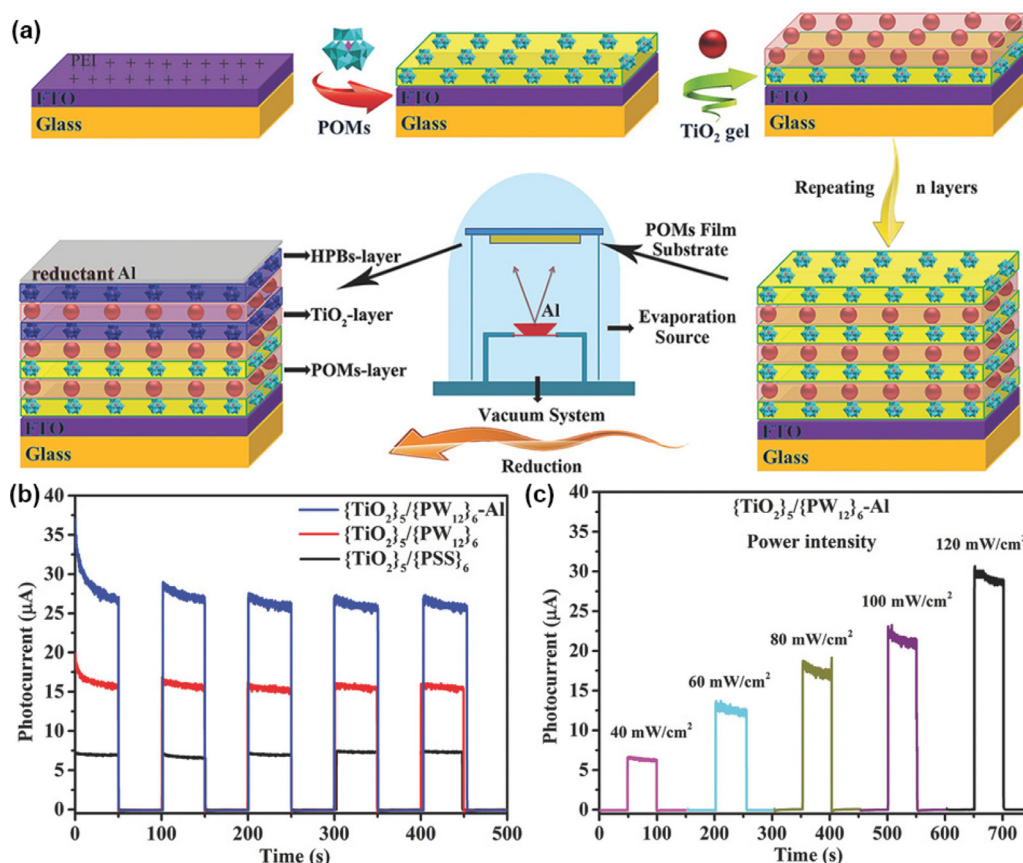


Fig. 34. (a) Schematic illustration of the vacuum thermal evaporation solid state reduction POMs. (b) Time-resolved photocurrent curves of the TiO₂/PW₁₂-Al (HPB) films under visible light ($\lambda > 420$ nm). (c) Photocurrent density of {TiO₂}₅/PW₁₂-Al (HPB) film under various power intensities. Reproduced with permission.³²² Copyright 2018, Wiley-VCH.

owing to the increased photogenerated carriers, the photocurrent of {TiO₂}₅/PW₁₂-Al (HPB) film demonstrated a smooth increase when the power intensity of incident sunlight is raised (Fig. 34c).

The POMs can act as electrolyte for DSSCs due to the redox properties.^{323–327} In 2006, a polymer electrolyte based on PW₁₂-impregnated polyvinylidene fluoride with I^{3−}/I[−] has been developed for DSSCs.³²³ And Yang et al. prepared a POM (PW₁₂) and polyethylene oxide composite electrolyte for DSSC that demonstrates high photovoltaic performance with an overall PCE of 3.1%.³²⁴ Additionally, Li et al. proposed a composite polymer electrolyte composed of ionic liquids and phosphotungstic acid (PWA) in a poly(2-hydroxyethyl methacrylate) matrix that was employed as a quasi-solid state electrolyte in DSSCs.³²⁵ And the Keggin-type POMs, K₆Co^{II}W₁₂O₄₀ and K₅Co^{III}W₁₂O₄₀, have also been employed as an inorganic redox couple in DSSCs.³²⁷

As one of the most viable clean energies, the research of solar cells develops rapidly, although it started relatively late compared with other energy applications. POMs, with semiconductor feature, electron acceptability, and redox properties have been utilized for DSSCs. The great progress made in this field demonstrates that POMs, as multi-functional materials, have great potential for further applications in solar cells. However, there is still a long way to go to optimize POMs properties for the enhanced PCE of DSSCs and to make use of POMs cooperating well with other DSSCs components.

CONCLUSIONS AND PERSPECTIVE

Nowadays, there is an increasing concern related to sustainable and clean energy that will become the most essential energy source in the future for human daily life, as a result of the serious issues arising from the overuse of fossil fuels and consequent non-renewable energy depletion and environmental problems. Thus, the achievement of the highly effective energy conversion catalytic processes and high-performance energy storage devices is of great significance, making it an urgent task to develop efficient, low-cost catalysts and electrode materials. The instinct plentiful redox properties, semiconductor-like feature and acidity of POMs make them and the related assemblies and derivatives as promising candidates for the electrocatalysts and photocatalysts involved in multi-electron transfer reactions, such as water reduction and oxidation, and CO₂ reduction, the electrode materials for the rechargeable batteries and pseudocapacitors, as well as platforms for proton conduction networks.

Here, we review and give a summary about the significant research progress on POM-based materials for the energy conversion among solar energy, electrical energy as well as chemical energy. The design and construction strategies of POM-based catalysts and electrode materials for several essential sustainable and clean energy conversion and storage systems have been organized and presented. The reported synthetic methodologies aiming at achieving effective and stable POM-based catalysts

or electrode materials can be classified into four strategies, including (1) constructing high nuclearity POMs containing several polyanion units or POMs with substituted center metal atoms to realize the controllable electronic structure and vigorous electron transfer, (2) incorporating POM into MOF structure to maintain its redox properties as well as prevent it from disintegration, (3) combining POM with conductive matrix to enhance the electronic conductivity and reduce its dissolution, especially in aqueous systems, and (4) employing POMs as platforms or precursors to prepare materials with abundant intermediate-valent metal species by pyrolysis.

The adjustment towards the instinct electronic and geometric structure of the POM-based catalysts via the about-mentioned routes, which leads to the tunable redox properties and fast electron transfer, is critical for catalysis processes. Although enormous research works has been devoted and much progress has been made using POM-based materials as catalysts in the field of hydrogen production, water oxidation and CO₂ reduction reaction, it still shows difficult to get sensible structure-reactivity correlations for obtaining desirable catalysts. To give a picture on how to rationally design POM-based catalysts for the energy-related electrocatalytic and photocatalytic reactions, a lot of researches could be further carried on. (1) Besides making full use of the unique properties of POMs, the retention of their structural integrity is also essential in all catalysis and energy conversion systems. Thus, the further study on the POM-based catalysts should take the stability, especially the structural maintenance of the POM clusters during the reaction processes, as an important aspect into consideration. (2) The crystallized POM clusters or POMOFs with precise and well-defined atomic structures are vital to achieve single-site or single-cluster catalysts, which can be ideal model catalysts to release precise catalysis with high-selectivity and catalytic activity in electro/photo-chemistry. (3) The POMs with tunable redox states, especially those oxidative POMs with a relatively low oxidation states, are quite promising active sites for the reduction reactions, such as CO₂ reduction and nitrogen reduction. The construction of POM-based catalysts with the specific catalytic active species for the CO₂ conversion to high-value products is of remarkable importance. (4) The *in-situ* electrochemical and photochemical characterizations should be developed to monitor the dynamic change of catalyst-electrode or catalyst-electrolyte interfaces during the reaction process and uncover the active catalytic species in the heterogeneous catalysis systems. (5) Another promising potential of POM-based materials is to utilize their proton/ion conductivity for high performance all-solid-state batteries or proton-exchange membrane fuel cells. Although the POMs have been proven to be high ionic conductive, even in the solid state, there is still a long way to go towards their industrialization in these fields. The further research should be carried on toward the rational design of POM-based membranes with high mechanical strength and stability.

Presently, the investigation of POMs as platforms for clean and sustainable energy is still on its way and much more efforts in the related fields will certainly contribute to the development and practical applications of future clean and renewable energy. It will be exciting to watch the rapid development of such new materials in the years to come.

■ ACKNOWLEDGEMENTS

This work was financially supported by NSFC (Nos. 21622104, 21701085, 21871141 and 21871142); the NSF of Jiangsu

Province of China (No. BK20171032); the Natural Science Research of Jiangsu Higher Education Institutions of China (No. 17KJB150025); Priority Academic Program Development of Jiangsu Higher Education Institutions and the Foundation of Jiangsu Collaborative Innovation Center of Biomedical Functional Materials.

■ AUTHOR CONTRIBUTIONS

Yu Zhang: Writing - original draft. **Jiang Liu:** Writing - review & editing. **Shun-Li Li:** Writing - review & editing. **Zhong-Min Su:** Writing - review & editing. **Ya-Qian Lan:** Writing - review & editing.

■ CONFLICT OF INTEREST

The authors declare no conflict of interest.

■ REFERENCES

1. Turner, J. A. Sustainable hydrogen production. *Science* **305**, 972–974 (2004).
2. Benson, E. E., Kubiak, C. P., Sathrum, A. J., Smieja, J. M. Electrocatalytic and homogeneous approaches to conversion of CO₂ to liquid fuels. *Chem. Soc. Rev.* **38**, 89–99 (2009).
3. Arico, A. S., Bruce, P., Scrosati, B., Tarascon, J. M., Van Schalkwijk, W. Nanostructured materials for advanced energy conversion and storage devices. *Nat. Mater.* **4**, 366–377 (2005).
4. Guo, Y.-G., Hu, J.-S., Wan, L.-J. Nanostructured materials for electrochemical energy conversion and storage devices. *Adv. Mater.* **20**, 2878–2887 (2008).
5. Gratzel, M. Photoelectrochemical cells. *Nature* **414**, 338–344 (2001).
6. Dolbecq, A., Dumas, E., Mayer, C. R., Mialane, P. Hybrid organic-inorganic polyoxometalate compounds: from structural diversity to applications. *Chem. Rev.* **110**, 6009–6048 (2010).
7. Miras, H. N., Yan, J., Long, D.-L., Cronin, L. Engineering polyoxometalates with emergent properties. *Chem. Soc. Rev.* **41**, 7403–7430 (2012).
8. Mueller, A., Gouzerh, P. From linking of metal-oxide building blocks in a dynamic library to giant clusters with unique properties and towards adaptive chemistry. *Chem. Soc. Rev.* **41**, 7431–7463 (2012).
9. Pope, M. T., Muller, A. Polyoxometalate chemistry-an old field with new dimensions in several disciplines. *Angew. Chem. Int. Ed.* **30**, 34–48 (1991).
10. Weinstock, I. A., Schreiber, R. E., Neumann, R. Dioxygen in polyoxometalate mediated reactions. *Chem. Rev.* **118**, 2680–2717 (2018).
11. Wang, S.-S., Yang, G.-Y. Recent advances in polyoxometalate-catalyzed reactions. *Chem. Rev.* **115**, 4893–4962 (2015).
12. Song, Y.-F., Tsunashima, R. Recent advances on polyoxometalate-based molecular and composite materials. *Chem. Soc. Rev.* **41**, 7384–7402 (2012).
13. Sadakane, M., Steckhan, E. Electrochemical properties of polyoxometalates as electrocatalysts. *Chem. Rev.* **98**, 219–237 (1998).
14. Liu, X., Inagaki, S., Gong, J. Heterogeneous molecular systems for photocatalytic CO₂ reduction with water oxidation. *Angew. Chem. Int. Ed.* **55**, 14924–14950 (2016).
15. Keita, B., Nadjo, L. Activation of electrode surfaces-application to the electrocatalysis of the hydrogen evolution reaction. *J. Electroanal. Chem.* **191**, 441–448 (1985).
16. Szczepankiewicz, S. H., Ippolito, C. M., Santora, B. P., Van de Ven, T. J., Ippolito, G. A., Fronckowiak, L., Wiatrowski, F., Power, T., Kozik, M. Interaction of carbon dioxide with transition-metal-substituted heteropolyanions in nonpolar solvents.

- Spectroscopic evidence for complex formation. *Inorg. Chem.* **37**, 4344–4352 (1998).
17. Howells, A. R., Sankarraj, A., Shannon, C. A diruthenium-substituted polyoxometalate as an electrocatalyst for oxygen generation. *J. Am. Chem. Soc.* **126**, 12258–12259 (2004).
 18. Toma, F. M., Sartorel, A., Iurlo, M., Carraro, M., Parisse, P., Maccato, C., Rapino, S., Rodriguez Gonzalez, B., Amenitsch, H., Da Ros, T., et al. Efficient water oxidation at carbon nanotube-polyoxometalate electrocatalytic interfaces. *Nat. Chem.* **2**, 826–831 (2010).
 19. Stracke, J. J., Finke, R. G. Electrocatalytic water oxidation beginning with the cobalt polyoxometalate $[\text{Co}_4(\text{H}_2\text{O})_2(\text{PW}_9\text{O}_{34})_2]^{10-}$: identification of heterogeneous CoO_x as the dominant catalyst. *J. Am. Chem. Soc.* **133**, 14872–14875 (2011).
 20. Qin, J.-S., Du, D.-Y., Guan, W., Bo, X.-J., Li, Y.-F., Guo, L.-P., Su, Z.-M., Wang, Y.-Y., Lan, Y.-Q., Zhou, H.-C. Ultrastable polymolybdate-based metal-organic frameworks as highly active electrocatalysts for hydrogen generation from water. *J. Am. Chem. Soc.* **137**, 7169–7177 (2015).
 21. Wu, H. B., Xia, B. Y., Yu, L., Yu, X.-Y., Lou, X. W. Porous molybdenum carbide nano-octahedrons synthesized via confined carburization in metal-organic frameworks for efficient hydrogen production. *Nat. Commun.* **6**, 6512 (2015).
 22. Li, J.-S., Wang, Y., Liu, C.-H., Li, S.-L., Wang, Y.-G., Dong, L.-Z., Dai, Z.-H., Li, Y.-F., Lan, Y.-Q. Coupled molybdenum carbide and reduced graphene oxide electrocatalysts for efficient hydrogen evolution. *Nat. Commun.* **7**, 11204 (2016).
 23. Ma, Y.-Y., Wu, C.-X., Feng, X.-J., Tan, H.-Q., Yan, L.-K., Liu, Y., Kang, Z.-H., Wang, E.-B., Li, Y.-G. Highly efficient hydrogen evolution from seawater by a low-cost and stable CoMoP@C electrocatalyst superior to Pt/C . *Energy Environ. Sci.* **10**, 788–798 (2017).
 24. Huang, Y., Ge, J., Hu, J., Zhang, J., Hao, J., Wei, Y. Nitrogen-doped porous molybdenum carbide and phosphide hybrids on a carbon matrix as highly effective electrocatalysts for the hydrogen evolution reaction. *Adv. Energy Mater.* **8**, 1701601 (2018).
 25. Blasco-Ahicart, M., Soriano-Lopez, J., Carbo, J. J., Poblet, J. M., Galan-Mascaros, J. R. Polyoxometalate electrocatalysts based on earth-abundant metals for efficient water oxidation in acidic media. *Nat. Chem.* **10**, 24–30 (2018).
Insoluble salts of Co-based POMs with barium counter-cations achieved high activity for oxygen evolution in acidic media with an overpotential of 189 mV at 1mA cm.
 26. Wang, Y.-R., Huang, Q., He, C.-T., Chen, Y., Liu, J., Shen, F.-C., Lan, Y.-Q. Oriented electron transmission in polyoxometalate-metalloporphyrin organic framework for highly selective electroreduction of CO_2 . *Nat. Commun.* **9**, 4466 (2018).
POM-metalloporphyrin organic framework showed a high CO RR FE of up to 99% with a turnover frequency of 1656 h.
 27. Yamase, T., Watanabe, R. Photoredox chemistry of Keggin dodecatungstoborate $\text{BW}_{12}\text{O}_{40}^{5-}$ and role of heterogeneous catalysis in hydrogen formation. *J. Chem. Soc. Dalton* **8**, 1669–1673 (1986).
 28. Geletii, Y. V., Botar, B., Koegerler, P., Hillesheim, D. A., Musaev, D. G., Hill, C. L. An all-inorganic, stable, and highly active tetraruthenium homogeneous catalyst for water oxidation. *Angew. Chem. Int. Ed.* **47**, 3896–3899 (2008).
 29. Sartorel, A., Carraro, M., Scorrano, G., Zorzi, R. D., Geremia, S., McDaniel, N. D., Bernhard, S., Bonchio, M. Polyoxometalate embedding of a tetraruthenium(IV)-oxo-core by template-directed metalation of $[\gamma\text{-SiW}_{10}\text{O}_{36}]^{8-}$: a totally inorganic oxygen-evolving catalyst. *J. Am. Chem. Soc.* **130**, 5006–5007 (2008).
 30. Huang, Z., Luo, Z., Geletii, Y. V., Vickers, J. W., Yin, Q., Wu, D., Hou, Y., Ding, Y., Song, J., Musaev, D. G., et al. Efficient light-driven carbon-free cobalt-based molecular catalyst for water oxidation. *J. Am. Chem. Soc.* **133**, 2068–2071 (2011).
 31. Song, F., Ding, Y., Ma, B., Wang, C., Wang, Q., Du, X., Fua, S., Song, J. $\text{K}_7[\text{Co}^{\text{II}}\text{Co}^{\text{III}}(\text{H}_2\text{O})\text{W}_{11}\text{O}_{39}]$: a molecular mixed-valence Keggin polyoxometalate catalyst of high stability and efficiency for visible light-driven water oxidation. *Energy Environ. Sci.* **6**, 1170–1184 (2013).
 32. Han, X.-B., Zhang, Z.-M., Zhang, T., Li, Y.-G., Lin, W., You, W., Su, Z.-M., Wang, E.-B. Polyoxometalate-based cobalt-phosphate molecular catalysts for visible light-driven water oxidation. *J. Am. Chem. Soc.* **136**, 5359–5366 (2014).
 33. Du, X., Zhao, J., Mi, J., Ding, Y., Zhou, P., Ma, B., Zhao, J., Song, J. Efficient photocatalytic H_2 evolution catalyzed by an unprecedented robust molecular semiconductor $\{\text{Fe}_{11}\}$ nanocluster without cocatalysts at neutral conditions. *Nano Energy* **16**, 247–255 (2015).
 34. Zhang, Z.-M., Zhang, T., Wang, C., Lin, Z., Long, L.-S., Lin, W. Photosensitizing metal-organic framework enabling visible-light-driven proton reduction by a Wells–Dawson-type polyoxometalate. *J. Am. Chem. Soc.* **137**, 3197–3200 (2015).
 35. Tian, J., Xu, Z.-Y., Zhang, D.-W., Wang, H., Xie, S.-H., Xu, D.-W., Ren, Y.-H., Wang, H., Liu, Y., Li, Z.-T. Supramolecular metal-organic frameworks that display high homogeneous and heterogeneous photocatalytic activity for H_2 production. *Nat. Commun.* **7**, 11580 (2016).
The first homogeneous supramolecular metal-organic framework (SMOF-1) in water at room temperature was synthesized by self-assembly and it showed high homogeneous and heterogeneous photocatalytic activity for H_2 production.
 36. Kong, X.-J., Lin, Z., Zhang, Z.-M., Zhang, T., Lin, W. Hierarchical integration of photosensitizing metal-organic frameworks and nickel-containing polyoxometalates for efficient visible-light-driven hydrogen evolution. *Angew. Chem. Int. Ed.* **55**, 6411–6416 (2016).
 37. Schwarz, B., Forster, J., Goetz, M. K., Yucel, D., Berger, C., Jacob, T., Streb, C. Visible-light-driven water oxidation by a molecular manganese vanadium oxide cluster. *Angew. Chem. Int. Ed.* **55**, 6329–6333 (2016).
 38. Xie, S.-L., Liu, J., Dong, L.-Z., Li, S.-L., Lan, Y.-Q., Su, Z.-M. Hetero-metallic active sites coupled with strongly reductive polyoxometalate for selective photocatalytic CO_2 -to- CH_4 conversion in water. *Chem. Sci.* **10**, 185–190 (2019).
 39. Freire, C., Fernandes, D. M., Nunes, M., Abdelkader, V. K. POM & MOF-based electrocatalysts for energy-related reactions. *Chemcatchem* **10**, 1703–1730 (2018).
 40. Ueda, T. Electrochemistry of polyoxometalates: from fundamental aspects to applications. *Chemelectrochem* **5**, 823–838 (2018).
 41. Lv, H., Geletii, Y. V., Zhao, C., Vickers, J. W., Zhu, G., Luo, Z., Song, J., Lian, T., Musaev, D. G., Hill, C. L. Polyoxometalate water oxidation catalysts and the production of green fuel. *Chem. Soc. Rev.* **41**, 7572–7589 (2012).
 42. Li, S.-L., Xu, Q. Metal-organic frameworks as platforms for clean energy. *Energy Environ. Sci.* **6**, 1656–1683 (2013).
 43. Symes, M. D., Cronin, L. Decoupling hydrogen and oxygen evolution during electrolytic water splitting using an electron-coupled-proton buffer. *Nat. Chem.* **5**, 403–409 (2013).
The polyoxometalate HPMoO used as electron-coupled-proton buffer (ECPB) to make the O_2 and H_2 produced at separate times during water electrolysis.
 44. Zeng, K., Zhang, D. Recent progress in alkaline water electrolysis for hydrogen production and applications. *Prog. Energ. Combust.* **36**, 307–326 (2010).
 45. Rausch, B., Symes, M. D., Chisholm, G., Cronin, L. Decoupled catalytic hydrogen evolution from a molecular metal oxide redox mediator in water splitting. *Science* **345**, 1326–1330 (2014).
 46. Wang, J., Xu, F., Jin, H., Chen, Y., Wang, Y. Non-noble metal-based carbon composites in hydrogen evolution reaction: fundamentals to applications. *Adv. Mater.* **29** (2017).
 47. Liu, R., Zhang, G., Cao, H., Zhang, S., Xie, Y., Haider, A., Kortz, U., Chen, B., Dalal, N. S., Zhao, Y., et al. Enhanced proton and electron reservoir abilities of polyoxometalate grafted on graphene for high-performance hydrogen evolution. *Energy Environ. Sci.* **9**, 1012–1023 (2016).

48. Fernandes, D. M., Araujo, M. P., Haider, A., Mougharbel, A. S., Fernandes, A. J. S., Kortz, U., Freire, C. Polyoxometalate-graphene electrocatalysts for the hydrogen evolution reaction. *ChemElectrochem* **5**, 273–283 (2018).
49. Huang, Y., Hu, J., Xu, H., Bian, W., Ge, J., Zang, D., Cheng, D., Lv, Y., Zhang, C., Gu, J., et al. Fine tuning electronic structure of catalysts through atomic engineering for enhanced hydrogen evolution. *Adv. Energy Mater.* **8**, 1800789 (2018).
50. Keita, B., Nadjo, L. New oxometalate-based materials for catalysis and electrocatalysis. *Mater. Chem. Phys.* **22**, 77–103 (1989).
51. Zhang, C., Hong, Y., Dai, R., Lin, X., Long, L.-S., Wang, C., Lin, W. Highly active hydrogen evolution electrodes via Co-deposition of Platinum and polyoxometalates. *ACS Appl. Mater. Interfaces* **7**, 11648–11653 (2015).
52. Barsukova-Stuckart, M., Izarova, N. V., Jameson, G. B., Ramachandran, V., Wang, Z., van Tol, J., Dalal, N. S., Biboum, R. N., Keita, B., Nadjo, L., et al. Synthesis and characterization of the dicopper(II)-containing 22-Palladate(II) $[\text{Cu}^{\text{II}}_2\text{Pd}^{\text{II}}_{22}\text{P}^{\text{V}}_{12}\text{O}_{60}(\text{OH})_8]^{20-}$. *Angew. Chem. Int. Ed.* **50**, 2639–2642 (2011).
53. Du, D.-Y., Qin, J.-S., Li, S.-L., Su, Z.-M., Lan, Y.-Q. Recent advances in porous polyoxometalate-based metal-organic framework materials. *Chem. Soc. Rev.* **43**, 4615–4632 (2014).
54. Nohra, B., El Moll, H., Rodriguez Albelo, L. M., Mialane, P., Marrot, J., Mellot-Draznieks, C., O'Keeffe, M., Biboum, R. N., Lemaire, J., Keita, B., et al. Polyoxometalate-based metal organic frameworks (POMOFs): structural trends, energetics, and high electrocatalytic efficiency for hydrogen evolution reaction. *J. Am. Chem. Soc.* **133**, 13363–13374 (2011).
55. Ensafi, A. A., Heydari-Soureshjani, E., Rezaei, B. Nanostructure polyoxometalates containing Co, Ni, and Cu as powerful and stable catalysts for hydrogen evolution reaction in acidic and alkaline solutions. *Int. J. Hydrog. Energy* **42**, 5026–5034 (2017).
56. Toma, F. M., Sartorel, A., Carraro, M., Bonchio, M., Prato, M. Dendron-functionalized multiwalled carbon nanotubes incorporating polyoxometalates for water-splitting catalysis. *Pure Appl. Chem.* **83**, 1529–1542 (2011).
57. Keita, B., Kortz, U., Holzle, L. R. B., Brown, S., Nadjo, L. Efficient hydrogen-evolving cathodes based on proton and electron reservoir behaviors of the phosphotungstate $[\text{H}_7\text{P}_8\text{W}_{48}\text{O}_{184}]^{33-}$ and the Co(II)-Containing silicotungstates $[\text{Co}_6(\text{H}_2\text{O})_{30}\{\text{Co}_9\text{Cl}_2(\text{OH})_3(\text{H}_2\text{O})_9(\beta\text{-SiW}_8\text{O}_{31})_3\}]^{5-}$ and $[\{\text{Co}_3(\text{B-}\beta\text{-SiW}_8\text{O}_{33}(\text{OH}))(\text{B-}\beta\text{-SiW}_8\text{O}_{29}(\text{OH}))_2\}]^{22-}$. *Langmuir* **23**, 9531–9534 (2007).
58. Xu, W., Liu, C., Xing, W., Lu, T. A novel hybrid based on carbon nanotubes and heteropolyanions as effective catalyst for hydrogen evolution. *Electrochem. Commun.* **9**, 180–184 (2007).
59. Yu, F., Gao, Y., Lang, Z., Ma, Y., Yin, L., Du, J., Tan, H., Wang, Y., Li, Y. Electrocatalytic performance of ultrasmall Mo_2C affected by different transition metal dopants in hydrogen evolution reaction. *Nanoscale* **10**, 6080–6087 (2018).
60. Zhang, J., Qu, L., Shi, G., Liu, J., Chen, J., Dai, L. N,P-codoped carbon networks as efficient metal-free bifunctional catalysts for oxygen reduction and hydrogen evolution reactions. *Angew. Chem. Int. Ed.* **55**, 2230–2234 (2016).
61. Hu, J., Huang, B., Zhang, C., Wang, Z., An, Y., Zhou, D., Lin, H., Leung, M. K. H., Yang, S. Engineering stepped edge surface structures of MoS_2 sheet stacks to accelerate the hydrogen evolution reaction. *Energy Environ. Sci.* **10**, 593–603 (2017).
62. Deng, J., Ren, P., Deng, D., Bao, X. Enhanced electron penetration through an ultrathin graphene layer for highly efficient catalysis of the hydrogen evolution reaction. *Angew. Chem. Int. Ed.* **54**, 2100–2104 (2015).
63. Tang, Y.-J., Gao, M.-R., Liu, C.-H., Li, S.-L., Jiang, H.-L., Lan, Y.-Q., Han, M., Yu, S.-H. Porous molybdenum-based hybrid catalysts for highly efficient hydrogen evolution. *Angew. Chem. Int. Ed.* **54**, 12928–12932 (2015).
64. Li, J.-S., Tang, Y.-J., Liu, C.-H., Li, S.-L., Li, R.-H., Dong, L.-Z., Dai, Z.-H., Bao, J.-C., Lan, Y.-Q. Polyoxometalate-based metal-organic framework-derived hybrid electrocatalysts for highly efficient hydrogen evolution reaction. *J. Mater. Chem. A* **4**, 1202–1207 (2016).
65. Yang, X., Feng, X., Tan, H., Zang, H., Wang, X., Wang, Y., Wang, E., Li, Y. N-Doped graphene-coated molybdenum carbide nanoparticles as highly efficient electrocatalysts for the hydrogen evolution reaction. *J. Mater. Chem. A* **4**, 3947–3954 (2016).
66. Zhang, L.-N., Li, S.-H., Tan, H.-Q., Khan, S. U., Ma, Y.-Y., Zang, H.-Y., Wang, Y.-H., Li, Y.-G. $\text{MoP}/\text{Mo}_2\text{C}@C$: a new combination of electrocatalysts for highly efficient hydrogen evolution over the entire pH range. *ACS Appl. Mater. Interfaces* **9**, 16270–16279 (2017).
67. Yan, G., Feng, X., Khan, S. U., Xiao, L., Xi, W., Tan, H., Ma, Y., Zhang, L., Li, Y. Polyoxometalate and resin-derived P-doped $\text{Mo}_2\text{C}@N$ -doped carbon as a highly efficient hydrogen-evolution reaction catalyst at all pH values. *Chem. Asian J.* **13**, 158–163 (2018).
68. Tang, Y.-J., Wang, Y., Wang, X.-L., Li, S.-L., Huang, W., Dong, L.-Z., Liu, C.-H., Li, Y.-F., Lan, Y.-Q. Molybdenum disulfide/nitrogen-doped reduced graphene oxide nanocomposite with enlarged interlayer spacing for electrocatalytic hydrogen evolution. *Adv. Energy Mater.* **6**, 1600116 (2016).
69. Huang, Y., Sun, Y., Zheng, X., Aoki, T., Pattengale, B., Huang, J., He, X., Bian, W., Younan, S., Williams, N., et al. Atomically engineering activation sites onto metallic 1T- MoS_2 catalysts for enhanced electrochemical hydrogen evolution. *Nat. Commun.* **10**, 982 (2019).
70. Sun, H., Ji, X., Qiu, Y., Zhang, Y., Ma, Z., Gao, G.-g. Hu, P. Poor crystalline MoS_2 with highly exposed active sites for the improved hydrogen evolution reaction performance. *J. Alloy Compd.* **777**, 514–523 (2019).
71. Tang, Y.-J., Chen, Y., Zhu, H.-J., Zhang, A. M., Wang, X.-L., Dong, L.-Z., Li, S.-L., Xu, Q., Lan, Y.-Q. Solid-phase hot-pressing synthesis of POMOFs on carbon cloth and derived phosphides for all pH value hydrogen evolution. *J. Mater. Chem. A* **6**, 21969–21977 (2018).
72. Yan, H., Xie, Y., Jiao, Y., Wu, A., Tian, C., Zhang, X., Wang, L., Fu, H. Holey reduced graphene oxide coupled with an $\text{Mo}_2\text{N}-\text{Mo}_2\text{C}$ heterojunction for efficient hydrogen evolution. *Adv. Mater.* **30**, 1704156 (2018).
73. Ma, Y.-Y., Lang, Z.-L., Yan, L.-K., Wang, Y.-H., Tan, H.-Q., Feng, K., Xia, Y.-J., Zhong, J., Liu, Y., Kang, Z.-H., et al. Highly efficient hydrogen evolution triggered by a multi-interfacial Ni/WC hybrid electrocatalyst. *Energy Environ. Sci.* **11**, 2114–2123 (2018).
74. Yan, H., Tian, C., Wang, L., Wu, A., Meng, M., Zhao, L., Fu, H. Phosphorus-modified tungsten nitride/reduced graphene oxide as a high-performance, non-noble-metal electrocatalyst for the hydrogen evolution reaction. *Angew. Chem. Int. Ed.* **54**, 6325–6329 (2015).
75. Huang, Y., Ma, Z., Hu, Y., Chai, D., Qiu, Y., Gao, G., Hu, P. An efficient $\text{WSe}_2/\text{Co}_{0.85}\text{Se}/\text{graphene}$ hybrid catalyst for electrochemical hydrogen evolution reaction. *RSC Adv* **6**, 51725–51731 (2016).
76. Tang, Y.-J., Zhang, A. M., Zhu, H.-J., Dong, L.-Z., Wang, X.-L., Li, S.-L., Han, M., Xu, X.-X., Lan, Y.-Q. Polyoxometalate precursors for precisely controlled synthesis of bimetallic sulfide heterostructure through nucleation-doping competition. *Nanoscale* **10**, 8404–8412 (2018).
77. Hou, J., Zhang, B., Li, Z., Cao, S., Sun, Y., Wu, Y., Gao, Z., Sun, L. Vertically aligned oxygenated- $\text{CoS}_2-\text{MoS}_2$ heteronanoshell architecture from polyoxometalate for efficient and stable overall water splitting. *ACS Catal* **8**, 4612–4621 (2018).
78. Shen, F.-C., Sun, S.-N., Xin, Z.-F., Li, S.-L., Dong, L.-Z., Huang, Q., Wang, Y.-R., Liu, J., Lan, Y.-Q. Hierarchically phosphorus doped bimetallic nitrides arrays with unique interfaces for efficient water splitting. *Appl. Catal. B-Environ.* **243**, 470–480 (2019).

79. Tang, Y.-J., Zhu, H.-J., Dong, L.-Z., Zhang, A. M., Li, S.-L., Liu, J., Lan, Y.-Q. Solid-phase hot-pressing of POMs-ZIFs precursor and derived phosphide for overall water splitting. *Appl. Catal. B-Environ.* **245**, 528–535 (2019).
80. Ruttinger, W., Dismukes, G. C. Synthetic water-oxidation catalysts for artificial photosynthetic water oxidation. *Chem. Rev.* **97**, 1–24 (1997).
81. Reier, T., Oezaslan, M., Strasser, P. Electrocatalytic oxygen evolution reaction (OER) on Ru, Ir, and Pt Catalysts: a comparative study of nanoparticles and bulk materials. *ACS Catal.* **2**, 1765–1772 (2012).
82. Sens, C., Romero, I., Rodriguez, M., Llobet, A., Parella, T., Benet-Buchholz, J. A new Ru complex capable of catalytically oxidizing water to molecular dioxygen. *J. Am. Chem. Soc.* **126**, 7798–7799 (2004).
83. Yin, Q., Tan, J. M., Besson, C., Geletii, Y. V., Musaev, D. G., Kuznetsov, A. E., Luo, Z., Hardcastle, K. L., Hill, C. L. A fast soluble carbon-free molecular water oxidation catalyst based on abundant metals. *Science* **328**, 342–345 (2010).
84. Stracke, J. J., Finke, R. G. Water oxidation catalysis beginning with $2.5\ \mu\text{M}$ $[\text{Co}_4(\text{H}_2\text{O})_2(\text{PW}_9\text{O}_{34})_2]^{10-}$: investigation of the true electrochemically driven catalyst at ≥ 600 mV overpotential at a glassy carbon electrode. *ACS Catal.* **3**, 1209–1219 (2013).
85. Goberna-Ferrón, S., Vigar, L., Soriano-López, J., Galán-Mascarós, J. R. Identification of a nonanuclear $\{\text{Co}^{\text{II}}_9\}$ polyoxometalate cluster as a homogeneous catalyst for water oxidation. *Inorg. Chem.* **51**, 11707–11715 (2012).
86. Soriano-Lopez, J., Goberna-Ferron, S., Vigar, L., Carbo, J. J., Poblet, J. M., Ramon Galan-Mascaros, J. Cobalt polyoxometalates as heterogeneous water oxidation catalysts. *Inorg. Chem.* **52**, 4753–4755 (2013).
87. Guo, S.-X., Liu, Y., Lee, C.-Y., Bond, A. M., Zhang, J., Geletii, Y. V., Hill, C. L. Graphene-supported $[\{\text{Ru}_4\text{O}_4(\text{OH})_2(\text{H}_2\text{O})_4\}(\gamma\text{-SiW}_{10}\text{O}_{36})_2]^{10-}$ for highly efficient electrocatalytic water oxidation. *Energy Environ. Sci.* **6**, 2654–2663 (2013).
88. Quintana, M., López, A. M., Rapino, S., Toma, F. M., Iurlo, M., Carraro, M., Sartorel, A., Maccato, C., Ke, X., Bittencourt, C., et al. Knitting the catalytic pattern of artificial photosynthesis to a hybrid graphene nanotexture. *ACS Nano* **7**, 811–817 (2013).
89. Lee, G. Y., Kim, I., Lim, J., Yang, M. Y., Choi, D. S., Gu, Y., Oh, Y., Kang, S. H., Nam, Y. S., Kim, S. O. Spontaneous linker-free binding of polyoxometalates on nitrogen-doped carbon nanotubes for efficient water oxidation. *J. Mater. Chem. A* **5**, 1941–1947 (2017).
90. Blasco-Ahicart, M., Soriano-Lopez, J., Ramon Galan-Mascaros, J. Conducting organic polymer electrodes with embedded polyoxometalate catalysts for water splitting. *Chemelectrochem* **4**, 3296–3301 (2017).
91. Luo, W., Hu, J., Diao, H., Schwarz, B., Streb, C., Song, Y.-F. Robust polyoxometalate/nickel foam composite electrodes for sustained solar-powered homogeneous water photolysis. *Angew. Chem. Int. Ed.* **56**, 4941–4944 (2017).
92. Tinker, L. L., McDaniel, N. D., Bernhard, S. Progress towards solar-powered homogeneous water photolysis. *J. Mater. Chem.* **19**, 3328–3337 (2009).
93. Seitz, L. C., Dickens, C. F., Nishio, K., Hikita, Y., Montoya, J., Doyle, A., Kirk, C., Vojvodica, A., Hwang, H. Y., Nørskov, J. K., et al. A highly active and stable $\text{IrO}_x/\text{SrIrO}_3$ catalyst for the oxygen evolution reaction. *Science* **353**, 1011–1014 (2016).
94. Ouattara, L., Fierro, S., Frey, O., Koudelka, M., Comninellis, C. Electrochemical comparison of IrO_2 prepared by anodic oxidation of pure iridium and IrO_2 prepared by thermal decomposition of H_2IrCl_6 precursor solution. *J. Appl. Electrochem.* **39**, 1361–1367 (2009).
95. Liu, C.-H., Tang, Y.-J., Wang, X.-L., Huang, W., Li, S.-L., Dong, L.-Z., Lan, Y.-Q. Highly active Co-Mo-C/NRGO composite as an efficient oxygen electrode for water-oxygen redox cycle. *J. Mater. Chem. A* **4**, 18100–18106 (2016).
96. Shen, F.-C., Wang, Y., Tang, Y.-J., Li, S.-L., Wang, Y.-R., Dong, L.-Z., Li, Y.-F., Xu, Y., Lan, Y.-Q. $\text{CoV}_2\text{O}_6\text{-V}_2\text{O}_5$ coupled with porous N-doped reduced graphene oxide composite as a highly efficient electrocatalyst for oxygen evolution. *ACS Energy Lett.* **2**, 1327–1333 (2017).
97. Gao, D., Liu, R., Biskupek, J., Kaiser, U., Song, Y.-F., Streb, C. Molecular design of noble-metal-free mixed metal oxide electrocatalysts for complete water splitting. *Angew. Chem. Int. Ed.* **58**, 4644–4648 (2019).
98. Chen, C., Wu, A., Yan, H., Xiao, Y., Tian, C., Fu, H. Trapping $[\text{PMo}_{12}\text{O}_{40}]^{3-}$ clusters into pre-synthesized ZIF-67 toward $\text{Mo}_x\text{Co}_x\text{C}$ particles confined in uniform carbon polyhedrons for efficient overall water splitting. *Chem. Sci.* **9**, 4746–4755 (2018).
99. Ma, Y., Wang, X., Jia, Y., Chen, X., Han, H., Li, C. Titanium dioxide-based nanomaterials for photocatalytic fuel generations. *Chem. Rev.* **114**, 9987–10043 (2014).
100. Pearson, P. N., Palmer, M. R. Atmospheric carbon dioxide concentrations over the past 60 million years. *Nature* **406**, 695–699 (2000).
101. Wang, C., Xie, Z., deKrafft, K. E., Lin, W. Doping metal-organic frameworks for water oxidation, carbon dioxide reduction, and organic photocatalysis. *J. Am. Chem. Soc.* **133**, 13445–13454 (2011).
102. Inoue, T., Fujishima, A., Konishi, S., Honda, K. Photoelectrocatalytic reduction of carbon-dioxide in aqueous suspensions of semiconductor powders. *Nature* **277**, 637–638 (1979).
103. Kuhl, K. P., Cave, E. R., Abram, D. N., Jaramillo, T. F. New insights into the electrochemical reduction of carbon dioxide on metallic copper surfaces. *Energy Environ. Sci.* **5**, 7050–7059 (2012).
104. Costentin, C., Robert, M., Saveant, J.-M. Catalysis of the electrochemical reduction of carbon dioxide. *Chem. Soc. Rev.* **42**, 2423–2436 (2013).
105. Girardi, M., Blanchard, S., Griveau, S., Simon, P., Fontecave, M., Bedioui, F., Proust, A. Electro-assisted reduction of CO_2 to CO and formaldehyde by $(\text{TOA})_6[\alpha\text{-SiW}_{11}\text{O}_{39}\text{Co}(_)]$ polyoxometalate. *Eur. J. Inorg. Chem.* **22**, 3642–3648 (2015).
106. Chen, Z., Chen, C., Weinberg, D. R., Kang, P., Concepcion, J. J., Harrison, D. P., Brookhart, M. S., Meyer, T. J. Electrocatalytic reduction of CO_2 to CO by polypyridyl ruthenium complexes. *Chem. Commun.* **47**, 12607–12609 (2011).
107. Kang, P., Meyer, T. J., Brookhart, M. Selective electrocatalytic reduction of carbon dioxide to formate by a water-soluble iridium pincer catalyst. *Chem. Sci.* **4**, 3497–3502 (2013).
108. Bourrez, M., Molton, F., Chardon-Noblat, S., Deronzier, A. $[\text{Mn}(\text{bipyridyl})(\text{CO})_3\text{Br}]$: An abundant metal carbonyl complex as efficient electrocatalyst for CO_2 reduction. *Angew. Chem.* **123**, 10077–10080 (2011).
109. Costentin, C., Drouet, S., Robert, M., Saveant, J.-M. A local proton source enhances CO_2 electroreduction to CO by a molecular Fe catalyst. *Science* **338**, 90–94 (2012).
110. Costentin, C., Drouet, S., Passard, G., Robert, M., Saveant, J.-M. Proton-coupled electron transfer cleavage of heavy-atom bonds in electrocatalytic processes. Cleavage of a C-O bond in the catalyzed electrochemical reduction of CO_2 . *J. Am. Chem. Soc.* **135**, 9023–9031 (2013).
111. Guo, S.-X., MacFarlane, D. R., Zhang, J. Bioinspired electrocatalytic CO_2 reduction by bovine serum albumin-capped silver nanoclusters mediated by $[\alpha\text{-SiW}_{12}\text{O}_{40}]^{4-}$. *Chemosuschem* **9**, 80–87 (2016).
112. Guo, S.-X., Li, F., Chen, L., MacFarlane, D. R., Zhang, J. Polyoxometalate-promoted electrocatalytic CO_2 reduction at nanostructured silver in dimethylformamide. *ACS Appl. Mater. Interface* **10**, 12690–12697 (2018).
113. Girardi, M., Platzer, D., Griveau, S., Bedioui, F., Alves, S., Proust, A., Blanchard, S. Assessing the Electrocatalytic Properties of the $\{\text{Cp}^*\text{Rh}^{\text{III}}\}^{2+}$ -Polyoxometalate Derivative $[\text{H}_2\text{PW}_{11}\text{O}_{39}\{\text{Rh}^{\text{III}}\text{Cp}^*(\text{OH})_2\}]^{3-}$ towards CO_2 Reduction. *Eur. J. Inorg. Chem.*, 387–393 (2019).
114. Zhang, J., Hao, J., Wei, Y., Xiao, F., Yin, P., Wang, L. Nanoscale

- chiral rod-like molecular triads assembled from achiral polyoxometalates. *J. Am. Chem. Soc.* **132**, 14–15 (2010).
115. Fang, X., Koegerler, P., Furukawa, Y., Speldrich, M., Luban, M. Molecular growth of a core-shell polyoxometalate. *Angew. Chem. Int. Ed.* **50**, 5212–5216 (2011).
 116. Miras, H. N., Vila-Nadal, L., Cronin, L. Polyoxometalate based open-frameworks (POMOFs). *Chem. Soc. Rev.* **43**, 5679–5699 (2014).
 117. Banerjee, A., Bassil, B. S., Röschenhaler, G.-V., Kortz, U. Diphosphates and diphosphonates in polyoxometalate chemistry. *Chem. Soc. Rev.* **41**, 7590–7604 (2012).
 118. Yoon, M., Chang, J. A., Kim, Y., Choi, J. R., Kim, K., Lee, S. J. Heteropoly acid-incorporated TiO₂ colloids as novel photocatalytic systems resembling the photosynthetic reaction center. *J. Phys. Chem. B* **105**, 2539–2545 (2001).
 119. Anandan, S., Yoon, M. Heteropolyacid-encapsulated TiHY zeolite as an inorganic photosynthetic reaction center mimicking the plant systems. *J. Photochem. Photobiol. A: Chem.* **160**, 181–184 (2003).
 120. Hou, W., Cronin, S. B. A review of surface plasmon resonance-enhanced photocatalysis. *Adv. Funct. Mater.* **23**, 1612–1619 (2013).
 121. DiSalle, B. F., Bernhard, S. Orchestrated photocatalytic water reduction using surface-adsorbing Iridium photosensitizers. *J. Am. Chem. Soc.* **133**, 11819–11821 (2011).
 122. Chen, X., Shen, S., Guo, L., Mao, S. S Semiconductor-based photocatalytic hydrogen generation. *Chem. Rev.* **110**, 6503–6570 (2010).
 123. Fujishima, A., Honda, K. Electrochemical photolysis of water at a semiconductor electrode. *Nature* **238**, 37–38 (1972).
 124. Zou, Z. G., Ye, J. H., Sayama, K., Arakawa, H. Direct splitting of water under visible light irradiation with an oxide semiconductor photocatalyst. *Nature* **414**, 625–627 (2001).
 125. Kudo, A., Miseki, Y. Heterogeneous photocatalyst materials for water splitting. *Chem. Soc. Rev.* **38**, 253–278 (2009).
 126. Guo, Y., Hu, C. Heterogeneous photocatalysis by solid polyoxometalates. *J. Mol. Catal. A-Chem.* **262**, 136–148 (2007).
 127. Papaconstantinou, E. Photochemistry of polyoxometalates of molybdenum and tungsten and/or vanadium. *Chem. Soc. Rev.* **18**, 1–31 (1989).
 128. Hiskia, A., Mylonas, A., Papaconstantinou, E. Comparison of the photoredox properties of polyoxometallates and semiconducting particles. *Chem. Soc. Rev.* **30**, 62–69 (2001).
 129. Renneke, R. F., Kadkhodayan, M., Pasquali, M., Hill, C. L. Roles of surface protonation on the photodynamic, catalytic, and other properties of polyoxometalates probed by the photochemical functionalization of alkanes. Implications for irradiated semiconductor metal oxides. *J. Am. Chem. Soc.* **113**, 8357–8367 (1991).
 130. Yamase, T. Photo- and electrochromism of polyoxometalates and related materials. *Chem. Rev.* **98**, 307–325 (1998).
 131. Hori, H., Koike, K., Sakai, Y., Murakami, H., Hayashi, K., Nomiya, K. New application of glycerin from a photochemical approach: Dihydrogen formation from aqueous glycerin by use of giant polyoxometalate photocatalysts. *Energ. Fuel* **19**, 2209–2213 (2005).
 132. Liu, R., Shang, X., Li, C., Xing, X., Yu, X., Zhang, G., Zhang, S., Cao, H., Bi, L. High nuclearity Co polyoxometalate based artificial photosynthesis for solar hydrogen generation. *Int. J. Hydrog. Energy* **38**, 9954–9960 (2013).
 133. Lv, H., Guo, W., Wu, K., Chen, Z., Bacsá, J., Musaev, D. G., Geletii, Y. V., Lauinger, S. M., Lian, T., Hill, C. L. A noble-metal-free, tetra-nickel polyoxotungstate catalyst for efficient photocatalytic hydrogen evolution. *J. Am. Chem. Soc.* **136**, 14015–14018 (2014).
 134. Zhao, J., Ding, Y., Wei, J., Du, X., Yu, Y., Han, R. A molecular Keggin polyoxometalate catalyst with high efficiency for visible-light driven hydrogen evolution. *Int. J. Hydrog. Energy* **39**, 18908–18918 (2014).
 135. Lv, H., Chi, Y., van Leusen, J., Koegerler, P., Chen, Z., Bacsá, J., Geletii, Y. V., Guo, W., Lian, T., Hill, C. L. $[\{Ni_4(OH)_3AsO_4\}_4(B-\alpha-PW_9O_{34})_4]^{28-}$: A new polyoxometalate structural family with catalytic hydrogen evolution activity. *Chem. Eur. J.* **21**, 17363–17370 (2015).
 136. Singh, V., Chen, Z., Ma, P., Zhang, D., Drew, M. G. B., Niu, J., Wang, J. Unprecedented $\{Fe_{14}\}/\{Fe_{10}\}$ polyoxotungstate-based nanoclusters with efficient photocatalytic H₂ evolution activity: synthesis, structure, magnetism, and electrochemistry. *Chem. Eur. J.* **22**, 10983–10989 (2016).
 137. Wang, Y., Weinstock, I. A. Polyoxometalate-decorated nanoparticles. *Chem. Soc. Rev.* **41**, 7479–7496 (2012).
 138. Xing, X., Liu, R., Yu, X., Zhang, G., Cao, H., Yao, J., Ren, B., Jiang, Z., Zhao, H. Self-assembly of CdS quantum dots with polyoxometalate encapsulated gold nanoparticles: enhanced photocatalytic activities. *J. Mater. Chem. A* **1**, 1488–1494 (2013).
 139. Guo, W., Lv, H., Chen, Z., Sullivan, K. P., Lauinger, S. M., Chi, Y., Sumliner, J. M., Lian, T., Hill, C. L. Self-assembly of polyoxometalates, Pt nanoparticles and metal-organic frameworks into a hybrid material for synergistic hydrogen evolution. *J. Mater. Chem. A* **4**, 5952–5957 (2016).
 140. Nie, Y., Chen, W., Liu, Z., Wang, E. Synthesis and photocatalytic hydrogen evolution activity of three Keggin-type polyoxometalates with different central atoms. *Inorg. Chem. Commun.* **61**, 184–186 (2015).
 141. Panagiotopoulos, A., Douvas, A. M., Argitis, P., Coutsolelos, A. G. Porphyrin-sensitized evolution of hydrogen using Dawson and Keplerate polyoxometalate photocatalysts. *Chemosuschem* **9**, 3213–3219 (2016).
 142. Schoenweiz, S., Rommel, S. A., Kuebel, J., Micheel, M., Dietzek, B., Rau, S., Streb, C. Covalent photosensitizer-polyoxometalate-catalyst dyads for visible-light-driven hydrogen evolution. *Chem. Eur. J.* **22**, 12002–12005 (2016).
 143. Prabu, R., Peramaiah, K., Palanisami, N., Pescarmona, P. P., Neppolian, B., Shanmugan, S. Non-covalent polyhedral oligomeric silsesquioxane-polyoxometalates as inorganic-organic-inorganic hybrid materials for visible-light photocatalytic splitting of water. *Inorg. Chem. Front.* **5**, 2666–2677 (2018).
 144. Zhai, X.-L., Liu, J., Hu, L.-Y., Bao, J.-C., Lan, Y.-Q. Polyoxometalate-decorated g-C₃N₄-wrapping snowflake-like CdS nanocrystal for enhanced photocatalytic hydrogen evolution. *Chem. Eur. J.* **24**, 15930–15936 (2018).
 145. Bu, Y., Liu, R., Zhen, M., Li, F., Sun, Z., Xu, L. A hybrid compound containing polyoxoanions and organic dye cations with visible-light photocatalytic H₂ evolution activity. *Inorg. Chem. Commun.* **62**, 34–36 (2015).
 146. Li, H., Yao, S., Wu, H.-L., Qu, J.-Y., Zhang, Z.-M., Lu, T.-B., Lin, W., Wang, E.-B. Charge-regulated sequential adsorption of anionic catalysts and cationic photosensitizers into metal-organic frameworks enhances photocatalytic proton reduction. *Appl. Catal. B-Environ.* **224**, 46–52 (2018).
 147. Li, X.-F., Yu, S.-B., Yang, B., Tian, J., Wang, H., Zhang, D.-W., Liu, Y., Li, Z.-T. A stable metal-covalent-supramolecular organic framework hybrid: enrichment of catalysts for visible light-induced hydrogen production. *Sci. China Chem.* **61**, 830–835 (2018).
 148. Yu, S.-B., Qi, Q., Yang, B., Wang, H., Zhang, D.-W., Liu, Y., Li, Z.-T. Enhancing hydrogen generation through nanoconfinement of sensitizers and catalysts in a homogeneous supramolecular organic framework. *Small* **14**, 1801037 (2018).
 149. Koutsouroubi, E. D., Papadas, I. T., Armatas, G. S. Ordered mesoporous polyoxometalate-organosilica frameworks as efficient photocatalysts of the hydrogen evolution reaction. *Chempluschem* **81**, 947–954 (2016).
 150. Tian, P., He, X., Li, W., Zhao, L., Fang, W., Chen, H., Zhang, F., Zhang, W., Wang, W. Zr-MOFs based on Keggin-type polyoxometalates for photocatalytic hydrogen production. *J. Mater. Sci.* **53**, 12016–12029 (2018).
 151. Vickers, J. W., Lv, H., Sumliner, J. M., Zhu, G., Luo, Z., Musaev, D. G., Geletii, Y. V., Hill, C. L. Differentiating homogeneous and heterogeneous water oxidation catalysis: confirmation that $[Co_4(H_2O)_2(\alpha-PW_9O_{34})_2]^{10-}$ is a molecular water oxidation catalyst. *J. Am. Chem. Soc.* **135**, 14110–14118 (2013).

152. Lv, H., Song, J., Geletii, Y. V., Vickers, J. W., Sumliner, J. M., Musaev, D. G., Kögerler, P., Zhuk, P. F., Bacsa, J., Zhu, G., et al. An exceptionally fast homogeneous carbon-free cobalt-based water oxidation catalyst. *J. Am. Chem. Soc.* **136**, 9268–9271 (2014).
153. Folkman, S. J., Finke, R. G. Electrochemical water oxidation catalysis beginning with Co(II) polyoxometalates: the case of the precatalyst $\text{Co}_4\text{V}_2\text{W}_{18}\text{O}_{68}^{10-}$. *ACS Catal.* **7**, 7–16 (2017).
154. Car, P.-E., Guttentag, M., Baldridge, K. K., Alberto, R., Patzke, G. R. Synthesis and characterization of open and sandwich-type polyoxometalates reveals visible-light-driven water oxidation via POM-photosensitizer complexes. *Green Chem.* **14**, 1680–1688 (2012).
155. Evangelisti, F., Car, P.-E., Blacque, O., Patzke, G. R. Photocatalytic water oxidation with cobalt-containing tungstobismutates: tuning the metal core. *Catal. Sci. Technol.* **3**, 3117–3129 (2013).
156. Santoni, M.-P., La Ganga, G., Mollica Nardo, V., Natali, M., Puntoriero, F., Scandola, F., Campagna, S. The use of a vanadium species as a catalyst in photoinduced water oxidation. *J. Am. Chem. Soc.* **136**, 8189–8192 (2014).
157. Umena, Y., Kawakami, K., Shen, J.-R., Kamiya, N. Crystal structure of oxygen-evolving photosystem II at a resolution of 1.9 angstrom. *Nature* **473**, 55–65 (2011).
158. Al-Oweini, R., Sartorel, A., Bassil, B. S., Natali, M., Berardi, S., Scandola, F., Kortz, U., Bonchio, M. Photocatalytic water oxidation by a mixed-valent $\text{Mn}^{\text{III}}_3\text{Mn}^{\text{IV}}\text{O}_3$ manganese oxo core that mimics the natural oxygen-evolving center. *Angew. Chem. Int. Ed.* **53**, 11182–11185 (2014).
159. Han, X.-B., Li, Y.-G., Zhang, Z.-M., Tan, H.-Q., Lu, Y., Wang, E.-B. Polyoxometalate-based nickel clusters as visible light-driven water oxidation catalysts. *J. Am. Chem. Soc.* **137**, 5486–5493 (2015).
160. Xu, Q., Li, H., Chi, L., Zhang, L., Wan, Z., Ding, Y., Wang, J. Identification of homogeneous $[\text{Co}_4(\text{H}_2\text{O})_4(\text{HPMIDA})_2(\text{PMIDA})_2]^{6-}$ as an effective molecular-light-driven water oxidation catalyst. *Appl. Catal. B-Environ.* **202**, 397–403 (2017).
161. Choi, Y., Jeon, D., Choi, Y., Kim, D., Kim, N., Gu, M., Bae, S., Lee, T., Lee, H.-W., Kim, B.-S., et al. Interface engineering of hematite with nacre-like catalytic multilayers for solar water oxidation. *ACS Nano* **13**, 467–475 (2019).
162. Quintana, M., López, A. M., Rapino, S., Toma, F. M., Iurlo, M., Carraro, M., Sartorel, A., Maccato, C., Ke, X., Bittencourt, C., et al. Knitting the catalytic pattern of artificial photosynthesis to a hybrid graphene nanotexture. *ACS Nano* **7**, 811–817 (2013).
163. He, P., Xu, B., Wang, P.-p., Liu, H., Wang, X. A monolayer polyoxometalate superlattice. *Adv. Mater.* **26**, 4339–4344 (2014).
164. Choi, Y., Jeon, D., Choi, Y., Ryu, J., Kim, B.-S. Self-assembled supramolecular hybrid of carbon nanodots and polyoxometalates for visible-light-driven water oxidation. *ACS Appl. Mater. Interfaces* **10**, 13434–13441 (2018).
165. Yu, L., Ding, Y., Deng, M. Polyoxometalate-based manganese clusters as catalysts for efficient photocatalytic and electrochemical water oxidation. *Appl. Catal. B-Environ.* **209**, 45–52 (2017).
166. Chakraborty, B., Gan-Or, G., Duan, Y., Raula, M., Weinstock, I. A. Visible-light-driven water oxidation with a polyoxometalate-complexed hematite core of 275 iron atoms. *Angew. Chem. Int. Ed.* **58**, 6584–6589 (2019).
167. Zhou, D., Han, B.-H. Graphene-based nanoporous materials assembled by mediation of polyoxometalate nanoparticles. *Adv. Funct. Mater.* **20**, 2717–2722 (2010).
168. Lan, Q., Zhang, Z.-M., Qin, C., Wang, X.-L., Li, Y.-G., Tan, H.-Q., Wang, E.-B. Highly dispersed polyoxometalate-doped porous Co_3O_4 water oxidation photocatalysts derived from POM@MOF crystalline materials. *Chem. Eur. J.* **22**, 15513–15520 (2016).
169. Shah, W. A., Waseem, A., Nadeem, M. A., Koegerler, P. Leaching-free encapsulation of cobalt-polyoxotungstates in MIL-100 (Fe) for highly reproducible photocatalytic water oxidation. *Appl. Catal. A-Gen.* **567**, 132–138 (2018).
170. Xi, L., Zhang, Q., Sun, Z., Song, C., Xu, L. Rational design of ternary composite photoanode $\text{BiVO}_4/\text{PW}_{12}/\text{NiTsPc}$ for improved photoelectrochemical water oxidation. *Chemelectrochem* **5**, 2534–2541 (2018).
171. Bodnarchuk, M. I., Erni, R., Krumeich, F., Kovalenko, M. V. Binary superlattices from colloidal nanocrystals and giant polyoxometalate clusters. *Nano Lett* **13**, 1699–1705 (2013).
172. Yin, P., Li, T., Forgan, R. S., Lydon, C., Zuo, X., Zheng, Z. N., Lee, B., Long, D., Cronin, L., Liu, T. Exploring the programmable assembly of a polyoxometalate-organic hybrid via metal ion coordination. *J. Am. Chem. Soc.* **135**, 13425–13432 (2013).
173. Paille, G., Gomez-Mingot, M., Roch-Marchal, C., Lassalle-Kaiser, B., Mialane, P., Fontecave, M., Mellot-Draznieks, C., Dolbecq, A. A fully noble metal-free photosystem based on cobalt-polyoxometalates immobilized in a porphyrinic metal-organic framework for water oxidation. *J. Am. Chem. Soc.* **140**, 3613–3618 (2018).
174. Shi, D., Zheng, R., Liu, C.-S., Chen, D.-M., Zhao, J., Du, M. Dual-functionalized mixed keggins- and lundqvist-type Cu_{24} -based POM@MOF for visible-light-driven H_2 and O_2 evolution. *Inorg. Chem.* **58**, 7229–7235 (2019).
175. Chang, X., Wang, T., Gong, J. CO_2 photo-reduction: insights into CO_2 activation and reaction on surfaces of photocatalysts. *Energy Environ. Sci.* **9**, 2177–2196 (2016).
176. Khenkin, A. M., Efremenko, I., Weiner, L., Martin, J. M. L., Neumann, R. Photochemical reduction of carbon dioxide catalyzed by a ruthenium-substituted polyoxometalate. *Chem. Eur. J.* **16**, 1356–1364 (2010).
177. Ettedgui, J., Diskin-Posner, Y., Weiner, L., Neumann, R. Photoreduction of carbon dioxide to carbon monoxide with hydrogen catalyzed by a rhenium(I) phenanthroline-polyoxometalate hybrid complex. *J. Am. Chem. Soc.* **133**, 188–190 (2011).
178. Ci, C., Carbo, J. J., Neumann, R., de Graaf, C., Poblet, J. M. Photoreduction mechanism of CO_2 to CO catalyzed by a rhenium(I)-polyoxometalate hybrid compound. *ACS Catal.* **6**, 6422–6428 (2016).
179. Haviv, E., Shimon, L. J. W., Neumann, R. Photochemical reduction of CO_2 with visible light using a polyoxometalate as photoreductant. *Chem. Eur. J.* **23**, 92–95 (2017).
180. Das, S., Kumar, S., Garai, S., Pochamoni, R., Paul, S., Roy, S. Softoxometalate $\{[\text{K}_{6.5}\text{Cu}(\text{OH})_{8.5}(\text{H}_2\text{O})_{7.5}]_{0.5} @ [\text{K}_3\text{PW}_{12}\text{O}_{40}]\}_n$ ($n = 1348\text{--}2024$) as an efficient inorganic material for CO_2 reduction with concomitant water oxidation. *ACS Appl. Mater. Interfaces* **9**, 35086–35094 (2017).
181. Das, S., Balaraju, T., Barman, S., Sreejith, S. S., Pochamoni, R., Roy, S. A molecular CO_2 reduction catalyst based on giant polyoxometalate $\{\text{Mo}_{368}\}$. *Front. Chem.* **6**, 514 (2018).
182. Liu, S.-M., Zhang, Z., Li, X., Jia, H., Ren, M., Liu, S. Ti-substituted Keggin-type polyoxotungstate as proton and electron reservoir encaged into metal-organic framework for carbon dioxide photoreduction. *Adv. Mater. Interfaces* **5**, 1801062 (2018).
183. Zhou, J., Chen, W., Sun, C., Han, L., Qin, C., Chen, M., Wang, X., Wang, E., Su, Z. Oxidative polyoxometalates modified graphitic carbon nitride for visible-light CO_2 reduction. *ACS Appl. Mater. Interfaces* **9**, 11689–11695 (2017).
184. Li, X.-X., Liu, J., Zhang, L., Dong, L.-Z., Xin, Z.-F., Li, S.-L., Huang-Fu, X.-Q., Huang, K., Lan, Y.-Q. Hydrophobic polyoxometalate-based metal-organic framework for efficient CO_2 photoconversion. *ACS Appl. Mater. Interfaces* **11**, 25790–25795 (2019).
185. Huang, Q., Liu, J., Feng, L., Wang, Q., Guan, W., Dong, L.-Z., Zhang, L., Yan, L.-K., Lan, Y.-Q., Zhou, H.-C. Multielectron transportation of polyoxometalate-grafted metalloporphyrin coordination frameworks for selective CO_2 -to- CH_4 photoconversion. *Natl. Sci. Rev.* (2019). <https://doi.org/10.1093/nsr/nwz096>.
186. Park, H., Choi, W. Photoelectrochemical investigation on electron transfer mediating behaviors of polyoxometalate in UV-illuminated suspensions of TiO_2 and Pt/TiO_2 . *J. Phys. Chem. B* **107**, 3885–3890 (2003).
187. Kim, H.-i., Kim, J., Kim, W., Choi, W. Enhanced photocatalytic and photoelectrochemical activity in the ternary hybrid of

- CdS/TiO₂/WO₃ through the cascaded electron transfer. *J. Phys. Chem. C* **115**, 9797–9805 (2011).
188. Walsh, J. J., Long, D.-L., Cronin, L., Bond, A. M., Forster, R. J., Keyes, T. E. Electronic and photophysical properties of adducts of [Ru(bpy)₃]²⁺ and Dawson-type sulfite polyoxomolybdates α/β -[Mo₁₈O₅₄(SO₃)₂]⁴⁻. *Dalton Trans* **40**, 2038–2045 (2011).
 189. Gao, L., Sun, Q., Wang, K. Photoelectrochemical properties of a series of electrostatically self-assembled films based on sandwich-type polyoxometalates and a bichromophore hemicyanine dye. *J. Colloid Interface Sci.* **393**, 92–96 (2013).
 190. Sun, Z., Li, F., Xu, L., Liu, S., Zhao, M., Xu, B. Effects of Dawson-type tungstophosphate on photoelectrochemical responses of cadmium sulfide composite film. *J. Phys. Chem. C* **116**, 6420–6426 (2012).
 191. Xie, Y. Photoelectrochemical reactivity of a hybrid electrode composed of polyoxophosphotungstate encapsulated in titania nanotubes. *Adv. Funct. Mater.* **16**, 1823–1831 (2006).
 192. Wang, M., Shang, X., Yu, X., Liu, R., Xie, Y., Zhao, H., Cao, H., Zhang, G. Graphene-CdS quantum dots-polyoxometalate composite films for efficient photoelectrochemical water splitting and pollutant degradation. *Phys. Chem. Chem. Phys.* **16**, 26016–26023 (2014).
 193. Xiang, X., Fielden, J., Rodriguez-Cordoba, W., Huang, Z., Zhang, N., Luo, Z., Musaev, D. G., Lian, T., Hill, C. L. Electron transfer dynamics in semiconductor-chromophore-polyoxometalate catalyst photoanodes. *J. Phys. Chem. C* **117**, 918–926 (2013).
 194. Zhang, Y., Tao, R., Zhao, X., Sun, Z., Wang, Y., Xu, L. A highly photoconductive composite prepared by incorporating polyoxometalate into perovskite for photodetection application. *Chem. Commun.* **52**, 3304–3307 (2016).
 195. Jeon, D., Kim, H., Lee, C., Han, Y., Gu, M., Kim, B.-S., Ryu, J. Layer-by-layer assembly of polyoxometalates for photoelectrochemical (PEC) water splitting: toward modular PEC devices. *ACS Appl. Mater. Interfaces* **9**, 40151–40161 (2017).
 196. Liu, R., Sun, Z., Song, X., Zhang, Y., Xu, L., Xi, L. Toward non-precious nanocomposite photocatalyst: an efficient ternary photoanode TiO₂ nanotube/Co₉S₈/polyoxometalate for photoelectrochemical water splitting. *Appl. Catal. A-Gen.* **544**, 137–144 (2017).
 197. Xi, L., Jin, Z., Sun, Z., Liu, R., Xu, L. Enhanced photoelectrocatalytic performance for water oxidation by polyoxometalate molecular doping in BiVO₄ photoanodes. *Appl. Catal. A-Gen.* **536**, 67–74 (2017).
 198. Bae, S., Kim, H., Jeon, D., Ryu, J. Catalytic multilayers for efficient solar water oxidation through catalyst loading and surface-state passivation of BiVO₄ Photoanodes. *ACS Appl. Mater. Interfaces* **11**, 7990–7999 (2019).
 199. Lauinger, S. M., Sumliner, J. M., Yin, Q., Xu, Z., Liang, G., Glass, E. N., Lian, T., Hill, C. L. High stability of immobilized polyoxometalates on TiO₂ nanoparticles and nanoporous films for robust, light-induced water oxidation. *Chem. Mater.* **27**, 5886–5891 (2015).
 200. Cao, X., Wang, Y., Lin, J., Ding, Y. Ultrathin CoO_x nanolayers derived from polyoxometalate for enhanced photoelectrochemical performance of hematite photoanodes. *J. Mater. Chem. A* **7**, 6294–6303 (2019).
 201. Tourneur, J., Fabre, B., Loget, G., Vacher, A., Meriadec, C., Ababou-Girard, S., Gouttefangeas, F., Joanny, L., Cadot, E., Haouas, M., et al. Molecular and material engineering of photocathodes derivatized with polyoxometalate-supported {Mo₃S₄} HER catalysts. *J. Am. Chem. Soc.* **141**, 11954–11962 (2019).
 202. Solarska, R., Bienkowski, K., Zoladek, S., Majcher, A., Stefaniuk, T., Kulesza, P. J., Augustynski, J. Enhanced water splitting at thin film tungsten trioxide photoanodes bearing plasmonic gold-polyoxometalate particles. *Angew. Chem. Int. Ed.* **53**, 14196–14200 (2014).
 203. Kim, H., Bae, S., Jeon, D., Ryu, J. Fully solution-processable Cu₂O-BiVO₄ photo-electrochemical cells for bias-free solar water splitting. *Green Chem* **20**, 3732–3742 (2018).
 204. Han, Y., Choi, K., Oh, H., Kim, C., Jeon, D., Lee, C., Lee, J. H., Ryu, J. Cobalt polyoxometalate-derived CoWO₄ oxygen-evolving catalysts for efficient electrochemical and photoelectrochemical water oxidation. *J. Catal.* **367**, 212–220 (2018).
 205. Sun, H., Guo, L.-Y., Li, J.-S., Bai, J.-P., Su, F., Zhang, L.-C., Sang, X.-J., You, W.-S., Zhu, Z.-M. Two New armtype polyoxometalates grafted on titanium dioxide films: towards enhanced photoelectrochemical performance. *Chemsuschem* **9**, 1125–1133 (2016).
 206. Poizat, P., Laruelle, S., Grugeon, S., Dupont, L., Tarascon, J. M. Nano-sized transition-metaloxides as negative-electrode materials for lithium-ion batteries. *Nature* **407**, 496–499 (2000).
 207. Sonoyama, N., Suganuma, Y., Kume, T., Quan, Z. Lithium intercalation reaction into the Keggin type polyoxomolybdates. *J. Power Sources* **196**, 6822–6827 (2011).
 208. Wang, H., Hamanaka, S., Nishimoto, Y., Irle, S., Yokoyama, T., Yoshikawa, H., Awaga, K. In operando X-ray absorption fine structure studies of polyoxometalate molecular cluster batteries: polyoxometalates as electron sponges. *J. Am. Chem. Soc.* **134**, 4918–4924 (2012).
- An operando X-ray absorption fine structure study showed the “electron sponge” feature of Keggin-type POM, [PMo₁₂O₄₀]³⁻.**
209. Chen, H.-Y., Friedl, J., Pan, C.-J., Haider, A., Al-Oweini, R., Cheah, Y. L., Lin, M.-H., Kortz, U., Hwang, B.-J., Srinivasan, M., et al. In situ X-ray absorption near edge structure studies and charge transfer kinetics of Na₆[V₁₀O₂₈] electrodes. *Phys. Chem. Chem. Phys.* **19**, 3358–3365 (2017).
 210. Wang, H., Isobe, J., Matsumura, D., Yoshikawa, H. In situ X-ray absorption fine structure studies of amorphous and crystalline polyoxovanadate cluster cathodes for lithium batteries. *J. Solid State Electrochem.* **22**, 2067–2071 (2018).
 211. Wang, H., Yamada, T., Hamanaka, S., Yoshikawa, H., Awaga, K. Cathode composition dependence of battery performance of polyoxometalate (POM) molecular cluster batteries. *Chem. Lett.* **43**, 1067–1069 (2014).
 212. Nishimoto, Y., Yokogawa, D., Yoshikawa, H., Awaga, K., Irle, S. Super-reduced polyoxometalates: excellent molecular cluster battery components and semipermeable molecular capacitors. *J. Am. Chem. Soc.* **136**, 9042–9052 (2014).
 213. Chen, J.-J., Symes, M. D., Fan, S.-C., Zheng, M.-S., Miras, H. N., Dong, Q.-F., Cronin, L. High-performance polyoxometalate-based cathode materials for rechargeable lithium-ion batteries. *Adv. Mater.* **27**, 4649–4654 (2015).
 214. Zhang, Z., Yoshikawa, H., Zhang, Z., Murayama, T., Sadakane, M., Inoue, Y., Ueda, W., Awaga, K., Hara, M. Synthesis of vanadium-incorporated, polyoxometalate-based open frameworks and their applications for cathode-active materials. *Eur. J. Inorg. Chem.* **8**, 1242–1250 (2016).
 215. Zhang, Z., Ishikawa, S., Kikuchi, M., Yoshikawa, H., Lian, Q., Wang, H., Ina, T., Yoshida, A., Sadakane, M., Matsumoto, F., et al. High-performance cathode based on microporous Mo-V-Bi oxide for Li Battery and investigation by operando X-ray absorption fine structure. *ACS Appl. Mater. Interfaces* **9**, 26052–26059 (2017).
 216. Chen, J.-J., Ye, J.-C., Zhang, X.-G., Symes, M. D., Fan, S.-C., Long, D.-L., Zheng, M.-S., Wu, D.-Y., Cronin, L., Dong, Q.-F. Design and performance of rechargeable sodium ion batteries, and symmetrical Li-ion batteries with supercapacitor-like power density based upon polyoxovanadates. *Adv. Energy Mater.* **8**, 1701021 (2018).
 217. Hartung, S., Bucher, N., Chen, H.-Y., Al-Oweini, R., Sreejith, S., Borah, P., Zhao, Y., Kortz, U., Stimming, U., Hoster, H. E., et al. Vanadium-based polyoxometalate as new material for sodium-ion battery anodes. *J. Power Sources* **288**, 270–277 (2015).
 218. Anjass, M. H., Deisböck, M., Greiner, S., Fichtner, M.,

- Streb, C. Differentiating molecular and solid-state vanadium oxides as active materials in battery electrodes. *Chemelectrochem* **6**, 398–403 (2019).
219. Kawasaki, N., Wang, H., Nakanishi, R., Hamanaka, S., Kitaura, R., Shinohara, H., Yokoyama, T., Yoshikawa, H., Awaga, K. Nanohybridization of polyoxometalate clusters and single-wall carbon nanotubes: applications in molecular cluster batteries. *Angew. Chem. Int. Ed.* **50**, 3471–3474 (2011).
 220. Wang, H., Kawasaki, N., Yokoyama, T., Yoshikawa, H., Awaga, K. Molecular cluster batteries of nano-hybrid materials between Keggin POMs and SWNTs. *Dalton Trans* **41**, 9863–9866 (2012).
 221. Ma, D., Liang, L., Chen, W., Liu, H., Song, Y.-F. Covalently tethered polyoxometalate-pyrene hybrids for noncovalent sidewall functionalization of single-walled carbon nanotubes as high-performance anode material. *Adv. Funct. Mater.* **23**, 6100–6105 (2013).
 222. Chen, W., Huang, L., Hu, J., Li, T., Jia, F., Song, Y.-F. Connecting carbon nanotubes to polyoxometalate clusters for engineering high-performance anode materials. *Phys. Chem. Chem. Phys.* **16**, 19668–19673 (2014).
 223. Huang, L., Hu, J., Ji, Y., Streb, C., Song, Y.-F. Pyrene-Anderson-modified CNTs as anode materials for lithium-ion batteries. *Chem. Eur. J.* **21**, 18799–18804 (2015).
 224. Ji, Y., Hu, J., Huang, L., Chen, W., Streb, C., Song, Y.-F. Covalent attachment of Anderson-type polyoxometalates to single-walled carbon nanotubes gives enhanced performance electrodes for lithium ion batteries. *Chem. Eur. J.* **21**, 6469–6474 (2015).
 225. Hu, J., Ji, Y., Chen, W., Streb, C., Song, Y.-F. “Wiring” redox-active polyoxometalates to carbon nanotubes using a sonication-driven periodic functionalization strategy. *Energy Environ. Sci.* **9**, 1095–1101 (2016).
 226. Xie, J., Zhang, Y., Han, Y., Li, C. High-capacity molecular scale conversion anode enabled by hybridizing cluster-type framework of high loading with amino-functionalized graphene. *ACS Nano* **10**, 5304–5313 (2016).
 227. Shen, F.-C., Wang, Y.-R., Li, S.-L., Liu, J., Dong, L.-Z., Wei, T., Cui, Y.-C., Wu, X. L., Xu, Y., Lan, Y.-Q. Self-assembly of polyoxometalate/reduced graphene oxide composites induced by ionic liquids as a high-rate cathode for batteries: “killing two birds with one stone”. *J. Mater. Chem. A* **6**, 1743–1750 (2018).
 228. Liu, W.-J., Yu, G., Zhang, M., Li, R.-H., Dong, L.-Z., Zhao, H.-S., Chen, Y.-J., Xin, Z.-F., Li, S.-L., Lan, Y.-Q. Investigation of the enhanced lithium battery storage in a polyoxometalate model: from solid spheres to hollow balls. *Small Methods* **2**, 1800154 (2018).
 229. Kume, K., Kawasaki, N., Wang, H., Yamada, T., Yoshikawa, H., Awaga, K. Enhanced capacitor effects in polyoxometalate/graphene nanohybrid materials: a synergetic approach to high performance energy storage. *J. Mater. Chem. A* **2**, 3801–3807 (2014).
 230. Ding, Y.-H., Peng, J., Khan, S.-U., Yuan, Y. A new polyoxometalate (POM)-based composite: fabrication through POM-assisted polymerization of dopamine and properties as anode materials for high-performance lithium-ion batteries. *Chem. Eur. J.* **23**, 10338–10343 (2017).
 231. Ni, E., Tsukada, T., Wen, Q., Sonoyama, N. Improved performance of nano-sized polyoxometalate as lithium-battery cathode by conductive polymer coating. *J. Electrochem. Soc.* **166**, 5226–5230 (2018).
 232. Yang, H., Song, T., Liu, L., Devadoss, A., Xia, F., Han, H., Park, H., Sigmund, W., Kwon, K., Paik, U. Polyaniline/polyoxometalate hybrid nanofibers as cathode for lithium ion batteries with improved lithium storage capacity. *J. Phys. Chem. C* **117**, 17376–17381 (2013).
 233. Lira-Cantú, M., Gómez-Romero, P. Electrochemical and chemical syntheses of the hybrid organic-inorganic electroactive material formed by phosphomolybdate and polyaniline. application as cation-insertion electrodes. *Chem. Mater.* **10**, 698–704 (1998).
 234. Sun, C.-Y., Liu, S.-X., Liang, D.-D., Shao, K.-Z., Ren, Y.-H., Su, Z.-M. Highly stable crystalline catalysts based on a microporous metal-organic framework and polyoxometalates. *J. Am. Chem. Soc.* **131**, 1883–1888 (2009).
 235. Song, J., Luo, Z., Britt, D. K., Furukawa, H., Yaghi, O. M., Hardcastle, K. I., Hill, C. L. A multiunit catalyst with synergistic stability and reactivity: a polyoxometalate–metal organic framework for aerobic decontamination. *J. Am. Chem. Soc.* **133**, 16839–16846 (2011).
 236. Yu, R., Kuang, X.-F., Wu, X.-Y., Lu, C.-Z., Donahue, J. P. Stabilization and immobilization of polyoxometalates in porous coordination polymers through host-guest interactions. *Coordin. Chem. Rev.* **253**, 2872–2890 (2009).
 237. Stock, N., Biswas, S. Synthesis of metal-organic frameworks (MOFs): routes to various MOF topologies, morphologies, and composites. *Chem. Rev.* **112**, 933–969 (2012).
 238. Yue, Y., Li, Y., Bi, Z., Veith, G. M., Bridges, C. A., Guo, B., Chen, J., Mullins, D. R., Surwade, S. P., Mahurin, S. M., et al. A POM-organic framework anode for Li-ion battery. *J. Mater. Chem. A* **3**, 22989–22995 (2015).
 239. Zhu, P.-P., Sheng, N., Li, M.-T., Li, J.-S., Liu, G.-D., Yang, X.-Y., Sha, J.-Q., Zhu, M.-L., Jiang, J. Fabrication and electrochemical performance of unprecedented POM-based metal-carbene frameworks. *J. Mater. Chem. A* **5**, 17920–17925 (2017).
 240. Yang, X., Zhu, P., Ren, J., Chen, Y., Li, X., Sha, J., Jiang, J. Surfactant-assisted synthesis and electrochemical properties of an unprecedented polyoxometalate-based metal-organic nanocaged framework. *Chem. Commun.* **55**, 1201–1204 (2019).
 241. Huang, Q., Wei, T., Zhang, M., Dong, L.-Z., Zhang, A. M., Li, S.-L., Liu, W.-J., Liu, J., Lan, Y.-Q. A highly stable polyoxometalate-based metal-organic framework with π - π stacking for enhancing lithium ion battery performance. *J. Mater. Chem. A* **5**, 8477–8483 (2017).
 242. Wang, Y.-Y., Zhang, M., Li, S.-L., Zhang, S.-R., Xie, W., Qin, J.-S., Su, Z.-M., Lan, Y.-Q. Diamondoid-structured polymolybdate-based metal-organic frameworks as high-capacity anodes for lithium-ion batteries. *Chem. Commun.* **53**, 5204–5207 (2017).
 243. Wei, T., Zhang, M., Wu, P., Tang, Y.-J., Li, S.-L., Shen, F.-C., Wang, X.-L., Zhou, X.-P., Lan, Y.-Q. POM-based metal-organic framework/reduced graphene oxide nanocomposites with hybrid behavior of battery-supercapacitor for superior lithium storage. *Nano Energy* **34**, 205–214 (2017).
 244. Yang, X.-Y., Wei, T., Li, J.-S., Sheng, N., Zhu, P.-P., Sha, J.-Q., Wang, T., Lan, Y.-Q. Polyoxometalate-incorporated metallapillararene/metallacalixarene metal-organic frameworks as anode materials for lithium ion batteries. *Inorg. Chem.* **56**, 8311–8318 (2017).
 245. Zhang, A. M., Zhang, M., Lan, D., Wang, H.-N., Tang, Y.-J., Wang, X.-L., Dong, L.-Z., Zhang, L., Li, S.-L., Lan, Y.-Q. Polyoxometalate-based metal-organic framework on carbon cloth with a hot-pressing method for high-performance lithium-ion batteries. *Inorg. Chem.* **57**, 11726–11731 (2018).
 246. Zhang, M., Zhang, A. M., Wang, X.-X., Huang, Q., Zhu, X., Wang, X.-L., Dong, L.-Z., Li, S.-L., Lan, Y.-Q. Encapsulating ionic liquids into POM-based MOFs to improve their conductivity for superior lithium storage. *J. Mater. Chem. A* **6**, 8735–8741 (2018).
 247. Xia, G., Liu, D., Zheng, F., Yang, Y., Su, J., Chen, Q. Preparation of porous MoO_2 @C nano-octahedrons from a polyoxometalate-based metal-organic framework for highly reversible lithium storage. *J. Mater. Chem. A* **4**, 12434–12441 (2016).
 248. Xu, X., Chen, S., Chen, Y., Sun, H., Song, L., He, W., Wang, X. Polyoxometalate cluster-incorporated metal-organic framework hierarchical nanotubes. *Small* **12**, 2982–2990 (2016).
 249. Ji, Y., Hu, J., Biskupek, J., Kaiser, U., Song, Y.-F., Streb, C. Polyoxometalate-based bottom-up fabrication of graphene quantum dot/manganese vanadate composites as lithium ion battery anodes. *Chem. Eur. J.* **23**, 16637–16643 (2017).
 250. Wang, H., Isobe, J., Shimizu, T., Matsumura, D., Ina, T., Yoshikawa, H. Preparation of γ - LiV_2O_5 from polyoxovanadate

- cluster $\text{Li}_7[\text{V}_{15}\text{O}_{36}(\text{CO}_3)]$ as a high-performance cathode material and its reaction mechanism revealed by *operando* XAFS. *J. Power Sources* **360**, 150–156 (2017).
251. Wang, P., Tian, J., Hu, J., Zhou, X., Li, C. Supernormal conversion anode consisting of high-density MoS_2 bubbles wrapped in thin carbon network by self-sulfuration of polyoxometalate complex. *ACS Nano* **11**, 7390–7400 (2017).
 252. Zhu, Y., Murali, S., Stoller, M. D., Ganesh, K. J., Cai, W., Ferreira, P. J., Pirkle, A., Wallace, R. M., Cychosz, K. A., Thommes, M., et al. Carbon-based supercapacitors produced by activation of graphene. *Science* **332**, 1537–1541 (2011).
 253. Winter, M., Brodd, R. J. What are batteries, fuel cells, and supercapacitors? *Chem. Rev.* **104**, 4245–4269 (2004).
 254. Wang, G., Zhang, L., Zhang, J. A review of electrode materials for electrochemical supercapacitors. *Chem. Soc. Rev.* **41**, 797–828 (2012).
 255. Yamada, A., Goodenough, J. B. Keggin-type heteropolyacids as electrode materials for electrochemical supercapacitors. *J. Electrochem. Soc.* **145**, 737–743 (1998).
 256. Herrmann, S., Aydemir, N., Naegele, F., Fantauzzi, D., Jacob, T., Travas-Sejdic, J., Streb, C. Enhanced capacitive energy storage in polyoxometalate-doped polypyrrole. *Adv. Funct. Mater.* **27** (2017).
 257. Suppes, G. M., Cameron, C. G., Freund, M. S. A polypyrrole/phosphomolybdic acid vertical bar poly(3,4-ethylenedioxythiophene)/phosphotungstic acid asymmetric supercapacitor. *J. Electrochem. Soc.* **157**, A1030–A1034 (2010).
 258. Wang, H.-N., Zhang, M., Zhang, A. M., Shen, F.-C., Wang, X.-K., Sun, S.-N., Chen, Y.-J., Lan, Y.-Q. Polyoxometalate-based metal-organic frameworks with conductive polypyrrole for supercapacitors. *ACS Appl. Mater. Interfaces* **10**, 32265–32270 (2018).
 259. Yang, M., Hong, S. B., Yoon, J. H., Kim, D. S., Jeong, S. W., Yoo, D. E., Lee, T. J., Lee, K. G., Lee, S. J., Choi, B. G. Fabrication of flexible, redoxable, and conductive nanopillar arrays with enhanced electrochemical performance. *ACS Appl. Mater. Interfaces* **8**, 22220–22226 (2016).
 260. Dong, Y., Chen, L., Chen, W., Zheng, X., Wang, X., Wang, E. rGO functionalized with a highly electronegative Keplerate-type polyoxometalate for high-energy-density aqueous asymmetric supercapacitors. *Chem. Asian J.* **13**, 3304–3313 (2018).
 261. Zhang, S., Liu, R., Li, S., Dolbecq, A., Mialane, P., Suo, L., Bi, L., Zhang, B., Liu, T., Wu, C., et al. Simple and efficient polyoxomolybdate-mediated synthesis of novel graphene and metal nanohybrids for versatile applications. *J. Colloid Interf. Sci.* **514**, 507–516 (2018).
 262. Pakulski, D., Gorczynski, A., Czepa, W., Liu, Z., Ortolani, L., Morandi, V., Patroniak, V., Ciesielski, A., Samori, P. Novel Keplerate type polyoxometalate-surfactant-graphene hybrids as advanced electrode materials for supercapacitors. *Energy Storage Mater.* **17**, 186–193 (2019).
 263. Xie, T., Zhang, L., Wang, Y., Wang, Y., Wang, X. Graphene-based supercapacitors as flexible wearable sensor for monitoring pulse-beat. *Ceram. Int.* **45**, 2516–2520 (2019).
 264. Chinnathambi, S., Ammam, M. A molecular hybrid polyoxometalate-organometallic moiety and its relevance to supercapacitors in physiological electrolytes. *J. Power Sources* **284**, 524–535 (2015).
 265. Hu, C., Zhao, E., Nitta, N., Magasinski, A., Berdichevsky, G., Yushin, G. Aqueous solutions of acidic ionic liquids for enhanced stability of polyoxometalate-carbon supercapacitor electrodes. *J. Power Sources* **326**, 569–574 (2016).
 266. Gomez-Romero, P., Chojak, M., Cuentas-Gallegos, K., Asensio, J. A., Kulesza, P. J., Casan-Pastor, N., Lira-Cantu, M. Hybrid organic-inorganic nanocomposite materials for application in solid state electrochemical supercapacitors. *Electrochem. Commun.* **5**, 149–153 (2003).
 267. Suppes, G. M., Deore, B. A., Freund, M. S. Porous conducting polymer/heteropolyoxometalate hybrid material for electrochemical supercapacitor applications. *Langmuir* **24**, 1064–1069 (2008).
 268. White, A. M., Slade, R. C. T. Polymer electrodes doped with heteropolymetallates and their use within solid-state supercapacitors. *Synthetic Met.* **139**, 123–131 (2003).
 269. White, A. M., Slade, R. C. T. Investigation of vapour-grown conductive polymer/heteropolyacid electrodes. *Electrochim. Acta* **48**, 2583–2588 (2003).
 270. White, A. M., Slade, R. C. T. Electrochemically and vapour grown electrode coatings of poly(3,4-ethylenedioxythiophene) doped with heteropolyacids. *Electrochim. Acta* **49**, 861–865 (2004).
 271. Genovese, M., Lian, K. Pseudocapacitive behavior of Keggin type polyoxometalate mixtures. *Electrochem. Commun.* **43**, 60–62 (2014).
 272. Genovese, M., Foong, Y. W., Lian, K. The unique properties of aqueous polyoxometalate (POM) mixtures and their role in the design of molecular coatings for electrochemical energy storage. *Electrochim. Acta* **199**, 261–269 (2016).
 273. Ruiz, V., Suarez-Guevara, J., Gomez-Romero, P. Hybrid electrodes based on polyoxometalate-carbon materials for electrochemical supercapacitors. *Electrochem. Commun.* **24**, 35–38 (2012).
 274. Suarez-Guevara, J., Ruiz, V., Gomez-Romero, P. Hybrid energy storage: high voltage aqueous supercapacitors based on activated carbon-phosphotungstate hybrid materials. *J. Mater. Chem. A* **2**, 1014–1021 (2014).
 275. Suarez-Guevara, J., Ruiz, V., Gomez-Romero, P. Stable graphene-polyoxometalate nanomaterials for application in hybrid supercapacitors. *Phys. Chem. Chem. Phys.* **16**, 20411–20414 (2014).
 276. Genovese, M., Lian, K. Polyoxometalate modified pine cone biochar carbon for supercapacitor electrodes. *J. Mater. Chem. A* **5**, 3939–3947 (2017).
 277. Dubal, D. P., Chodankar, N. R., Vinu, A., Kim, D.-H., Gomez-Romero, P. Asymmetric supercapacitors based on reduced graphene oxide with different polyoxometalates as positive and negative electrodes. *ChemSuschem* **10**, 2742–2750 (2017).
 278. Mu, A., Li, J., Chen, W., Sang, X., Su, Z., Wang, E. The composite material based on Dawson-type polyoxometalate and activated carbon as the supercapacitor electrode. *Inorg. Chem. Commun.* **55**, 149–152 (2015).
 279. Chen, Y., Han, M., Tang, Y., Bao, J., Li, S., Lan, Y., Dai, Z. Polypyrrole-polyoxometalate/reduced graphene oxide ternary nanohybrids for flexible, all-solid-state supercapacitors. *Chem. Commun.* **51**, 12377–12380 (2015).
 280. Dubal, D. P., Suarez-Guevara, J., Tonti, D., Enciso, E., Gomez-Romero, P. A high voltage solid state symmetric supercapacitor based on graphene-polyoxometalate hybrid electrodes with a hydroquinone doped hybrid gelelectrolyte. *J. Mater. Chem. A* **3**, 23483–23492 (2015).
 281. Wang, G., Chen, T., Wang, X., Ma, H., Pang, H. High-performance supercapacitor afforded by a high-connected Keggin-based 3D coordination polymer. *Eur. J. Inorg. Chem.* **45**, 5350–5355 (2017).
 282. Chai, D., Hou, Y., O'Halloran, K. P., Pang, H., Ma, H., Wang, G., Wang, X. Enhancing energy storage via TEA-dependent controlled syntheses: two series of polyoxometalate-based inorganic-organic hybrids and their supercapacitor properties. *ChemElectrochem* **5**, 3443–3450 (2018).
 283. Prabhakaran, V., Mehdi, B. L., Ditto, J. J., Engelhard, M. H., Wang, B., Gunaratne, K. D. D., Johnson, D. C., Browning, N. D., Johnson, G. E., Laskin, J. Rational design of efficient electrode-electrolyte interfaces for solid-state energy storage using ion soft landing. *Nat. Commun.* **7**, 11399 (2016).
 284. Prabhakaran, V., Lang, Z., Clotet, A., Poblet, J. M., Johnson, G. E., Laskin, J. Controlling the activity and stability of electrochemical interfaces using atom-by-atom metal substitution of redox species. *ACS Nano* **13**, 458–466 (2019).
 285. Liu, J., Chen, Z., Chen, S., Zhang, B., Wang, J., Wang, H., Tian, B., Chen, M., Fan, X., Huang, Y., et al. "Electron/ion sponge"-like

- V-based polyoxometalate: toward high-performance cathode for rechargeable sodium ion batteries. *ACS Nano* **11**, 6911–6920 (2017).
286. Lin, C.-C., Lin, W.-H., Huang, S.-C., Hu, C.-W., Chen, T.-Y., Hsu, C.-T., Yang, H., Haider, A., Lin, Z., Kortz, U., et al. Mechanism of sodium ion storage in $\text{Na}_7[\text{H}_2\text{PV}_{14}\text{O}_{42}]$ anode for sodium-ion batteries. *Adv. Mater. Interfaces* **5**, 1800491 (2018).
 287. Choi, W., Im, D., Park, M. S., Ryu, Y.-G., Hwang, S. S., Kim, Y. S., Kim, H., Doo, S.-G., Chang, H. Keggin-type polyoxometalates as bidirectional redox mediators for rechargeable batteries. *Electrochemistry* **84**, 882–886 (2016).
 288. Yao, W., Liu, L., Wu, X., Qin, C., Xie, H., Su, Z. Polyoxometalates/active carbon thin separator for improving cycle performance of lithium-sulfur batteries. *ACS Appl. Mater. Interfaces* **10**, 35911–35918 (2018).
 289. Ye, J. C., Chen, J. J., Yuan, R. M., Deng, D. R., Zheng, M. S., Cronin, L., Dong, Q. F. Strategies to explore and develop reversible redox reactions of Li-S in electrode architectures using silver-polyoxometalate clusters. *J. Am. Chem. Soc.* **140**, 3134–3138 (2018).
 290. Lee, J.-S., Lee, C., Lee, J.-Y., Ryu, J., Ryu, W.-H. Polyoxometalate as a nature-inspired bifunctional catalyst for lithium-oxygen batteries. *ACS Catal* **8**, 7213–7221 (2018).
 291. Etesami, M., Abouzari-Lotf, E., Sha'rani, S. S., Miyake, M., Nia, P. M., Ripin, A., Ahmad, A. Self-assembled heteropolyacid on nitrogen-enriched carbon nanofiber for vanadium flow batteries. *Nanoscale* **10**, 13212–13222 (2018).
 292. Friedl, J., Holland-Cunz, M. V., Cording, F., Pfanschilling, F. L., Wills, C., McFarlane, W., Schrick, B., Fleck, R., Wolfschmidt, H., Stimming, U. Asymmetric polyoxometalate electrolytes for advanced redox flow batteries. *Energy Environ. Sci.* **11**, 3010–3018 (2018).
 293. VanGelder, L. E., Matson, E. M. Heterometal functionalization yields improved energy density for charge carriers in nonaqueous redox flow batteries. *J. Mater. Chem. A* **6**, 13874–13882 (2018).
 294. Chen, J.-J., Symes, M. D., Cronin, L. Highly reduced and protonated aqueous solutions of $[\text{P}_2\text{W}_{18}\text{O}_{62}]^{6-}$ for on-demand hydrogen generation and energy storage. *Nat. Chem.* **10**, 1042–1047 (2018).
 295. Ito, T., Otobe, S., Oda, T., Kojima, T., Ono, S., Watanabe, M., Kiyota, Y., Misawa, T., Koguchi, S., Higuchi, M., et al. Polymerizable ionic liquid crystals comprising polyoxometalate clusters toward inorganic-organic hybrid solid electrolytes. *Polymers* **9**, 290 (2017).
 296. Tong, X., Thangadurai, V. Hybrid gel electrolytes derived from Keggin-type polyoxometalates and imidazolium-based ionic liquid with enhanced electrochemical stability and fast ionic conductivity. *J. Phys. Chem. C* **119**, 7621–7630 (2015).
 297. Ji, Y., Huang, L., Hu, J., Streb, C., Song, Y.-F. Polyoxometalate-functionalized nanocarbon materials for energy conversion, energy storage and sensor systems. *Energy Environ. Sci.* **8**, 776–789 (2015).
 298. Siroma, Z., Kakitsubo, R., Fujiwara, N., Ioroi, T., Yamazaki, S.-i., Yasuda, K. Depression of proton conductivity in recast Nafion (R) film measured on flat substrate. *J. Power Sources* **189**, 994–998 (2009).
 299. Xu, L., Wang, Z., Lu, Y., Yan, T., Tian, H., Li, X., Wang, S., Sun, X., Zhang, Z., Dang, T., et al. Synthesis and proton conductivity of two novel molybdate polymers. *New J. Chem.* **42**, 16516–16522 (2018).
 300. Miao, J., Liu, Y., Tang, Q., He, D., Yang, G., Shi, Z., Liu, S., Wu, Q. Proton conductive watery channels constructed by Anderson polyanions and lanthanide coordination cations. *Dalton Trans* **43**, 14749–14755 (2014).
 301. Liu, Y., Liu, S., Lai, X., Miao, J., He, D., Li, N., Luo, F., Shi, Z., Liu, S. Polyoxometalate-modified sponge-like graphene oxide monolith with high proton-conducting performance. *Adv. Funct. Mater.* **25**, 4480–4485 (2015).
 302. Lai, X., Liu, Y., Yang, G., Liu, S., Shi, Z., Lu, Y., Luo, F., Liu, S. Controllable proton-conducting pathways via situating polyoxometalates in targeting pores of a metal-organic framework. *J. Mater. Chem. A* **5**, 9611–9617 (2017).
 303. Li, Z., Lin, L.-D., Yu, H., Li, X.-X., Zheng, S.-T. All-inorganic ionic porous material based on giant spherical polyoxometalates containing core-shell $\text{K}_6@ \text{K}_{36}$ -Water Cage. *Angew. Chem. Int. Ed.* **57**, 15777–15781 (2018).
 304. Chand, S., Pal, S. C., Pal, A., Ye, Y., Lin, Q., Zhang, Z., Xi-ang, S., Das, M. C. Metallo hydrogen-bonded organic frameworks (MHOs) as new class of crystalline materials for protonic conduction. *Chem. Eur. J.* **25**, 1691–1695 (2019).
 305. Yang, P., Alsufyani, M., Emwas, A.-H., Chen, C., Khashab, N. M. Lewis acid guests in a $\{\text{P}_8\text{W}_{48}\}$ archetypal polyoxotungstate host: enhanced proton conductivity via metal-oxo cluster within cluster assemblies. *Angew. Chem. Int. Ed.* **57**, 13046–13051 (2018).
 306. Parayil, S. K., Lee, Y. M., Yoon, M. Photoelectrochemical solar cell properties of heteropolytungstic acid-incorporated TiO_2 nanodisc thin films. *Electrochem. Commun.* **11**, 1211–1216 (2009).
 307. Zhang, L., Yang, X., Wang, W., Gurdzadyan, G. G., Li, J., Li, X., An, J., Yu, Z., Wang, H., Cai, B., et al. 13.6% efficient organic dye-sensitized solar cells by minimizing energy losses of the excited state. *ACS Energy Lett* **4**, 943–951 (2019).
 308. Chen, L., Chen, W.-L., Wang, X.-L., Li, Y.-G., Su, Z.-M., Wang, E.-B. Polyoxometalates in dye-sensitized solar cells. *Chem. Soc. Rev.* **48**, 260–284 (2019).
 309. Jin, G., Wang, S.-M., Chen, W.-L., Qin, C., Su, Z.-M., Wang, E.-B. A photovoltaic system composed of a keplerate-type polyoxometalate and a water-soluble poly(p-phenylenevinylene) derivative. *J. Mater. Chem. A* **1**, 6727–6730 (2013).
 310. Xu, S., Wang, Y., Zhao, Y., Chen, W., Wang, J., He, L., Su, Z., Wang, E., Kang, Z. Keplerate-type polyoxometalate/semiconductor composite electrodes with light-enhanced conductivity towards highly efficient photoelectronic devices. *J. Mater. Chem. A* **4**, 14025–14032 (2016).
 311. Li, J.-S., Sang, X.-J., Chen, W.-L., Zhang, L.-C., Zhu, Z.-M., Li, Y.-G., Su, Z.-M., Wang, E.-B. A strategy for breaking the MOF template to obtain small-sized and highly dispersive polyoxometalate clusters loaded on solid films. *J. Mater. Chem. A* **3**, 14573–14577 (2015).
 312. Zheng, X., Chen, W., Chen, L., Wang, Y., Guo, X., Wang, J., Wang, E. A strategy for breaking polyoxometalate-based MOFs to obtain high loading amounts of nanosized polyoxometalate clusters to improve the performance of dye-sensitized solar cells. *Chem. Eur. J.* **23**, 8871–8878 (2017).
 313. He, L., Chen, L., Zhao, Y., Chen, W., Shan, C., Su, Z., Wang, E. TiO_2 film decorated with highly dispersed polyoxometalate nanoparticles synthesized by micelle directed method for the efficiency enhancement of dye-sensitized solar cells. *J. Power Sources* **328**, 1–7 (2016).
 314. Wang, Y.-J., Chen, W.-L., Chen, L., Zheng, X.-T., Xu, S.-S., Wang, E.-B. Sandwich-type silicotungstate modified TiO_2 microspheres for enhancing light harvesting and reducing electron recombination in dye-sensitized solar cells. *Inorg. Chem. Front.* **4**, 559–565 (2017).
 315. Shan, C.-H., Zhang, H., Chen, W.-L., Su, Z.-M., Wang, E.-B. Pure inorganic D-A type polyoxometalate/reduced graphene oxide nanocomposite for the photoanode of dye-sensitized solar cells. *J. Mater. Chem. A* **4**, 3297–3303 (2016).
 316. Sang, X., Li, J., Chen, W., Wang, E. Polyoxometalate-assisted synthesis of the ZnO polyhedra in an alkali solution and their photoelectrical properties. *Mater. Lett.* **87**, 39–42 (2012).
 317. Li, N., Sun, Z., Liu, R., Xu, L., Xu, K., Song, X.-M. Enhanced power conversion efficiency in phthalocyanine-sensitized solar cells by modifying TiO_2 photoanode with polyoxometalate. *Sol. Energy Mater. Sol. Cells* **157**, 853–860 (2016).

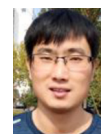
318. Liu, R., Sun, Z., Zhang, Y., Xu, L., Li, N. Polyoxometalate-modified TiO₂ nanotube arrays photoanode materials for enhanced dye-sensitized solar cells. *J. Phys. Chem. Solids* **109**, 64–69 (2017).
319. Barrows, J. N., Jameson, G. B., Pope, M. T. Structure of a heteropoly blue-the 4-electron reduced β -12-molybdophosphate anion. *J. Am. Chem. Soc.* **107**, 1771–1773 (1985).
320. Sang, X., Li, J., Zhang, L., Wang, Z., Chen, W., Zhu, Z., Su, Z., Wang, E. A novel carboxyethyltin functionalized sandwich-type germanotungstate: synthesis, crystal structure, photosensitivity, and application in dye-sensitized solar cells. *ACS Appl. Mater. Interfaces* **6**, 7876–7884 (2014).
321. Li, J.-S., Sang, X.-J., Chen, W.-L., Zhang, L.-C., Zhu, Z.-M., Ma, T.-Y., Su, Z.-M., Wang, E.-B. Enhanced visible photovoltaic response of TiO₂ thin film with an all-inorganic donor-acceptor type polyoxometalate. *ACS Appl. Mater. Interfaces* **7**, 13714–13721 (2015).
322. Li, J., Chen, W., Chen, L., Zheng, X., Zhu, G., Wang, E. A Strategy to obtain long-term stable heteropoly blues for photosensitive property investigations. *Adv. Optical Mater.* **6**, 1800225 (2018).
323. Anandan, S., Pitchumani, S., Muthuraaman, B., Maruthamuthu, P. Heteropolyacid-impregnated PVDF as a solid polymer electrolyte for dye-sensitized solar cells. *Sol. Energy Mater. Sol. Cells* **90**, 1715–1720 (2006).
324. Akhtar, M. S., Cheralathan, K. K., Chun, J.-M., Yang, O. B. Composite electrolyte of heteropolyacid (HPA) and polyethylene oxide (PEO) for solid-state dye-sensitized solar cell. *Electrochim. Acta* **53**, 6623–6628 (2008).
325. Chen, D., Zhang, Q., Wang, G., Zhang, H., Li, J. A novel composite polymer electrolyte containing room-temperature ionic liquids and heteropolyacids for dye-sensitized solar cells. *Electrochem. Commun.* **9**, 2755–2759 (2007).
326. Yuan, C.-C., Wang, S.-M., Chen, W.-L., Liu, L., Qin, C., Su, Z.-M., Wang, E.-B. Polyoxometalate supported complexes as effective electron-transfer mediators in dye-sensitized solar cells. *Dalton Trans* **43**, 1493–1497 (2014).
327. Yuan, C.-C., Wang, S.-M., Chen, W.-L., Liu, L., Zhang, Z.-M., Lu, Y., Su, Z.-M., Zhang, S.-W., Wang, E.-B. The research of employing polyoxometalates as pure-inorganic electron-transfer mediators on dye-sensitized solar cells. *Inorg. Chem. Commun.* **46**, 89–93 (2014).

AUTHOR BIOGRAPHIES

Yu Zhang received her Ph.D. degree from School of Chemistry and Chemical Engineering, Nanjing University in 2018. Now, she is a postdoctoral researcher in Ya-Qian Lan's group in Nanjing Normal University. Her current research interests mainly focus on the structural design and mechanism study of electro-/photo-catalysts for CO₂ reduction reaction.



Jiang Liu, associate professor of College of Chemistry and Materials Science of Nanjing Normal University, received his Ph.D. degree from Sun Yat-Sen University. His main research interests focus on the development of metal-organic crystalline materials in energy storage and conversion, proton conductivity and photo/electric heterogeneous catalysis applications.



Prof. Shun-Li Li was born in 1979 in Jilin, P. R. China. She received her BS (2002) in Chemistry and PhD degree (2008) from Northeast Normal University under the supervision of Prof. Jian-Fang Ma. She carried out postdoctoral studies with Prof. Zhong-Min Su in Environmental Chemistry at Northeast Normal University. Then she worked as a JSPS (Japan Society for the Promotion of Science) invited fellow at AIST (National Institute of Advanced Industrial Science and Technology) in 2012. She is a professor of Chemistry at Nanjing Normal University. Her current research interest lies in the syntheses, structures and properties of organic-norganic hybrid materials.



Prof. Zhong-Min Su received his BS (1983) and then his PhD in inorganic chemistry under the supervision of Prof. Rong-Shun Wang and Prof. Chi-Ming Che from NENU (1997). He has been a full professor at NENU since 1994. Later, he worked as a visiting scholar in the group of Prof. Chi-Ming Che and Prof. Guan-Hua Chen (The University of Hong Kong), in Prof. Koji Ohta's group (National Industrial Technology Research Institute), Roesch's group (Technical University of Munich, Germany). His research interests focus on the functional material chemistry and quantum chemistry.



Prof. Ya-Qian Lan was born in 1978 in Jilin, P. R. China. He received his BS and PhD degree (2009) from Faculty of Chemistry, Northeast Normal University, under the supervision of Prof. Zhong-Min Su. In 2010, he worked as a JSPS postdoctoral fellow at AIST. Since the fall of 2012, he has been a Professor of Chemistry at Nanjing Normal University. His current research interests focus on synthesis of porous crystalline materials and catalytic research related to clean energy applications.

